Implementation of dosimetry audits in Radiotherapy



Diana Lopes Silva
Master in Medical Physics
Department of Physics and Astronomy
Faculty of Sciences of University of Porto
2024

Implementation of dosimetry audits in Radiotherapy

Diana Lopes Silva

Dissertation carried out as part of the Master in Medical Physics

Department of Physics and Astronomy

2024

Supervisor, PhD
Anabela Gregório Dias
Medical Physicist Expert
Instituto Português de Oncologia do Porto Francisco Gentil, E.P.E.

Co-supervisor, MSc
Ana Catarina Santos Souto
Medical Physicist Expert
Instituto Português de Oncologia do Porto Francisco Gentil, E.P.E.

“Life is not easy for any of us. But what of that? We must have perseverance and above all confidence in ourselves. We must believe that we are gifted for something, and that this thing must be attained.”

Marie Curie

Acknowledgements | Agradecimentos

Quero começar por agradecer às minhas orientadoras, Anabela Dias e Catarina Souto. Obrigada pela orientação, paciência e dedicação durante todo o trabalho, e pelo voto de confiança.

Estendo este agradecimento ao resto da equipa do serviço de Física Médica do IPO-Porto. Obrigada por todas as sugestões e por me ajudarem sempre que precisei.

Nunca teria conseguido percorrer este caminho sozinha e, por isso, tenho de agradecer à minha família. Mãe e pai, nunca vou encontrar as palavras certas para vos agradecer por tudo. Obrigada pelo amor incondicional e estarem sempre ao meu lado. Avó, obrigada por acreditares sempre que eu era capaz.

Ao meu namorado, Pedro, obrigada pelos conselhos, pela ajuda e, acima de tudo, pela amizade. Tens sido o meu porto seguro.

Também tenho de agradecer aos meus amigos, que acreditaram em mim e me deram força quando precisei. Em especial à Inês Rolo, que esteve sempre lá para mim nos últimos 6 anos. Felicidade, Maria, Bea, Emma, obrigada pela amizade, mesmo durante as minhas ausências. Este percurso foi ainda mais bonito com vocês ao meu lado.

Não teria sido a mesma coisa sem vocês. Obrigada, do fundo do coração.

Resumo

O cancro é a segunda principal causa de morte a nível global, com mais de metade dos casos a serem tratados com radioterapia. A radioterapia é uma modalidade de tratamento que utiliza radiação ionizante e, por isso, exige precisão em todas as etapas. Os avanços tecnológicos permitiram a introdução de novas técnicas em radioterapia, destacando a necessidade de assegurar tratamentos seguros e consistentes. As auditorias dosimétricas são ferramentas essenciais para verificação da precisão dos sistemas e da uniformidade dos processos entre diferentes centros.

Este trabalho tem como objetivo principal o desenvolvimento de um protocolo de auditoria, composto por duas partes: (1) uma auditoria à metodologia de determinação da dose absoluta e (2) uma auditoria à dosimetria de campos pequenos, mais especificamente à determinação dos *output factors* de campos pequenos. Para a auditoria à dose absoluta, foi criado um inquérito sobre práticas em dosimetria de referência, e foi construída uma folha de cálculo para determinação da dose absorbida em água, seguindo as indicações da revisão do protocolo TRS-398, publicada em fevereiro de 2024. De forma a validar a metodologia desenvolvida, o IPO-Porto foi o centro-piloto. Foram realizadas verificações de medidas de dose absoluta para feixe de fotões, nos 8 aceleradores lineares instalados na instituição.

Relativamente à dosimetria de campos pequenos, foi desenvolvido um inquérito sobre práticas em dosimetria de campos pequenos e medições de *output factors*, contendo um ficheiro Excel para recolha dos valores dos *output factor* medidos. No IPO-Porto, foram realizadas as medições de *output factors* de campos pequenos, usando dois detetores, nomeadamente um detetor de diamante e um detetor díodo, seguindo as recomendações do protocolo TRS-483.

Os inquéritos desenvolvidos foram enviados a nível nacional para 20 centros de radioterapia. Até ao momento, apenas 6 centros mostraram disponibilidade para participarem e fornecerem os seus dados. Esta distribuição permitiu uma comparação multicentro, que não foi conseguida na sua totalidade. Para acompanhar as verificações de ambos os procedimentos, foram, ainda, criadas duas *checklists* de verificação de boas práticas.

As respostas a ambos os inquéritos foram analisadas, permitindo comparar a implementação dos protocolos em diferentes serviços e identificar discrepâncias. Os

valores de dose foram calculados utilizando a folha de cálculo desenvolvida durante este trabalho e a folha de cálculo fornecida pela IAEA, e foi possível observar que todos os valores estavam dentro dos limites de tolerância. No que respeita, aos valores de *output factors* de campos pequenos, foram analisadas as medidas realizadas no centro-piloto com dois detetores diferentes. Similarmente, os dados fornecidos pelos centros de radioterapia que participaram no estudo demonstraram boa concordância entre eles.

Foram, ainda, calculadas as incertezas associadas à determinação de dose absorvida em água e à determinação dos *output factors* de campos pequenos, com base nas verificações do centro piloto e nos dados fornecidos pelos participantes.

Palavras-chave: [auditorias dosimétricas, dosimetria, dose absoluta, campos pequenos, output factors, incertezas]

Abstract

Cancer ranks as the second leading cause of death worldwide, with over half of cases undergoing radiation therapy. Radiotherapy is a treatment modality that uses ionizing radiation, and, for that reason, demands precision throughout its processes. Technological advancements have introduced new techniques in radiotherapy, emphasizing the critical need for safe and consistent treatment delivery. Dosimetry audits serve as pivotal tools to verify system accuracy and process uniformity across different centres.

This study aimed to develop a dosimetry audit protocol comprising two parts: (1) an absolute dose audit and (2) a small field dosimetry audit, specifically focusing on small field output factors determination.

For absolute dose auditing, a survey on reference dosimetry practices was conducted, and a worksheet for calculating absorbed dose in water was created following the revision of the TRS-398 protocol, published in February 2024. To validate the developed methodology, IPO-Porto was the pilot-centre. Local verifications of absolute dose measurements were performed at IPO-Porto, for photon beams, in the 8 linear accelerators installed at the facility.

Regarding small field dosimetry, a survey on small field dosimetry practices and field output factor measurements was developed. It included an Excel file to collect field output factors data. At IPO, field output factor measurements were performed, using two detectors, namely a diamond detector and a diode detector, following the TRS-483 recommendations.

The developed surveys were sent to 20 national radiotherapy centres. So far, only 5 centres were available to participate and provide their data. Two verification checklists for best practices were devised to accompany local verifications for both parts of the audit.

Survey responses were analysed for both parts of the audit, enabling comparison of protocol use across facilities and identification of discrepancies. Dose values were calculated using self-developed and IAEA-provided spreadsheets, and it was possible to observe that all within tolerance limits. For field output factors, local measurements at IPO using two different detectors were compared. Similarly, data from the different radiotherapy centres were also compared, demonstrating good agreement among them.

Uncertainties associated with the determination of absorbed dose in water and small field output factors were also calculated based on pilot-centre verifications and information provided by the participants.

Keywords: [dosimetry audits, dosimetry, absolute dose, small fields, output factors, uncertainties]

Table of Contents

List of Tables ix

List of Figures xi

List of Abbreviations xiii

Introduction 1

1. State of the Art 3

1.1. Dosimetry audits 3

1.2. Radiation dosimetry 8

1.2.1. Photon beam characterization 8

1.2.2. Formalism for absorbed dose determination 12

1.2.3. Equipment for absolute dose measurements 16

1.3. Small field dosimetry 18

1.3.1. Small field characterization 19

1.3.2. Formalism for small field dosimetry 23

1.3.3. Equipment for small field dosimetry 26

1.4. Uncertainties 33

2. Methods and Materials 36

2.1. Audit outline 36

2.2. Multicentre survey on dosimetry practices in Radiotherapy 37

2.3. Worksheet for determination of absorbed dose to water 39

2.4. On-site measurements at pilot-centre: absolute dose 39

2.4.1. Stability verification procedure 40

2.4.2. Solid water slab phantom 42

2.4.3. Water tank phantom 43

2.5. Multicentre survey on dosimetry of small fields practices 44

2.6. Remote audit: small field OF 46

2.7. On-site measurements at pilot-centre: small field OF 47

2.8. Uncertainties determination 50

2.8.1. Absolute dose determination 50
2.8.2. Field output factors determination 53
2.9. Audit report 54
3. Results and discussion 55
3.1. Multicentre survey on dosimetry practices in absolute dose 55
3.2. On-site measurements at pilot-centre: absolute dose 57
3.2.1. Stability verification procedure 57
3.2.2. Absolute dose determination 57
3.3. Multicentre survey on dosimetry of small fields practices 59
3.4. Field output factors determination 60
3.4.1. On-site measurements at pilot-centre 60
3.4.2. Remote audit 62
3.5. Uncertainties determination 67
3.5.1. Uncertainties associated with absolute dose determination 67
3.5.2. Uncertainties associated field output factors determination 72
4. Conclusions 75
4.1. Future work 76
References 77
Attachments 89
Attachment 1 89
Attachment 2 95
Attachment 3 97
Attachment 4 101
Attachment 5 108
Attachment 6 111

List of Tables

Table 1: Classification of different types of dosimetry audits (Adapted from [20]). 6
Table 2: Overview of the ionization chamber models used to measure absolute dose across different RT facilities. 55
Table 3: Overview of the tolerance level for dose deviation adopted by the participating RT facilities. 56
Table 4: Relative variations in dose and beam quality correction factor kQ values, between the two dose determination worksheets, for each beam energy of IPO LINACs. 57
Table 5: Overview of the number of LINACs and respective setups for field output factors determination. 59
Table 6: Overview of the detectors used for field output factors determination. 60
Table 7: $Sclin$ measured for the TrueBeam small field sizes, as a function of the nominal square field sizes. 61
Table 8: Field Output Factors determined with MicroDiamond and MicroSilicon detectors and relative standard deviation (SD) of the values, for photon beams with energies 6 MV and a 6 MV FFF. 62
Table 9: Mean and standard deviation of field OFs submitted, and number of beams considered for photon beams with energies 6 MV and a 6 MV FFF, for Varian TrueBeam LINACs. 63
Table 10: Mean and standard deviation of field OFs with the TRS-483 correction factor applied, and number of beams considered for photon beams with energies 6 MV and a 6 MV FFF, for Varian TrueBeam LINACs 63
Table 11: Mean and standard deviation of field OFs submitted, and number of beams considered for photon beams with energies 6 MV and a 6 MV FFF, for Elekta Versa HD LINACs. 64
Table 12: Mean and standard deviation of field OFs submitted, and number of beams considered for photon beams with energies 10 MV and a 10 MV FFF, for Elekta Versa HD LINACs. 65
Table 13: Mean and standard deviation of field OFs with the TRS-483 correction factor applied, and number of beams considered for photon beams with energies 6 MV and a 6 MV FFF, for Elekta Versa HD LINACs. 65
Table 14: Mean and standard deviation of field OFs with the TRS-483 correction factor applied, and number of beams considered for photon beams with energies 10 MV and a 10 MV FFF, for Elekta Versa HD LINACs. 65

Table 15: Uncertainty budget of the determination of absorbed dose to water. 70
Table 16: Field OF uncertainty and its respective relative standard uncertainty, according to TRS-483 [9]. 73
Table 17: Uncertainty budget of field output factors determination. 74

List of Figures

Figure 1: 6 MV, 10 MV, 15 MV, 6 MV FFF and 10 MV FFF PDDs for the TrueBeam LINAC (IPO-Porto), measured at a 10 cm × 10 cm field size, and 100 cm SSD. 9
Figure 2: 6 MV and 6 FFF MV profiles for the TrueBeam LINAC (IPO-Porto), measured at a 10 cm × 10 cm field size, 100 cm SSD and 10 cm depth. 10
Figure 3: Scheme of the setup that should be used to determine dose absorbed to water, recommended by the TRS-398 [8]. 13
Figure 4: Scheme of a cylindrical ionization chamber (Adapted from [54]). 17
Figure 5: In a large field, there's LCPE; in a small field, the number of charged particles exiting the chamber's cavity is not compensated by the number of charged particles entering the cavity – loss of LCPE (Adapted from [62]). 20
Figure 6: Schematic illustration of source occlusion (Adapted from IPEM report 103 [65]). 21
Figure 7: Apparent profile widening associated with small fields (Adapted from [47]). 22
Figure 8: Lateral charged particle equilibrium (LCPE) range (Adapted from [62]). 23
Figure 9: Overview of the dosimetry of small static fields with reference to a machine specific reference field, according to the formalism of TRS-483 [9], [46] (Reproduced from Alfonso et al. [46]). 25
Figure 10: TLD and OSLD detectors (Adapted from [83]). 28
Figure 11: Comparison of different diode dosimeters models (Adapted from [85]). 29
Figure 12: Schematic diagram of a diode detector (Adapted from [88]). 30
Figure 13: a. Scheme of a water-equivalent diamond detector. b. Photography of a diamond detector with a graphite cover. (Adapted from [74]). 31
Figure 14: Scheme of a MOSFET detector design (Adapted from [54]). 31
Figure 15: a. Irradiated films with different known doses. b Calibration curve of the film sheet (Adapted from [92]). 33
Figure 16: Exemplification of the uncertainty interval (Adapted from [97]). 34
Figure 17: A-priori distributions (Adapted from JCGUM [98]). 35
Figure 18: PTW 30013 Farmer chamber used in absorbed dose to water measurements. 40
Figure 19: PTW Radioactive Check Device type T48010. 41
Figure 20: Setup for absorbed dose determination, assembled with RW3 slab phantom. 42
Figure 21: Setup for absorbed dose determination, assembled with a water phantom.43

Figure 22: Setup for field output factors determination, assembled with a water phantom. 48
Figure 23: a) PTW 60019 MicroDiamond; b) PTW 6023 MicroSilicon 49
Figure 24: Absorbed dose determined for each beam energy for the TrueBeam LINAC, calculated using the IAEA worksheet and the new worksheet. The red line indicates the tolerance limit of 2%. 58
Figure 25: Field output factors, and respective uncertainty, for 3 field sizes (1 cm × 1 cm, 2 cm × 2 cm, and 3 cm × 3 cm), determined with MicroDiamond and MicroSilicon detectors, for 6 MV and 6 MV FFF photon beams. 61
Figure 26: Absorbed dose determined for each beam energy for the TrueBeam LINAC, calculated using the IAEA worksheet and the new worksheet, and respective uncertainties. The red line indicates the tolerance limit of 2%..... 71

List of Abbreviations

AAPM	AMERICAN ASSOCIATION OF PHYSICISTS IN MEDICINE
CAX	CENTRAL AXIS
DP	DOSE PROFILES
ESTRO	EUROPEAN SOCIETY FOR RADIOTHERAPY AND ONCOLOGY
IAEA	INTERNATIONAL ATOMIC ENERGY AGENCY
IMRT	INTENSITY-MODULATED RADIATION THERAPY
FF	FLATENNING FILTER
FFF	FLATENNING FILTER FREE
FWHM	FULL WIDTH AT HALF MAXIMUM
LCPE	LATERAL CHARGE PARTICLE EQUILIBRIUM
LINAC	LINEAR PARTICLE ACCELERATOR
MSR	MACHINE SPECIFIC REFERENCE
MU	MONITOR UNIT
OF	OUTPUT FACTOR
PDD	PERCENT DEPTH DOSE
QA	QUALITY ASSURANCE
RT	RADIOTHERAPY
SBRT	STEREOTACTIC BODY RADIOTHERAPY
SD	STANDARD DEVIATION
SSD	SOURCE-TO-SURFACE DISTANCE
SRS	STEREOTACTIC RADIOSURGERY
TPR	TISSUE-PHANTOM RATIO
TRS	TECHNICAL REPORTS SERIES
WFF	WITH FLATENNING FILTER
WHO	WORLD HEALTH ORGANIZATION

Introduction

Cancer is the second leading cause of death worldwide, and according to the World Health Organization (WHO), it was responsible for nearly 20 million new cases and 9.6 million deaths in 2022. In the same year, in Portugal, almost 70 thousand new cases emerged and there were 33 thousand recorded deaths [1]. Over 60% of cases require treatment with radiotherapy (RT), either alone or in combination with other treatment modalities such as surgery and chemotherapy [2].

Radiotherapy is a high-risk procedure because it is a complex multi-step process that involves ionizing radiation, requiring a high level of accuracy at every step [3]. Inadequate clinical dosimetry places the patient at risk, as the dose has an impact on local tumour control and radiation toxicity, consequently affecting quality of life [3], [4], in other words, underdosing can disrupt the therapeutic effectiveness of a radiotherapy treatment, while overdosing can harm healthy tissues. Due to this, it is very important to ensure safe radiotherapy with consistent doses. Dosimetry audits are an effective way of checking whether the quality of dosimetry in radiotherapy centres is adequate for the treatment objectives [4], [5], [6]. The required accuracy for dose delivery is typically considered to be $\pm$ 5% [7], [8], [9], [10], [11].

Dosimetry audit has demonstrated to be an efficient tool in improving the quality and patient safety during radiotherapy treatments as well as identifying significant parameters that can have an impact on patient dosimetry [6], [12], [13]. The development of new and more complex techniques and treatment modalities requires testing the most complex aspects of systems [6], to ensure more rigorous treatment and greater patient safety [14]. There is also the need to ensure even more consistency between different systems and medical institutions [5]. Several authors and studies report that dosimetry audits reduce uncertainty and increase the consistency of dosimetry between different centres [4], [10].

Modern linear accelerator photon beams are calibrated in water at a 10 cm depth according to AAPM TG-51 [15] and IAEA TRS-398 [8] recommendations, standards that are widely adopted globally. This represents a significant improvement over previous methods, offering greater accuracy and consistency. Most linear accelerators are configured so that 1 monitor unit (MU) corresponds to 1 cGy at depth of maximum dose, d_{max}. Once calibrated, the accuracy of delivered dose should be assessed through an independent audit, part of a complete quality assurance program [4], [13].

The use of small fields has become widespread in advanced radiotherapy techniques, such as intensity modulated radiotherapy (IMRT), stereotactic radiosurgery (SRS) and stereotactic body radiotherapy (SBRT). Small-field dosimetry represents an added challenge in terms of acquiring and characterising beam data during the commissioning process. The latest revision of IAEA TRS-483 protocol [9] includes different recommendations, including the use of different detectors and the application of output fact (OF) correction factors. The correct implementation of this protocol is crucial to guaranteeing the quality and safety of radiotherapy treatments, and local procedures should be supported and validated by independent external audits.

The purpose of this work is to create a methodology for dosimetry audits in radiotherapy facilities. The main objectives are:

- Conduct a survey on dosimetry practices for absolute dose measurements.
- Conduct a survey on small field dosimetry.
- Develop a new worksheet for absorbed dose determination based on the revision of the TRS-398 [8], published in 2024.
- Perform a national multicentre comparison of dosimetry practices.
- Estimate the uncertainties associated with absolute dose measurements and small field output factors measurements.

This dissertation is divided into four main chapters. The current chapter introduces the theme and outlines the objectives of the work. Chapter 1 presents the state of the art with a literature review on dosimetry audits, radiation dosimetry in reference fields and small fields, and uncertainties calculation. Chapter 2 describes the materials and methods of the work, including the audit methodology, with the description of the surveys, all the measurements performed, and the determination of the associated uncertainties. Chapter 3 reviews and discusses the results of the work. The final chapter presents conclusions and reflections on future work.

Attachment 1 includes the survey on dosimetry practices for absorbed dose determination. Attachment 2 features the worksheet for determination of absorbed dose to water for photon beams. Attachment 3 includes the checklist developed for the absolute dose dosimetric audit. Attachment 4 contains the survey on small field dosimetry practices. Attachment 5 features the checklist developed for small field dosimetric audit. And, finally, Attachment 6 includes the audit report developed.

1. State of the Art

Dosimetry audits have proven to be an effective tool for improving quality and patient safety in Radiotherapy (RT). Numerous examples show how dosimetry audits have played a key role in defining and improving standards of care, as well as identifying issues that can cause harm to patients, such as errors in reference dosimetry. They are also crucial for supporting the implementation of complex techniques [6], [12], [14], [16], [17], [18].

There are more than 7000 registered radiotherapy centres worldwide, operating 13800 RT machines – 11400 linear accelerators and 2200 Cobalt-60 units. In 2013, only about 66% of these centres had received some type of dosimetry audit. Participation in dosimetry audits is voluntary and it is based on the motivation to perform high-quality Radiotherapy [4]. Several authors and studies report that dosimetry audits reduce uncertainty and increase the consistency of dosimetry between different institutions [4], [18], [19], [20].

1.1. Dosimetry audits

In 1925, Rolf Maximilian Sievert established a department to regulate the use of radiation in medicine, in Sweden. This department identified the appropriate dosimeters and reported the need for better protective equipment for radiation professionals. Meanwhile, the data collected from percent depth dose (PDD) measurements began to be used as reference values. Inspired by Marie Curie's idea to establish a laboratory for measuring the dose of X-rays and the radioactive isotope radium used in hospitals, the laboratory for dosimetry measurements was founded in 1936, in Poland [21].

Dosimetry audits were officially introduced by the International Atomic Energy Agency (IAEA) [13], that, in 1966, organized the first postal dosimetry service. In 1968, the World Health Organization (WHO) joined the dose project [17], [22]. Since 1969, the IAEA, in collaboration with the WHO, has conducted thermoluminescence dosimetry (TLD) audits by mail to verify the calibration of teletherapy beams in radiation therapy departments in developing countries. Over 50 years, the program has verified the calibration of more than 6200 photon beams in approximately 1500 radiotherapy facilities [21], [22].

In 2018, Izewska et al. [4] reported an IAEA database describing activities of dosimetry audit network in radiotherapy (DAN). This database is based on a

questionnaire started in 2010 with responses from more than 80 departments of radiotherapy in 59 countries.

The European Society for Radiotherapy and Oncology (ESTRO) identified dosimetry audits as a strategy to support quality improvement through standardization of RT practices across Europe [17]. But, due to the development of new and complex RT techniques, dosimetry audits challenges are increasing [16], [23]. In 2017, ESTRO held two workshops to address how IAEA and clinical trial quality assurance groups can work together to develop audit methodologies that address specific issues [6], [17]. Additionally, a course on dosimetric audits has been included in the ESTRO training program, in 2023, highlighting the importance of this topic [24].

A clinical audit is a process of quality assurance (QA) that seeks to improve patient care and outcomes by reviewing the clinical activity performed. A dosimetry audit in radiotherapy is part of this process. The main goal of this form of QA is to improve patient care by maximizing the effectiveness of clinical activities and minimizing harm to both individuals and society as a whole [20], [25].

In accordance with the Portuguese national legislation, namely Decree-Law 108/2018, radiological facilities must carry out clinical audits with the appropriate periodicity, whether internal or external, transposing Council Directive 2013/59/Euratom of 5 December 2013, laying down basic safety standards to protect against the dangers arising from exposure to ionizing radiation. Auditing is defined as a systematic analysis or review of medical radiological procedures with the aim of improving the quality and results of patient care, through a structured review in which medical radiological practices, procedures and outcomes are scrutinized against approved standards of good medical radiological procedures, leading to the amendment of the practices concerned, where appropriate, and the application, if necessary, of new standards. However, and unlike some countries that follow national guidelines [4], [26], Portugal does not have any. Since 2011, the IAEA has conducted two national audits in Portugal, one in 2011 and 2012 and another in 2018, both carried out by local physicists. The audit carried out in 2011/2012 was a 3D-CRT TPS audit. The audit methodology simulated all steps of 3D-CRT external beam radiotherapy workflow, from image acquisition to treatment planning and dose delivery. All 24 radiotherapy centres in Portugal have participated [27]. The audit carried out in 2018 focused on Intensity Modulated Radiotherapy (IMRT) technique. The audit methodology tested basic small field dosimetry and MLC performance. At the time, 20 out of 24 centres had already introduced IMRT into clinical practice, and all 20 centres participated in the study [28].

Dosimetry audits worldwide are organized in different ways, often due to geographical, economic, or political reasons [21], [26]. Audits are limited by available resources, such as new and well-calibrated equipment [4], [29], which is one of the reasons why in low and middle-income countries the percentage of results outside the acceptance limits were higher [22].

Audits can be classified as internal or external, depending on whether they are conducted by the organization's own staff or by an independent external team. Internal audits are performed within a single RT facility, typically by physicists from that institution [17], [25]. At an institutional level, external audits are conducted through independent procedures, by external professionals, who are not responsible for the performance of the activities subject to the audit [21], [25]. External audits ensure that the clinical requirements for the quality of RT treatments are met, minimizing errors and incidents [21].

A multicentre audit is a form of audit conducted by an external team that involves multiple RT facilities. It allows for comparative dosimetry studies, which are crucial for assessing the uniformity and consistency of dose delivery [30]. This type of audit has proven to be useful in detecting differences between beam outputs, ensuring that patients receive a standardized level of care regardless of the facility they attend [31], [32]. When comparing data from different facilities, it is important to ensure that the procedures used to obtain the data were consistent, so that measurements are not influenced by factors that are not being evaluated. [31], [33]. Errors in measurements commonly result from different measurement instruments, such as the phantom or the dosimeters [12], [31].

There are several types of radiation dosimetry audits, which span from basic measurements under reference conditions to audits involving complex irradiation plans or *in vivo* dosimetry on patient treatment [6], [13], [17]. Dosimetry audits can be either partial, focusing solely on specific parts of the RT process, or comprehensive, evaluating the entire process [13]. Depending on the availability of dosimetry equipment and logistics, audit measurements can be conducted on-site, with the auditor present during the measurements and tests, or remotely, where the auditing team requests the values and analyses them without being at the centre at the time of the measurements [4], [21], [25].

As per the IAEA, dosimetry audits can be classified according to their complexity [23] and the aspect of the radiotherapy treatment they assess. The classification of the different audit types can be found in Table 1. Regardless of the approach, dosimetry

audits primarily verify the fundamental measurement, which is the absorbed dose in reference conditions — the beam output. This measurement determines whether the system is well calibrated and suitable to deliver dose to patients [21]. The absolute output measurement of high-energy beams produced by a linear accelerator under reference conditions is known as Level 1 dosimetry [30].

Conventionally, audits are conducted independently, where each procedure is audited separately. In this method, physicists audit each system or process individually using phantoms and dosimeters to assess the accuracy and compliance of each component. Alternatively, audits can be performed through an end-to-end process – Level 4 audits, testing the entire chain of procedures from the CT to the actual treatment, using, typically, an anthropomorphic phantom [29], [34]. First, the phantom is used to generate a computed tomography (CT) image, which is used to plan the treatment. Then, the phantom is irradiated, following the plan, and dose measurements are performed and compared with the calculated plan [13], [14], [17].

There are audit methods based on phantoms (phantom-detector combinations) and methods that don't use any phantom (portal dosimetry, transmission detectors, log files). These have the potential to enable parallel audits (across multiple institutions simultaneously), automate data analysis, and assess various treatment steps. These evolving methods may also significantly reduce the time required for conducting an audit [25], [29].

Table 1: Classification of different types of dosimetry audits (Adapted from [21]).

Level	Tasks	Dosimetry equipment	Phantom
Level 1	Verification of the beam under reference conditions.	**R**[1]: TLD, OSLD, RPLD, Alanine **O**[2]: Ion chamber, 2D & 3D array, TLD, OSLD, Alanine	Water or solid water/geometric
Level 2	Verification of the photon beam relative dosimetry parameters under non-reference conditions on- and off-central axis.	**R**: TLD, OSLD, RPLD, Alanine, films, diodes **O**: Ion chamber, 2D & 3D array, films, diodes, TLD, OSLD, Alanine	Water or solid water/geometric

[1] Remote audits
[2] On-site audits

Level 3	Verification of complex dosimetry parameters using geometric phantom or anthropomorphic phantom. Treatment planning system (TPS) dose calculations are compared to audit measurements.	**R**: TLD, OSLD, RPLD, Alanine, films, diodes, 2D & 3D array **O**: Ion chamber, 2D & 3D array, films, diodes, TLD, OSLD, RPLD, Alanine	Water or solid water/geometric Anthropomorphic
Level 4	End-to-end verification of advanced treatment modalities, using an anthropomorphic phantom that approaches a patient treatment, including targets, organs at risk and heterogeneities.	**R**: TLD, OSLD, RPLD, Alanine, films, diodes, 3D dosimeters **O**: Ion chamber, 2D & 3D array, films, diodes, TLD, OSLD, RPLD, Alanine, 3D dosimeters	Anthropomorphic

In recent years, several articles have been published on multicentre audit studies of small field output factors, which reflect the growing use of small fields in special radiotherapy techniques, like Intensity Modulated Radiotherapy (IMRT), Stereotactic Radiosurgery (SRS), or Stereotactic Body Radiation Therapy (SBRT). These studies aim to ensure consistency and accuracy in small field dosimetry across different centres. For example, Russo et al. (2016) [35] audited 30 Italian RT facilities, equipped with Siemens, Varian, and Elekta linear accelerator (LINACs), testing a diamond detector for output factor measurements and concluding it is a suitable detector. Akino et al. (2018) [36] studied 19 institutions with Novalis (Varian) LINACs, revealing that detector choice affects measurement consistency across institutions and highlighting the need for careful management of small fields due to detected measurement errors. Russo et al. (2019) [37] examined five institutions using CyberKnife LINACs, finding significant uncertainties in small field dosimetry and recommending careful detector selection and the creation of a database for less experienced RT departments to reference. Talamonti et al. (2019) [38] conducted a national multicentre audit in Italy across 24 centres, auditing Elekta and Varian LINACs. Akino et al. (2019) [39] also investigated 12 institutions with TrueBeam (Varian) LINACs, showing that detector-dependent interinstitutional variations in beam data can lead to dose delivery uncertainties for patients. Dufreneix et al. (2021) [20] audited field output factors in 23 institutions in France, including RT treatment machines

from CyberKnife, Elekta, and Varian, underlining the variability in measurements due to different detectors and practices.

1.2. Radiation dosimetry

Radiation dosimetry, or simply dosimetry, is the field concerned with measuring the absorbed dose deposited in a medium by ionizing radiation [40]. The International Commission on Radiation Units and Measurements (ICRU) [41] defined the absorbed dose, D, as the energy absorbed per unit mass of tissue:

$$D = \frac{dE}{dm} \quad (1)$$

dE is the mean energy imparted by the ionizing radiation to a mass, dm. The unit for absorbed dose is the Gray (Gy) [40], [41].

Radiation dosimetry includes reference dosimetry and relative dosimetry [42]. The term reference dosimetry refers to the measurement of absorbed dose in water with an ionization chamber [43], necessary for calibration of treatment equipment, establish baseline measurements and maintain the accuracy and safety of radiation treatments [42]. Relative dosimetry involves the measurement of the dose under non-reference conditions. These measurements include dosimetry of different radiation fields by comparing them to a reference field, calculating outputs factors (OFs), and determining depth dose distributions [8], [40]. Relative dosimetry allows the evaluation of variations and consistency in dose delivery across different conditions and setups, ensuring accurate and effective radiation treatments [40], [42].

1.2.1. Photon beam characterization

Clinical photon beams are characterized during the commissioning procedure through percentage depth dose (PDDs), off-axis profiles, and output factor (OF) measurements.

PDDs are obtained for various field sizes to characterize beam quality and depth dose deposition along the central axis. A PDD curve is defined as the ratio, expressed as a percentage, of the absorbed dose at a given depth along the beam's central axis, D_d, to the absorbed dose at a reference depth, D_{max}:

$$\mathrm{PDD}(\%) = \frac{D_d}{D_{max}} \times 100\% \quad (2)$$

The PDD is influenced by factors such as the irradiated material, the field size, beam energy, and the source-to-surface distance (SSD). The region from the surface to the depth of D_{max}, where the dose progressively increases with depth, is known as the buildup region. This region is significantly larger for photons compared to electrons due to the longer range of energetic secondary charged particles produced by photon interactions. These particles travel through the medium, depositing their energy at a certain distance from their initial interaction point. Beyond the buildup region, the PDD increases with higher beam energy for both photons and electrons, as higher energy particles have greater penetrating power. PDDs for energies 6, 10 and 15 MV are presented in Figure 1.

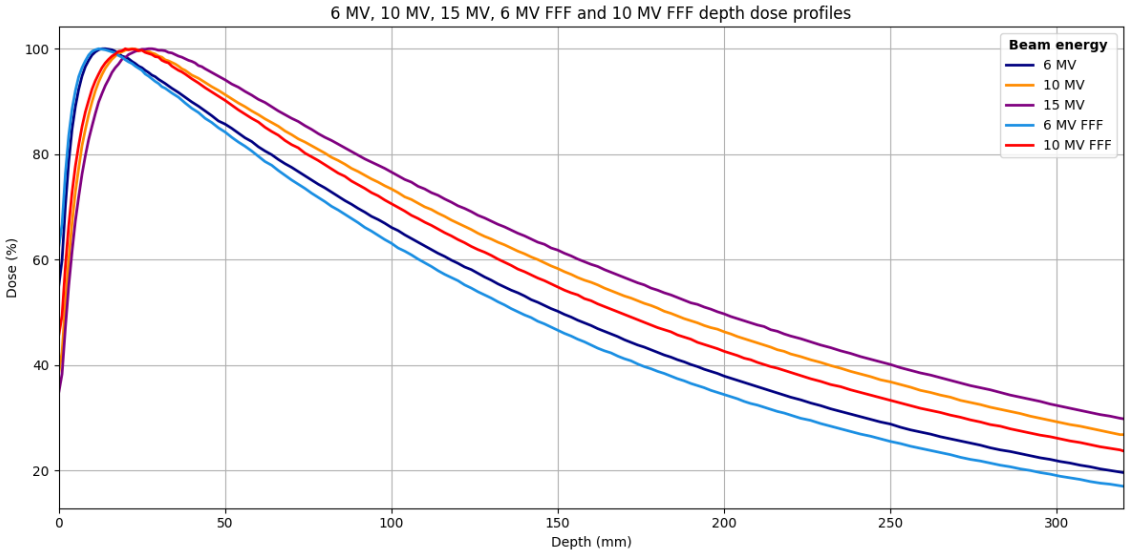


Figure 1: 6 MV, 10 MV, 15 MV, 6 MV FFF and 10 MV FFF PDDs for the TrueBeam LINAC (IPO-Porto), measured at a 10 cm × 10 cm field size, and 100 cm SSD.

The beam quality index Q for high-energy photon beams is given by the tissue phantom ratio (TPR) for a square field of 10 cm × 10 cm and SSD of 100 cm. The $\mathrm{TPR}_{20,10}$ is determined using the percentage of dose at depths 20 cm and 10 cm, PDD_{20} and PDD_{10}, respectively, for reference conditions:

$$\mathrm{TPR}_{20,10}(10) = 1{,}2661 \times \frac{\mathrm{PDD}_{20}}{\mathrm{PDD}_{10}} - 0{,}0595 \qquad (3)$$

For an accurate description of the energy deposited in the patient, essential for determining dose distributions in two or three dimensions, lateral profiles are also necessary for beam characterization. This off-axis data is obtained by measuring beam

profiles perpendicular to the beam's central axis at various depths in a water phantom. The measured dose distribution depends on collimation, which affects the beam edges, and the presence of the flattening filter, which controls the beam centre dose. Consequently, there is a dose variation from the beam axis to the off-axis region due to the influence of different structures within the linear accelerator. The profile is expressed as a percentage, of the dose at a point away from the beam central axis at a given depth, $D_{x,y}$, to the dose at the point on the central axis of the beam at the same depth, D_{x_0,y_0}, thus:

$$\text{Profile}(\%) = \frac{D_{x,y}}{D_{x_0,y_0}} \times 100 \quad (4)$$

The curve that illustrates the profile as function of the distance from the central axis is called the transverse beam profile, and it can be seen in Figure 2.

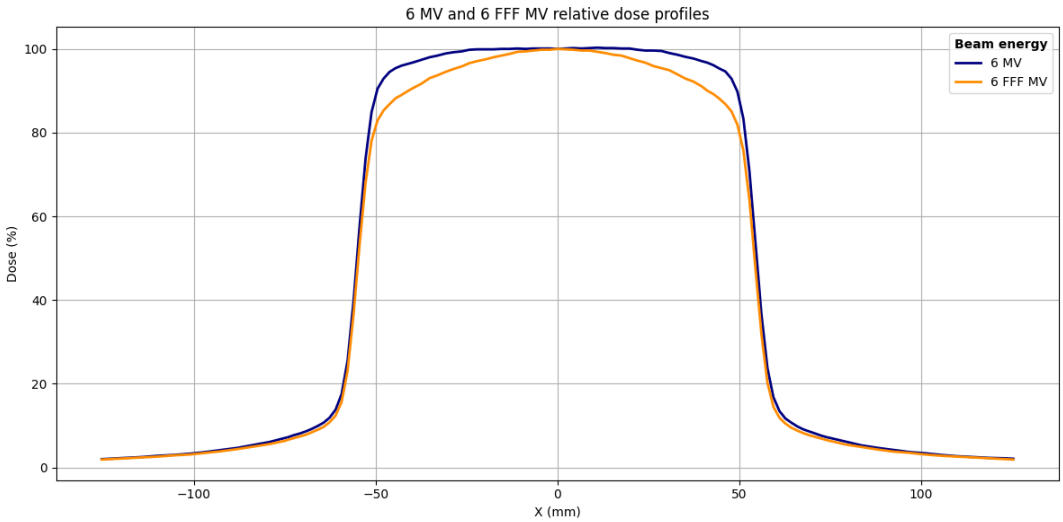


Figure 2: 6 MV and 6 FFF MV profiles for the TrueBeam LINAC (IPO-Porto), measured at a 10 cm × 10 cm field size, 100 cm SSD and 10 cm depth.

The transverse beam profile is usually divided in three zones:

1. Central Dose Region: This region encompasses the central part of the profile, extending from the central axis to about 1.0 cm to 1.5 cm from the geometric field edges. It contains 80% to 100% of the dose at the beam's central axis.
2. Penumbra Region: Located near the geometric field edges, this zone experiences rapid dose changes. It is influenced by the field-defining collimators, the size of the radiation source, and lateral electronic disequilibrium. The

penumbra can be defined as the distance between the 20% and 80% dose levels at the field edge once the profile is normalized.

3. Umbra Region: This is the area outside the radiation field, away from the field edges, where the dose is residual. It characterizes the radiation transmitted through the collimator and head shielding and contains less than 20% of the dose at the beam's central axis.

In broad beams, the full width at half maximum (FWHM) of the lateral profiles, which indicates the irradiation field size at the 50% relative dose level, matches the collimator setting and aligns with the geometrical field size. Therefore, the collimator setting accurately corresponds to the FWHM of the lateral beam profile at the isocentre depth, making FWHM measurement a common method for verifying the field size setting. However, in small fields, due to partial occlusion of the finite primary photon source and loss of lateral charged particle equilibrium (LCPE), resulting in a significant reduction of beam output, this alignment no longer holds true, as detailed in Section 1.3.1.

The characteristics of the transverse beam profiles can be quantified through parameters that evaluate its uniformity, namely symmetry and flatness. Symmetry, S, is the maximum ratio of the dose at two points symmetric with respect to the central axis of the beam, $D_{x,y}$ and $D_{-x,-y}$, is used to calculate symmetry, thus:

$$S(\%) = \frac{D_{x,y}}{D_{-x,-y}} \times 100 \quad (5)$$

Symmetry can also be determined by the calculation of the areas below the transverse beam profile ranging from the central axis to the point where the dose is 50% of the central axis dose, to the left, A_{left}, and to the right, A_{right}, of the beam central axis:

$$S(\%) = \frac{A_{left} - A_{right}}{A_{left} + A_{right}} \times 100 \quad (6)$$

Beam flatness, F, is characterized by the maximum D_{max} and minimum D_{min} dose point values on the beam profile within the central 80% of the beam width:

$$F(\%) = \frac{D_{max} - D_{max}}{D_{max} + D_{max}} \times 100 \quad (7)$$

For flattening filter free (FFF) beams, the flatness parameter is not applicable. The purpose of using a flattening filter is to convert the forward-peaked MeV bremsstrahlung photon intensity into a uniform intensity pattern, creating a clinically acceptable beam profile. However, advanced radiotherapy techniques now modulate the

intensity pattern of the flattened photon beam, indicating that initial beam flattening is not necessary for these treatments. Recent modified versions of LINAC designs incorporate the options of generating also unflattened photon beam for clinical use, by removing the flattening filter. This removal significantly increases the dose rate, softens the x-ray spectra, and reduces scattered radiation.

The peak shape of the FFF profile can be assessed by the “slope” parameter, which describes the left and right inclinations of the curves. This parameter can be calculated as the slope of the line passing through two fixed points on the profiles located at 1/3 and 2/3 of the half beam (defined by the field size), according to:

$$\text{Slope} = \frac{(x1 - x2) \times (y1 - y2)}{(x1 - x2)2} \quad (8)$$

Where $x1, y1$ are the coordinates (as dose value y at position x) on the half-profile for the first point and $x2, y2$ are the coordinates of the second point.

The output factor (OF) will be discussed in Section 1.3.2.

1.2.2. Formalism for absorbed dose determination

The procedure for determining the absorbed dose in water was implemented following the guidelines of the International Atomic Energy Agency (IAEA), as outlined in TRS-398 [8]. TRS-398 is an IAEA publication titled "Absorbed Dose Determination in External Beam Radiotherapy: An International Code of Practice for Dosimetry Based on Standards of Absorbed Dose to Water." This publication was originally released in 2000, but a revision was recently published in February 2024. This code of practice establishes standards and recommendations for dosimetry of external beams from radiotherapy machines and provides a detailed methodology for the calibration of radiation beams, the use of ionization chambers, and other dosimetry instruments. Additionally, TRS-398 addresses procedures for determining absorbed dose in water for low, medium, and high-energy photon beams, electron beams, proton beams, and heavy ion beams used in external radiotherapy. In this chapter, the formalism for the determination of absorbed dose to water using photon beams will be discussed. TRS-398 is an important reference in the field of medical dosimetry and is internationally used to ensure consistency and accuracy in absorbed dose measurements during radiotherapy treatments. Experimentally, the absorbed dose measurements can be performed in a water tank or solid water phantoms. While using solid water phantoms, a correction factor must be applied to account for differences in material density. Absorbed dose to water should be

determined in reference conditions, which correspond to a SSD of 100 cm, a depth of 10 cm and a field size of 10 cm × 10 cm, as shown in Figure 3.

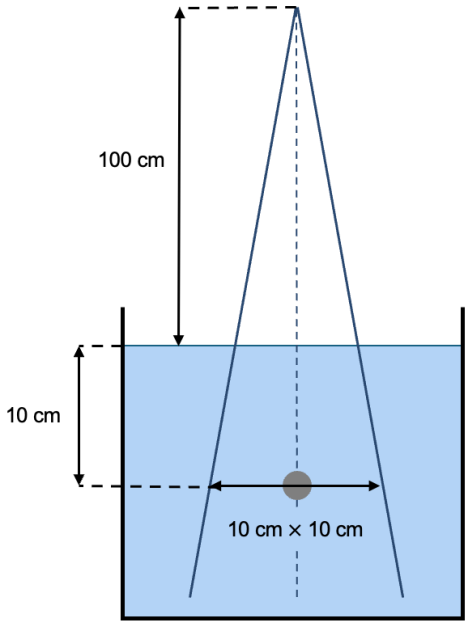


Figure 3: Scheme of the setup that should be used to determine dose absorbed to water, recommended by the TRS-398 [8].

The absorbed dose in water, D_{w,Q_0}, at the reference depth, z_{ref}, for a reference beam of quality Q_0, in the absence of the ionization chamber, is given by:

$$D_{w,Q_0} = M_{Q_0} N_{D,w,Q_0} \tag{9}$$

M_{Q_0} is the chamber reading under reference conditions used in the standards laboratory and N_{D,w,Q_0} is the calibration factor for the dose absorbed to water obtained from the standards laboratory. $N_{D,w}$ is the combined calibration factor for the ionization chamber and the electrometer. However, when the ionization chamber and the electrometer are calibrated separately, the calibration laboratory provides a calibration factor for each. In this case, the calibration factor $N_{D,w}$ is given only for the ionization chamber and k_{elec} is the electrometer calibration factor, which is included in the calculation of the correction factors.

The influence quantities are defined as factors that are not directly related to measurement but affect it. These quantities can be of different natures, related to the environment, such as pressure, temperature, humidity or voltage, the dosimeter, or the radiation field, like beam quality, dose rate, field size or depth in the phantom. When

working with a radiation detector, influence quantities must be measured. When performing measurements under non-reference conditions, all influence quantities must be measured, and a correction must be applied to the dose calculation, since the measurement conditions in a medical facility setting do not match the reference conditions used in standards laboratories. Correction factors are crucial to ensure the accuracy of absorbed dose measurements in different situations.

The measurements performed with ionization chambers require the application of an air pressure correction, since the mass of air in the chamber volume depends on the ambient temperature and pressure [8], [44]. During the calibration, the chamber is under reference conditions and, typically, the temperature, T_0, is 20ºC and the pressure, P_0, is 101,325 kPa, but these values should always be checked in the chamber calibration certificate.

$$k_{TP} = \frac{(273{,}25 + T)}{(273{,}25 + T_0)} \frac{P_0}{P} \tag{10}$$

P and T are the pressure and temperature values of the cavity at the time of measurements, which is approximately the same as the phantom temperature.

Water vapor in the air has a relatively small effect on the measurements, although, in certain situations, a humidity correction factor is needed. It is not necessary to apply a relative humidity correction if the calibration was done at 50% relative humidity and the camera is used with relative humidity between 20% and 80%. However, when performing measurements in dry air (relative humidity below 20%), a humidity correction factor, k_h, must be equal to 0,997. Humid air, on the other hand, can affect the chamber's stability since it alters the density of the gas in the chamber cavity. For that reason, it is not recommended to measure dose with humidity above 80% [45].

The effect of polarization potential of opposite polarity on the camera reading must always be considered.

$$k_{pol} = \frac{|M_+| + |M_-|}{2M} \tag{11}$$

M_+ and M_- are the electrometer readings obtained with positive and negative polarity, respectively, and M is the normally used polarity, either positive or negative.

In the chamber's cavity two effects occur: the recombination of ions formed by bands of separate ionizing particles, called general or volume recombination, which depends on the density of the ionizing particles and, therefore, on the dose rate; the

recombination of ions formed by a single band of ionizing particles, referred to as initial recombination, which is independent of dose rate. Both effects depend on the camera geometry and the applied bias voltage and imply the use of a correction factor. The code of practice recommends that it be calculated using the two-voltage method:

$$k_s = a_0 + a_1\left(\frac{M_1}{M_2}\right) + a_2\left(\frac{M_1}{M_2}\right)^2 \quad (12)$$

a_0, a_1 and a_2 depend on the voltage ratio V_1/V_2 and on the type of radiation beam (pulsed or pulse scanned).

Ionization chambers are calibrated with a reference radiation beam, typically Co-60, which differs in quality from the LINAC beams. The beam correction factor, denoted as k_{Q,Q_0}, quantifies the dosimetric correction required to standardize the response of ionization chambers in different radiation beams. Q is the quality of the beam used and Q_0 is the quality of the calibration beam.

The k_{Q,Q_0} values generally used are those provided by the IAEA TRS-398. This protocol includes tables of the determined factor as a function of beam quality and ionization chamber type. For beam quality values not listed in the tables, the correction factor is obtained through linear interpolation.

The revised version of TRS-398 [8] gives updated k_Q values along with the respective equation to obtain them, eliminating the need to use a linear interpolation. The new set of values was obtained by Monte Carlo calculations and by a robust data set of measurements at standards laboratories. For high-energy photon beams and a chamber calibrated with a Co-60 beam, k_Q can be obtained using the beam quality $\mathrm{TPR}_{20,10}$:

$$k_Q\left(\mathrm{TPR}_{20,10}\right) = \frac{1+\exp\left(\frac{a-0{,}57}{b}\right)}{1+\exp\left(\frac{a-\mathrm{TPR}_{20,10}}{b}\right)} \quad (13)$$

a and b are constants specific to each ionization chamber and they are presented in the Appendix II of TRS-398 [8].

The dose is obtained by multiplying the uncorrected reading by all the correction factors. For with FF (WFF) photon beams, the dose is given by:

$$D_{w,Q_0} = M_{Q_0} N_{D,w,Q_0} k_Q k_{TP} k_h k_{pol} k_s \quad (14)$$

Since the transverse profile of an FFF beam is non-flat, the sensitive area of a chamber is unevenly irradiated during exposure. The chamber's reading is averaged across its volume, resulting in an underestimation of the dose reading. The revision of TRS-398 [8] suggests a new correction factor to account for this effect. The volume averaging correction factor is applied only to FFF beams and considers the length of the ionization chamber, L:

$$k_{vol} = 1 + \left(0{,}0062 \times \mathrm{TPR}_{20,10} - 0{,}0036\right)\left(\frac{100}{SDD}\right)^2 \times L^2 \quad (15)$$

For FFF beams the dose is, then, given by:

$$D_{w,Q_0} = M_{Q_0} N_{D,w,Q_0} k_Q k_{TP} k_h k_{pol} k_s k_{vol} \quad (16)$$

1.2.3. Equipment for absolute dose measurements

A dosimeter is a radiation detector that can measure a physical quantity that is a measure of the absorbed dose, D, deposited in a volume by ionizing radiation [40]. The dosimeter along with its reader, which is typically an electrometer, is referred to as a dosimetry system [44].

Ionization chambers

Ionization chambers are the standard radiation detector for dosimetry [46], [47], because of their instant readout, dose rate independence, small energy dependence ease of use, high signal-to-noise, long term stability, and the extensive research supporting their use [44], [47], [48], [49], [50]. Ionization chambers can be used for both reference and relative dosimetry [51], and they are the recommended dosimeter for beam calibration [44], [47]. Dosimetric protocols for absolute dose determination, such as AAPM TG-51 [15] and IAEA TRS-398 [8], are based on ionometric measurements with an air-filled ionization chamber, with the application of adequate correction factors, in reference conditions. The types and models of chambers may vary depending on the beam being measured, such as low or high-energy photon beams, with flattening filter (WFF) or flattening filter free (FFF) photon beams [9], [47].

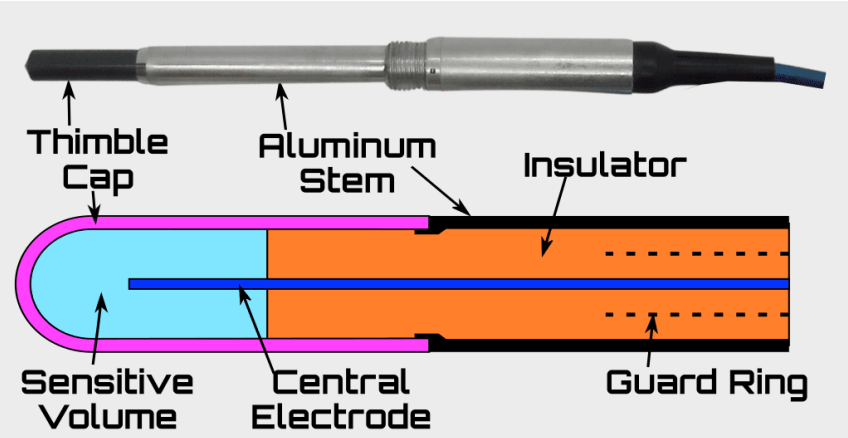


Figure 4: Scheme of a cylindrical ionization chamber (Adapted from [56]).

An ionization chamber is constituted by an air-filled cavity – sensitive zone, with a central collecting electrode, bounded by a conductive outer wall, as shown in Figure 4. The wall and the electrode are separated by an insulator to reduce leakage current [44], [51]. Upon irradiation of the air-filled cavity, both excited and ionized molecules are created. When a neutral molecule is ionized, it results in a positive ion and a free electron, known as an electron-ion pair. The electron-ion pair is, then, collected by the electrode. In the presence of an electric field, the drift of the charged particles establishes an electric current. If the cavity is undergoing steady-state irradiation, the rate of formation of ion pairs is constant, and if all the charges are efficiently collected, the current produced is an accurately measure of the rate at which electron-ion pairs are formed [42], [50], [51], [52]. The ionization chambers used in radiation dosimetry in RT can be cylindrical or plane-parallel [44]. Cylindrical chambers' active volume ranges from 0,1 to 1,0 cm^3, ensuring a balance between sensitivity and the capability to measure dose at a point [8]. Usually, they feature an internal length of less than 15 mm and an internal diameter of less than 7 mm. The wall material should ideally have a low atomic number Z and a thickness not exceeding 0,1 g/cm^2 [47]. The chamber construction should be as homogeneous as possible, although an aluminum central electrode with a diameter of approximately 1 mm is commonly used to ensure flat energy dependence [44]. Farmer-type ionization chambers are the primary choice for performing output measurements under reference conditions and in conventional fields, due to their well-defined geometry, which ensures reproducible measurements, and their linear response to radiation dose, providing accurate and reliable dose readings across a wide range of energies and modalities in clinical radiotherapy [53], [54], [55], [56].

As the name suggests, plane-parallel chambers consist of two parallel flat walls: one serves as the window as polarizing electrode, while the other serves as the back wall and collecting electrode, as well as a guard ring system. The back wall is typically made of a conducting plastic or a non-conducting material, like polystyrene, with a thin conducting layer of graphite that forms the collecting electrode [44]. The diameter of the collecting electrode should be smaller than 20 mm to attenuate the influence of non-uniformities in the beam profile, and the height of the cavity should be smaller than 2 mm [8]. These chambers are recommended for electron dosimetry with energies below 10 MeV because their design minimizes scattering perturbation effects. Electrons enter through the chamber's front window, making the contribution of electrons entering through the side walls negligible [8]. Plane-parallel chambers are also used for photon dosimetry, including surface dose and depth dose measurements in the buildup region [8], [44].

1.3. Small field dosimetry

Small-field dosimetry has been studied for more than 20 years, with the development of advanced radiotherapy techniques, that imply the use of relatively small fields, like IMRT, SRS, or SBRT [19], [49], [57], [58], [59].

IMRT is a type of therapy where the intensity of the radiation beams is modulated across the treatment area, and many small fields are superimposed to get the full dose [60], [61]. IMRT is commonly used to treat tumors in areas where preserving nearby critical structures is essential, such as the head and neck, prostate, and central nervous system [60]. The radiation beam is modulated by the multi-leaf collimator (MLC). The MLC consists of multiple individual leaves that can move independently of each other. These leaves are made of absorbing material and are controlled by a computer to create precise openings and blocks in the radiation beam [32], [44]. SRS is a technique used to treat small brain tumors and other brain abnormalities. Despite its name, SRS is not a surgical procedure but rather a form of highly focused radiation therapy, where numerous small radiation beams are precisely targeted at the tumor from different angles, converging at the tumor site to deliver a high dose of radiation while sparing surrounding healthy brain tissue. SRS is highly effective for controlling small, well-defined brain tumours or metastases, and the treatment is typically completed in a single session [60]. SBRT is a highly precise form of radiation therapy that delivers very high doses of radiation to small, well-defined tumors in a shorter treatment course compared to conventional radiation therapy [6], [60]. It is typically used to treat tumors in the body,

such as those in the lungs, liver, spine, and pancreas [6]. In the last couple of years, the number of SBRT machines has increased substantially, however the study of small field dosimetry has not followed this trend. It is necessary to carry out this type of studies to identify systematic dosimetric uncertainties [62].

The most widely used dosimetry protocols include the TRS-398 [8], published by the IAEA, and the TG-51 [15], by the American Association of Physicists in Medicine (AAPM). However, for small field dosimetry, there's the need to use specialized protocols due to the unique dosimetry challenges posed by these fields, such as the IAEA TRS-483 [9], the AAPM TG-155 [63], or the ICRU-91 [60]. These protocols provide guidelines and procedures tailored specifically for accurate dosimetry in small fields.

1.3.1. Small field characterization

Small fields are typically defined between 0,3 cm × 0,3 cm and 4 cm × 4 cm. Such small fields require special attention in both dose calculation and measurements, as well as in dosimeter selection [49], [63].

Small fields are created through downstream collimation of either flattened or non-flattened photon beams. Different collimation methods are used, such as jaws, MLCs and, in some cases, cones or adjustable tertiary collimators [8]. A small field is characterized by meeting at least one of the following conditions:

1. Loss of lateral charged-particle equilibrium (LCPE) on the beam axis;
2. Partial source occlusion by the collimating devices;
3. The size of the detector is similar or larger than the radiation field.

The first two conditions are beam related, while the third one is detector related. All these conditions lead to an overlap between the field penumbrae and the detector volume [8].

Loss of lateral charged-particle equilibrium (LCPE) on the beam axis

Charged particle equilibrium (CPE) is achieved within a volume when each charged particle exiting the sensitive volume (chamber's cavity) is replaced by an identical particle entering the volume, resulting in absorbed dose equaling collision kerma [42], [49], [64]. In small field conditions where the field dimensions are smaller than the lateral range of secondary electrons contributing to absorbed dose, loss of lateral charged-particle equilibrium (LCPE) may occur on the central axis [8], [60], [65].

In small fields, there is no LCPE within the radiation detector region, in penumbra regions, and narrow fields [49], [63]. This effect is illustrated in Figure 5.

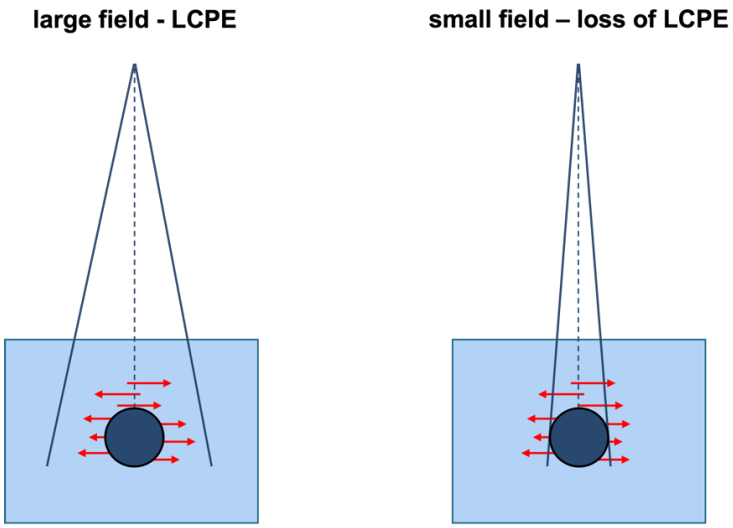


Figure 5: In a large field, there's LCPE; in a small field, the number of charged particles exiting the chamber's cavity is not compensated by the number of charged particles entering the cavity – loss of LCPE (Adapted from [64]).

One can define a parameter called lateral charge particle equilibrium range (r_{LCPE}), which represents the range of laterally scattered electrons and determines the smallest field size where absorbed dose and collision kerma are proportional [51], [65]. r_{LCPE}, can be determined based on photon beam quality index, $\mathrm{TPR}_{20,10}$, for the reference field size of 10 cm × 10 cm:

$$r_{LCPE}\,(\mathrm{cm}) = 8{,}369\ \times \mathrm{TPR}_{20,10}(10) - 4{,}382 \qquad (17)$$

If the radiation field extends at least a distance r_{LCPE} around the outer boundaries of the ionization chamber, there's LCPE [64]. This effect is particularly notable for higher energy photons, since the generated charged particles will have longer ranges [51], [66], and it can be further intensified in regions with tissue heterogeneity, such as between lung and bone [49], [66].

Partial Source Occlusion by the collimating devices

As the collimation aperture is reduced to define a small field, there is a point at which the radiation field size is comparable to the photon source size as seen from the detector [49], [51]. Further reduction of the field size results in partial occlusion of the photon source [51]. As a result, the beam output is reduced compared with that in bigger

field sizes, where the detector can see the full source [49], [60]. A schematic illustration of partial source occlusion is shown in Figure 6.

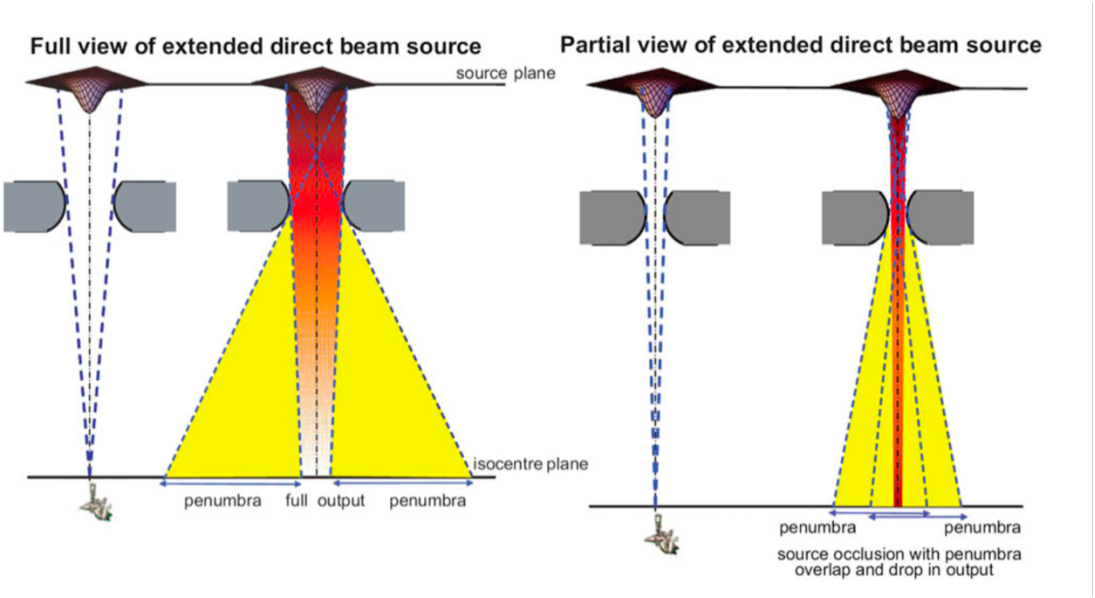


Figure 6: Schematic illustration of source occlusion (Adapted from IPEM report 103 [67]).

Additionally, the penumbras of the opposed collimation jaws overlap, affecting the dose profiles [51]. In this condition, the field size shouldn't be defined by conventional methods, such as full width at half maximum (FWHM), because the field size specified by FWHM is larger than the actual field size [49], as seen in Figure 7. The extent of this widening depends on the lateral electron ranges [67].

Partial source occlusion affects the response of detectors in small fields, since it disturbs the energy and angular fluence distribution. Both the loss of LCPE and the partial source occlusion effect are responsible for a decrease in the output factors when reducing the field size. The beam output drop becomes more significant when the photon beam energy increases or the density of the medium decreases, since, in both instances, the electron ranges increase [9], [49].

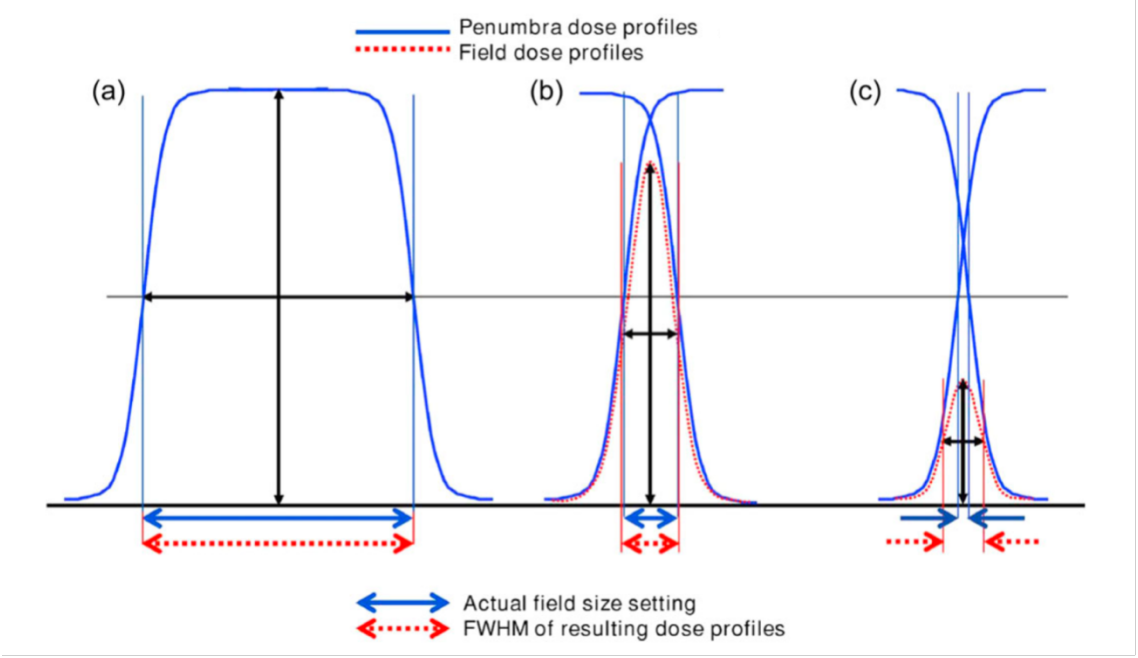


Figure 7: Apparent profile widening associated with small fields (Adapted from [49]).

The size of the detector is similar or larger than the radiation field

The third aspect that characterizes a small field is the detector size relative to the radiation field size. When the dosimeter is large in comparison with the radiation field size, occurs volume averaging [49]. In high gradient dose regions, the dose value has a great change over the dosimeters' active volume. The detector reading is averaged throughout the active volume and, since only a part of the active volume is exposed to radiation, the measured dose is lower than the actual dose [67].

Additionally, most used detectors are relatively large relative to the size of the radiation field [9]. TRS-483 [9] recommends the use of a smaller detector with high resolution, to avoid volume averaging in small fields [49]. LCPE exists in regions that are at least a distance r_{LCPE} beyond the outer boundaries of the ionization chamber [51], [64], as shown in Figure 8.

$$FWHM \geq 2r_{LCPE} + d \tag{18}$$

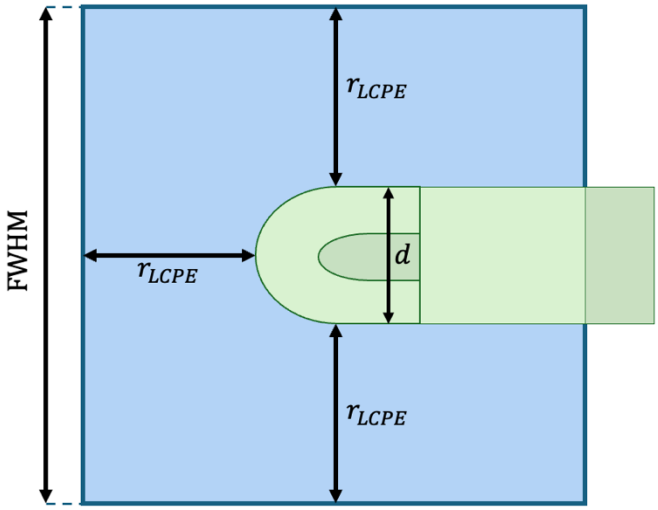


Figure 8: Lateral charged particle equilibrium (LCPE) range (Adapted from [64]).

1.3.2. Formalism for small field dosimetry

For machines where the conventional 10 cm × 10 cm reference field cannot be established at a SSD of 100 cm, such as CyberKnife, GammaKnife or TomoTherapy, TRS-483 [9] defines a machine specific reference, denoted as f_{msr}. This reference field should have dimensions as close as possible to the conventional reference field [9], [48], [58], [63].

The formalism for small field dosimetry is described according to TRS-483 [9], that adopted the formalism proposed by Alfonso et al, in 2008 [48]. The formalism for reference dosimetry is based on an ionization chamber that has been calibrated in a standard laboratory. The TRS-483 protocol presents three different approaches that depend on the type of calibration and the availability of beam quality correction factors.

If the chamber was calibrated for the machine specific reference field, at a reference depth, z_{ref}, with a beam with quality Q_{msr}, the absorbed dose to water is given by:

$$D_{w,Q_{msr}}^{f_{msr}} = M_{Q_{msr}}^{f_{msr}} N_{D,w,Q_{msr}}^{f_{msr}} \tag{19}$$

$M_{Q_{msr}}^{f_{msr}}$ is the reading of the ionization chamber calibrated for the msr field and $N_{D,w,Q_{msr}}^{f_{msr}}$ is the calibration coefficient of the chamber obtained by the standard laboratory at the reference beam of quality Q_{msr} and field size f_{msr}.

If the chamber was calibrated using a beam of quality Q_0 and in a conventional reference field size f_{ref}, and given that a beam quality correction factor is available to correct for the use of the calibration coefficient in the f_{msr} field:

$$D_{w,Q_{msr}}^{f_{msr}} = M_{Q_{msr}}^{f_{msr}} N_{D,w,Q_0}^{f_{ref}} k_{Q_{msr},Q_0}^{f_{msr},f_{ref}} \tag{20}$$

The correction factor $k_{Q_{msr},Q_0}^{f_{msr},f_{ref}}$ accounts for the change of field size, shape, and beam quality from the reference conditions. It is defined as the ratio of the ionization chamber's calibration coefficients in the machine specific field and in the conventional reference field.

If the chamber was calibrated for a beam quality Q_0 and a conventional reference field size f_{ref}, but the correction factor is not available:

$$D_{w,Q_{msr}}^{f_{msr}} = M_{Q_{msr}}^{f_{msr}} N_{D,w,Q_0}^{f_{ref}} k_{Q,Q_0}^{f_{ref}} k_{Q_{msr},Q}^{f_{msr},f_{ref}} \tag{21}$$

The correction factor $k_{Q,Q_0}^{f_{ref}}$ accounts for the difference in the chamber's response between beam quality Q and Q_0.

For FFF beams, the formalism is the same except for the values of the correction factor $k_{Q,Q_0}^{f_{ref}}$. Since the ionization chamber responds differently to FFF beam quality Q^{FFF} and with flattening filter (WFF) beam quality Q^{WFF}, $k_{Q,Q_0}^{f_{ref}}$ is replaced with the product of two factors:

$$D_{w,Q_{msr}}^{f_{msr}} = M_{Q_{msr}^{FFF}}^{f_{msr}} N_{D,w,Q_0}^{f_{ref}} k_{Q^{WFF},Q_0}^{f_{ref}} k_{Q^{FFF},Q^{WFF}}^{f_{ref}} k_{Q_{msr}^{FFF},Q^{FFF}}^{f_{msr},f_{ref}} \tag{22}$$

Relative dosimetry refers to the determination of the ratio of absorbed doses under either reference or non-reference conditions. Output factors (OF) and dose profiles are some of the most important relative dosimetry measurements [63].

Field output factors can also be called field factors or scatter factors [15], [51]. The dose absorbed in a non-reference field, also known as the clinical field f_{clin}, differs from the dose absorbed in a machine specific reference field f_{msr}. The field output factor, denoted as $\Omega_{Q_{clin}Q_{msr}}^{f_{clin}f_{msr}}$, is defined as the ratio of these two doses [48], [60]:

$$\Omega_{Q_{clin},Q_{msr}}^{f_{clin},f_{msr}} = \frac{D_{w,Q_{clin}}^{f_{clin}}}{D_{w,Q_{msr}}^{f_{msr}}} \tag{23}$$

Q_{msr} and Q_{clin} are the beam quality in the reference field and in the clinical field, respectively.

The introduction of the detector specific field output correction factor $k_{Q_{clin},Q_{msr}}^{f_{clin},f_{msr}}$ accounts for the differences between the detector's response in a clinical field and in a reference field [9], [68]. This correction factor is specific to each detector, since this correction is needed to account for material perturbations and volume averaging effects [51], [58]. $k_{Q_{clin},Q_{msr}}^{f_{clin},f_{msr}}$ varies depending on the linear accelerator and detector configuration [69]. The equation for field output factors can be written as:

$$\Omega_{Q_{clin},Q_{msr}}^{f_{clin},f_{msr}} = \frac{M_{w,Q_{clin}}^{f_{clin}}}{M_{w,Q_{msr}}^{f_{msr}}} k_{Q_{clin},Q_{msr}}^{f_{clin},f_{msr}} \quad (24)$$

The readings $M_{w,Q_{clin}}^{f_{clin}}$ and $M_{w,Q_{msr}}^{f_{msr}}$ are obtained from detector measurement in the clinical field and in the msr field [60].

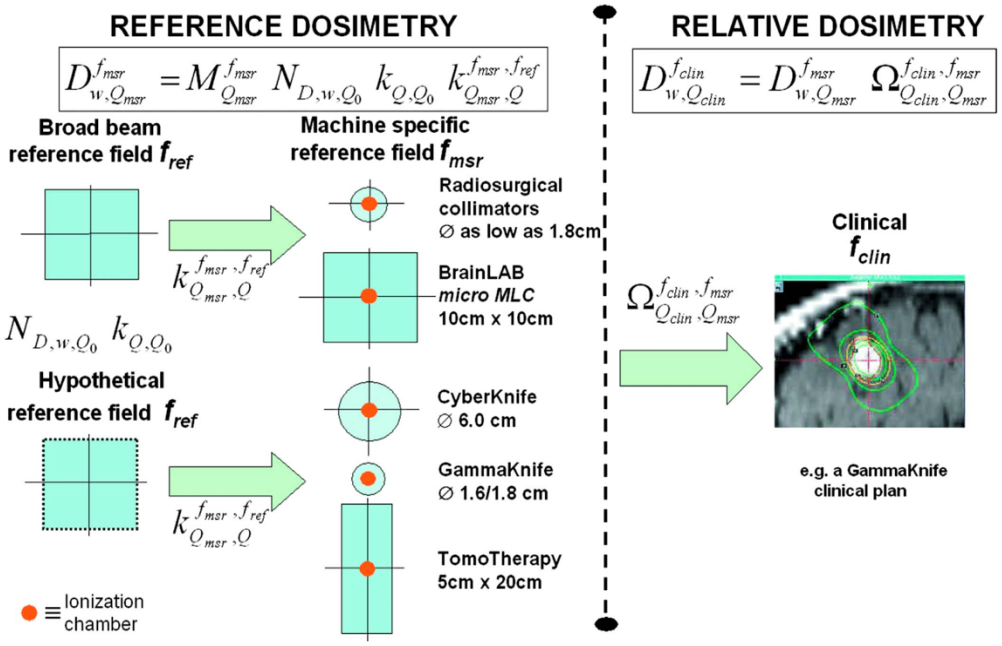


Figure 9 summarizes the dosimetry of small fields.

Figure 9: Overview of the dosimetry of small static fields with reference to a machine specific reference field, according to the formalism of TRS-483 [9], [48] (Reproduced from Alfonso et al. [48]).

Accurate detector positioning in the centre of the field is far more important in small fields dosimetry, as the dose distribution does not reach a uniform and flat level in the centre of the field. The detector should be aligned to the field centre according to its central axis (CAX) value [59]. Therefore, before performing OF measurements, the

physicist should measure dose profiles at the chosen depth for each field size [70]. The lateral beam profile is the absorbed dose distribution at the reference depth, perpendicular to the beam axis and parallel to the phantom surface [9].

Differently to what happens in conventional fields, in small fields the nominal field size indicated by the collimation system will not coincide with the FWHM of a dose profile, measured at 10 cm depth, normalized to the central axis, occurring an apparent widening of the field. The partial occlusion also reduces the relative central-axis dose, which decreases the machine output. Then, output factors must be reported according to the equivalent square small field size, and not the nominal field size [9], [20], [71].

For rectangular small fields with uneven in-plane and cross-plane FWHMs, the equivalent square small field size, S_{clin}, is determined by the geometric mean where A and B correspond to the in-plane and cross-plane dosimetric field widths, respectively, defined as the FWHM of the dose profiles at the measurement depth [9]:

$$S_{clin} = \sqrt{AB} \tag{25}$$

For circular small fields with a FWHM radius r [9]:

$$S_{clin} = r\sqrt{\pi} = 1{,}77r \tag{26}$$

Small-field output factors are especially sensitive to the source size, due the photon beam penumbra overlap [19], [72].

1.3.3. Equipment for small field dosimetry

An ideal detector for small field dosimetry must offer high spatial resolution, high stability, a high signal-to-noise ratio, low energy dependence, low directional and dose rate dependency, and high-water equivalence [49], [59], [69]. Since no single detector currently meets all these criteria simultaneously, it is recommended to use multiple detectors to obtain redundant measurements more accurate and reliable measurements [49]. The IAEA TRS-483 [9] provides a comprehensive analysis of the choice of detectors for small field dosimetry measurements.

To choose a suitable detector, it is first necessary to determine the basic requirements, keeping in mind the minimum and maximum field sizes, and the quantity that is going to measured, and then find a compromise between all the requirements [49], [59]. A thorough understanding of the physics of small field dosimetry is essential, as is knowledge of the suitability of different detectors' specifications for the required data

measurements [9], [44], [72]. Several publications address this issue, including articles that provide comparative analyses of the performance of various detectors [49], [51], [72], [73].

Ionization chambers are the most common dosimeters used in radiation dosimetry; however, they are not suitable for measures in small radiation fields, due to effects as volume averaging and loss of electronic equilibrium, which require a region of uniform beam intensity surrounding the detector [48], [49], [51]. Although, there is no standard dosimeter for small field dosimetry [49], solid-state detectors, such as silicon diodes, diamonds, plastic scintillators, and MOSFETs, are commonly used in small field dosimetry [49], [69]. Solid-state detectors have a higher mass density compared to the air in ionization chambers, allowing for small detector volumes with high signal-to-noise ratios, that enable high spatial resolution while minimizing partial volume effects. Additionally, solid-state detectors overcome some limitations of small chambers, such as signal-to-noise ratio, polarity corrections, stem effects, and leakage, making them increasingly favoured over micro-ionization chambers [37], [49], [74]. However, certain perturbations intrinsic to the detector material and design may require significant corrections for the smallest field sizes [9]. These detectors have other disadvantages, for instance, diodes are dependent on dose rate, energy, and direction, diamond detectors are energy dependent, and MOSFETs may have angular dependency issues [49], [75], [76], [77].

Differences of the fluence inside some detectors can be due to the difference of the mass stopping power of the radiation sensitive volume of the detector relative to water and due to the constructional specificities of the detector, causing an over-estimation of the measured value [9], [78]. The decreasing of the field size has also an additional impact on the energy spectrum of the beam. Decreasing the field size will reduce the scattering originated in the LINAC components and in the phantom. The result is the elimination of the low energy photon and the hardening of the energy spectrum [79].

Small field measurements should be performed in a water phantom. The measurement is made at a depth and SSD defined by the user. It is recommended to perform the measurements at a depth of 5 cm or 10 cm to avoid electron contamination [51], [60].

To obtain field output factors, it can be used an ionization chamber down to the field size where the volume averaging effect sets in, and use a small detector, like a diode or a scintillator, for smaller fields. The field output factors derived from the

measurements with the small detectors are renormalized at the smallest field size where the ionization chamber is used. This type of procedure is an intermediate field method and has been known as the “daisy-chaining” [9]. If not using an intermediate field method, the most used detectors for output factor measurements are solid-state detectors, such as silicon diodes, diamond detectors and MOSFETs [9], [73], [80].

Solid-state detectors

Solid-state detectors encompass a wide range of devices, including thermoluminescent dosimeters (TLDs), optically stimulated luminescent dosimeter (OSLDs), scintillators, and semiconductors such as diodes and diamonds [74].

The process of radiation measurement with TLDs or OSLDs is essentially the same. TLDs and OSLDs are made of small polycrystals bound by a binder. Ionizing radiation generates free electrons that may recombine with holes or settle into traps capable of retaining electrons for extended periods of time. When the dosimeter is heated or backlighted, the trapped electrons are freed and release energy as light. The light output is measured, and it is a function of the ionizing radiation that interacted with the detector [81], [82], [83]. If the material is excited by heat, it undergoes thermoluminescence and is called a thermoluminescent dosimeter (TLD); if excited by light, it experiences optically stimulated luminescence and it is called an optically stimulated luminescent dosimeter (OSLD) [44], [83]. TLDs and OSLDs are widely used for *in vivo* dosimetry, to determine patient dose in radiology and in external beam RT [74], [82]. These detectors are advantageous due to their small volume, allowing point dose measurements, no associated voltage, high precision and accuracy, and their availability in different formats [44], [82], [84], [85]. They can be manufactured in various materials, and commonly are denser than water and have an atomic composition different than water and tissue [44], [81], [82], [83]. A TLD and a OSLD can be seen in Figure 10.

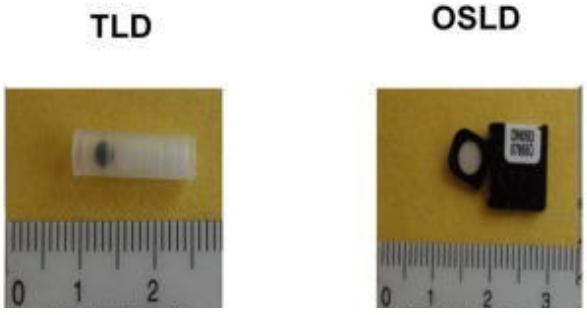


Figure 10: TLD and OSLD detectors (Adapted from [85]).

A semiconductor dosimeter is a radiation detector base on a semiconductor material, such as silicon or germanium. Diodes and diamond detectors are semiconductor-based detectors [74], [86]. These detectors can be used in diagnostic and therapy quality assurance to check x-ray systems and dose measurements, and they can also serve in *in vivo* patient dosimetry [74].

Diodes are often used for relative dosimetry and can be manufactured in small sizes while maintaining high sensitivity [44], [51]. Additionally, diode radiation detectors offer immediate response and high spatial resolution. On the flip side, semiconductor measurements are dependent on dose rate, energy, and temperature [49], [74], [86]. Diodes have an active volume of approximately 1 mm^3 and a diameter ranging from 0,5 to 1,2 mm [44], [87]. Four different models of diodes are shown in Figure 11.



Figure 11: Comparison of different diode dosimeters models (Adapted from [87]).

A diode dosimeter consists of a p-n junction formed by doping a semiconductor material to create a region with excess positive charges (p-type) and a region with excess negative charges (n-type) [44], [86]. The diode operates in reverse bias mode, so the p-type region is connected to the negative terminal and the n-type region is connected to the positive terminal of the power supply. When ionizing radiation strikes the diode, it results in the production of electron-hole pairs. Due to the reverse bias, the electron-hole pairs drift in opposite directions, and the pairs are separated. The movement generates a current that is proportional to the amount of radiation energy [50], [52], [86]. This process is schematized in Figure 12.

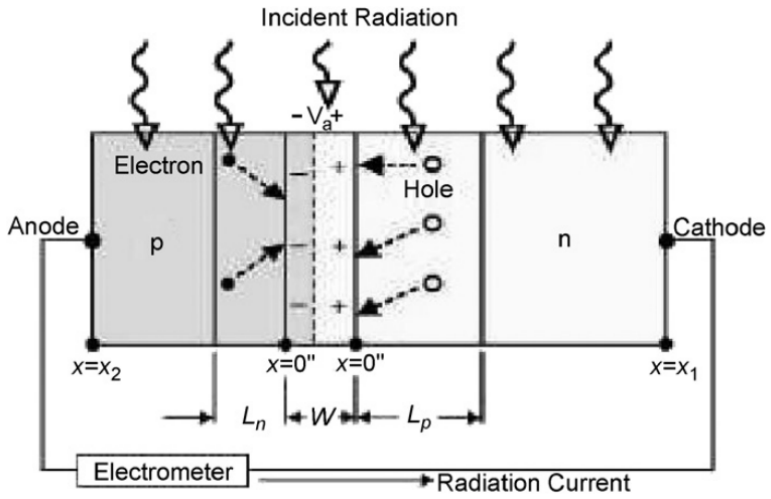


Figure 12: Schematic diagram of a diode detector (Adapted from [90]).

Diamond semiconductors are highly convenient detectors for relative dosimetry in small fields, as they can be manufactured in small dimensions and are water equivalent, due to similarity of carbon's atomic number to tissue [44], [49], [88], [89]. Typically, these detectors are made of natural diamonds, with a sensitive volume radius ranging from 1,0 to 2,2 mm, and a thickness varying between 0,2 mm and 0,4 mm [74]. These detectors have high sensitivity and resistance to radiation damage [44], [88]. Diamonds also offer high spatial resolution due to their small sensitive volume, typically in the order of a few cubic millimetres. Additionally, these detectors offer other advantages such as immediate readout, no requirement for external bias voltage, and their chemical inertness. Diamond detectors are also waterproof, enabling for measurements in a water phantom [44], [74], [82]. On the other hand, diamond detectors require pre-irradiation to stabilize detector response and address dose rate dependence [44], [90]. The long manufacturing time, high cost, and insufficiency of high-quality diamonds make their use in RT dosimetry challenging. However, there is a growing interest in studying synthetic alternatives. Synthetic diamonds are attractive due to their low cost, availability, and reproducibility [74], [89]. A scheme of a diamond dosimeter is shown in Figure 13.

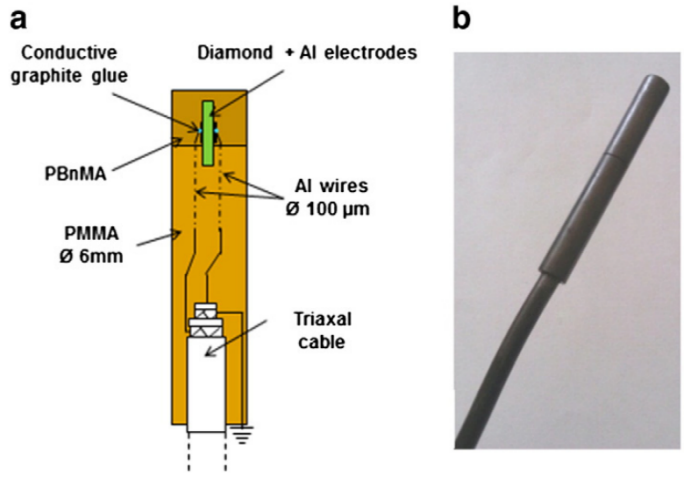


Figure 13: a. Scheme of a water-equivalent diamond detector. b. Photography of a diamond detector with a graphite cover. (Adapted from [76]).

A metal-oxide semiconductor field effect transistor, commonly called MOSFET, is a miniature silicon transistor. MOSFETs have high spatial resolution and are typically used for *in vivo* dosimetry, due to its small dimensions. These detectors can be used in the full range of energies of photon and electron beams; however, the energy response depends on the radiation quality [44], [91]. They offer other advantages, such as permanent dose storage, high reproducibility, immediate readouts of information, reusability. However, they are dependent from dose rate, beam incidence angle and temperature [49], [77], [91]. The ionizing radiation that crosses the detector generates charged particles that end up trapped, causing a changing in threshold voltage. The threshold voltage measured is a function of the absorbed dose [44]. MOSFETs require a bias voltage [44], [91]. Figure 14 presents a schematic diagram of a MOSFET detector.

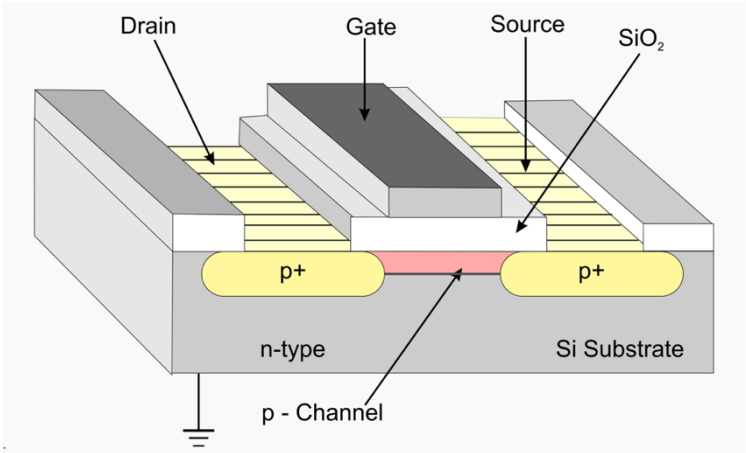


Figure 14: Scheme of a MOSFET detector design (Adapted from [56]).

Film detectors

Films can be employed in qualitative and quantitative dose measurements, such as verification of dose distributions of high dose gradient fields, and in quality control of radiotherapy machines, to verify parameters such as correspondence of light and radiation fields, determination of the position of a collimator axis, dose profile at depth in phantom [44], [92], [93]. Their main advantages are the water equivalence, the 2D spatial resolution, the minimal energy dependence and the fact they are very thin and don't perturb the beam propagation [44], [51]. These factors make film detectors suitable for both clinical and research dosimetry, including brachytherapy, electron therapy, skin dose measurements, total body irradiation, and phantom measurements [93], [94]. Dose is assessed by applying a calibration curve of a film detector, which relates the measured optical density (OD) values to known radiation dose values, allowing for the conversion of OD readings to actual dose measurements [92], [93]. The most widely used films in RT are the radiochromic films. The first radiochromic films adapted for radiotherapy applications were introduced to the market in 2004 by GAFCHROMIC. Since then, various models have been developed and their structure optimized [95].

In its most recent model, the active layer is composed of small needle-shaped crystals of lithium pentacosa-10,12-diynoate (LiPCDA). These crystals are aligned so the longest axis of the needles is arranged parallel to the shortest axis of the film. When the film is exposed to ionizing radiation, the deposition of energy in the active layer induces the formation of cross-linking between the LiPCDA monomers, leading to the formation of a polymer that is arranged parallel to the longest axis of the needles. With the formation of this polymer, changes appear in the electronic configuration, changing the absorption spectrum, which depends on the irradiated dose. The active layer also contains a yellow marker that minimizes sensitivity to ultraviolet radiation, and stabilizers and other additives, giving the film its near energy-independent response [95], [96]. A set of irradiated films and its respective calibration curve is shown in Figure 15.

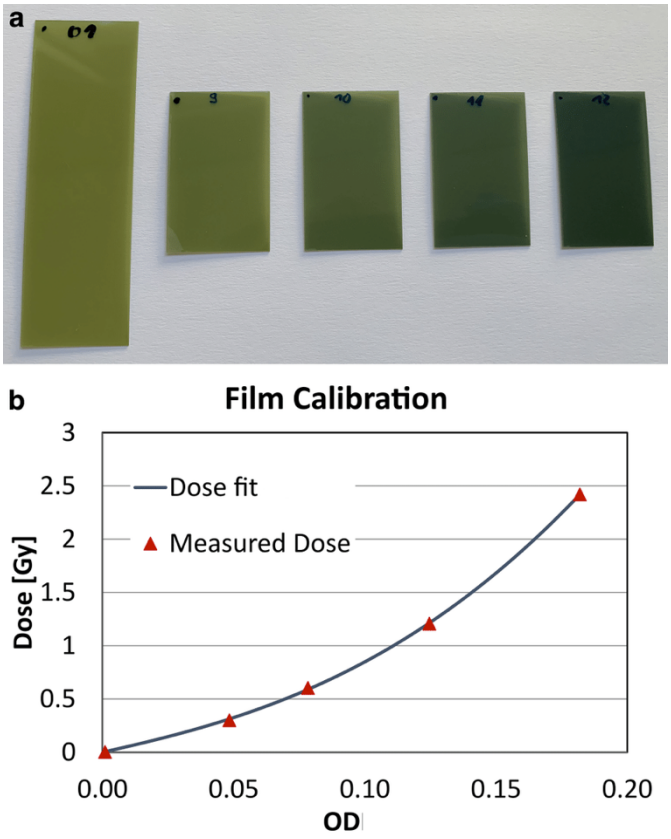


Figure 15: a. Irradiated films with different known doses. b Calibration curve of the film sheet (Adapted from [94]).

1.4. Uncertainties

Given that no measurement can be performed perfectly, every step in RT has an associated uncertainty [97]. This uncertainty should always be estimated, because it characterizes the dispersion of values for a measurement [97]. To enhance the accuracy of RT treatments, it is essential to minimize uncertainty throughout each stage of the process and account for uncertainties in all measured quantities during dose determination [30], [98].

The estimated or measured value of the dose, $D_{w,m}$, should always be reported with an associated uncertainty:

$$D_{w,true} = D_{w,m} \pm u \tag{27}$$

The "true" value, $D_{w,true}$, lies in the interval $\left[D_{w,m} - u,\ D_{w,m} + u\right]$ [99], as exemplified in Figure 16.

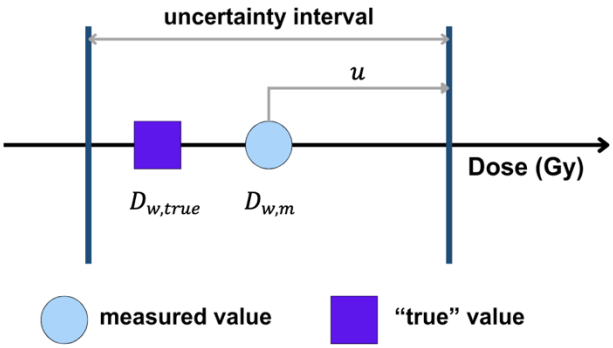


Figure 16: Exemplification of the uncertainty interval (Adapted from [97]).

In some cases, a measurand it's not measured directly, but it is determined from other quantities. In this case, it's necessary to estimate the combined uncertainty. The expression of the absorbed dose only contains products and quotients; therefore, the combined uncertainty will be the quadratic sum of the uncertainties of each component [100]:

$$u = +\sqrt{\sum_{i=1}^{N}\left(\frac{\partial g}{\partial x_i}\right)^2 \cdot u^2(x_i)} \tag{28}$$

$\left(\frac{\partial g}{\partial x_i}\right)^2$ is the sensitivity factor, which represents the weight that each component has in the final uncertainty.

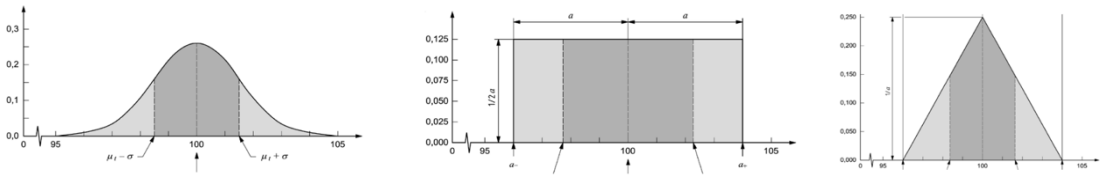
The components to the overall uncertainty can be categorized as type A or type B according to how the associated distribution is being evaluated. A type A uncertainty is a component which is evaluated by statistical analysis of repeated of observations; to evaluate these components, first we must determine the mean value from a series of observations:

$$\overline{x_i} = \frac{1}{N}\sum_{k=1}^{N} x_{i,k} \tag{29}$$

Then, determine the variance of the distribution, and, finally, determine the standard uncertainty of the mean:

$$s^2 = \frac{1}{N-1}\sum_{i=1}^{N}(x_i - \overline{x_i})^2 \tag{30}$$

A type B uncertainty applies to components that are evaluated by any other means; in this case the uncertainty cannot be evaluated by repeating the measurement, so the corresponding distribution must be evaluated as an a-priori distribution based on any other available information such as previous measurement, experience, general knowledge, or manufacturer's specification. An a-priori distribution can be a gaussian, rectangular or triangle, as illustrated in Figure 17.



(a) Gaussian distribution (b) Rectangular distribution (c) Triangle distribution

Figure 17: A-priori distributions (Adapted from JCGUM [100]).

The uncertainty budget is the compilation of all input uncertainties and associated sensitivity factors with subsequent evaluation [100]. Accordingly, to the IAEA, each user should have the responsibility to establish an uncertainty budget for their determination of absorbed dose to water [8].

IAEA codes of practice outline the uncertainties associated with each measurement. According to TRS-398 [8], the relative combined standard uncertainty of the absorbed dose to water, $D_{w,Q}$, for a high energy photon beam is approximately 1,0%. Within this, 0,6% accounts for uncertainties from the components related to the standards laboratory, such as the uncertainty of the user dosimeter's calibration, $N_{D,w}$, and the long-term stability of the standard. The remaining 0,8% is associated with the calibration of the user beam with regard to the uncertainties associated with the measurements, including long term stability of user dosimeter, establishment of reference conditions, dosimeter reading, M_Q, correction for influence quantities, k_i, and beam quality factor, k_Q.

2. Methods and Materials

2.1. Audit outline

The audit plan was divided in two major parts: an audit of absolute dose measurements of photon beams and an audit of small field output factors.

The absolute dose audit included the following steps:

1. **Pre-visit survey:** the medical physicists were asked to complete a survey on dosimetry practices in Radiotherapy. The surveys included questions about the equipment, dosimetry measurements, correction factors applied, dose determination.
2. **Development of a worksheet for dose determination:** considering the 2024 revision of TRS-398 [8], an updated worksheet for absorbed dose determination was developed.
3. **On-site measurements:**
    a. Pilot-centre audit: monitorization of the reference dosimetry verifications of IPO-Porto's linear accelerators. The verification of the reference dosimetry practices and dose determination at IPO can be considered an internal audit.
    b. On-site measurements: monitorization of the reference dosimetry verifications in different radiotherapy centres. This step was not carried out at this point due to project constraints
4. **Post-visit analysis:** Analysis of the survey's answers. Analysis of dose measurements performed, assessment of their deviation from the reference value, comparison between the results obtained with the two worksheets and estimation of associated uncertainties.

The small field output factors audit included the steps listed below:

1. **Pre-visit survey:** the medical physicists were asked to complete a survey on small fields dosimetry. The survey included questions about the equipment, dosimetry measurements, correction factors applied, and used setup.
2. **Remote audit:** 20 radiotherapy centres in Portugal were asked to submit their commissioning OFs, aiming to compare the data between centres.

3. **On-site measurements:**
    a. Pilot-centre audit: at IPO-Porto, measurement of small OFs with a water tank.
    b. On-site measurements: small field OF verification in different radiotherapy centres. This step was not carried out at this point due to project constraints.
4. **Post-visit analysis:** Analysis of the survey's answers. Analysis of the OFs measurements performed estimation of associated uncertainties. Review and comparison of OFs measured by participants.

The audit results are presented and analysed in a comprehensive report providing the specifics of the audit, results, conclusions and main recommendations. The audit report will be sent to the medical physicist responsible of the Radiotherapy Department.

2.2. Multicentre survey on dosimetry practices in Radiotherapy

A multicentre survey on dosimetry practices in radiotherapy was developed. The aim of the survey was to evaluate the measurement procedures used to determine absolute dose with photon beams, analyse the methodology used, identify any discrepancies among centres, and gather the necessary information to calculate the uncertainty associated with the process of verifying the absolute dose in water. The survey was designed to cover various aspects of absolute dose measurements in radiotherapy, from equipment characterization to measurement setup and practices. The survey's questions were organized in the following sections:

- Radiotherapy service details
- Equipment characterization
- Set-up
- Formalism for dose determination
- Measurements

This survey can be fully accessed in Attachment 1.

Radiotherapy Service Details

This section gathers basic contact information about the institution and the responsible physicist, facilitating follow-up if necessary.

Equipment Characterization

The aim of this section was to gather details about the equipment, which can influence measurement practices and help in understanding discrepancies. The details relating to the calibration certificates will also allow the calculation of the uncertainty associated with the absolute dose verification process. This section requests details about the used equipment in each RT facility, such as:

- linear accelerators, including manufacturer, model, and available photon energies.
- ionization chambers used for absolute dose measurement, including calibration details and uncertainties.
- electrometer details, including model, manufacturer, and calibration information.
- thermometer and barometer specifications, including model, manufacturer, and calibration information.

Set-up

This part of the survey requests for information related to the setup, such as reference setup details, distance measurement methodology and phantoms used.

Formalism for dose determination

This section pertains questions related to the calibration protocol and dose calculation worksheet used. It is also questioned if the updated correction factors are used as per the 2024 TRS-398 [8] revision. This section aims to ensure if the followed protocol is adequate, as well as the correction factors applied.

Measurements

Detailing the measurement process helps in understanding how centres ensure accurate dose measurements. In this part of the survey, there are questions about the actual measurement methodology, such as:

- the minimum number of charge measurements taken, and acceptance criteria.
- tolerance levels for dose deviation.
- application of uncertainty limits to dose calculation.

2.3. Worksheet for determination of absorbed dose to water

A worksheet for determining the absorbed dose in water was developed, considering the 2024 update of TRS-398 [8]. The absolute dose is calculated following the formalism presented in Chapter 1.2.3.

In this new worksheet, the dose is calculated using the updated values of the beam quality correction factor, k_Q, and applying the volume averaging correction factor, k_{vol}, when using FFF beams. Additionally, if the selected phantom is solid water, the respective correction factor is automatically added. It also indicates the relative deviation from the reference value of 1 cGy/MU and automatically calculates the ideal charge. The dose calculation worksheet can be fully consulted in Attachment 2.

2.4. On-site measurements at pilot-centre: absolute dose

For this audit stage, a checklist to verify the if the methodology was implemented following the TRS-398 [9] protocol recommendations. This checklist includes the steps that must be followed to determine absorbed dose to water, and the recommended value or tolerance for each of them. The aim is to verify each part of the process in order and following an objective methodology. This document can be fully consulted in Attachment 3.

This step of the audit included on-site absolute dose measurements. These verifications were performed at the pilot-centre, IPO. IPO-Porto is equipped with 8 linear accelerators (LINACs) manufactured by Varian (Varian Medical Systems, Palo Alto, USA) [101]. The LINAC models include Clinac (4), TrueBeam (1), Trilogy (2) and Novalis (1). During this step, 19 photon beams with nominal energies of 4 MV, 6 MV, 6 MV FFF, 6 MV SRS, 10 MV, 10 MV FFF, and 15 MV were analysed

Absorbed dose was determined following the IAEA Code of Practice TRS-398 [8]. For dose measurements, two setups were assembled: one with solid water slab phantoms and the other with a water tank phantom. The reference conditions were depth of 10 cm, SSD of 100 cm, and a field size of 10 cm × 10 cm.

The chamber used is a PTW 30013 Farmer (PTW, Freiburg, Germany) [102], which is the standard ionization chamber for absolute dose measurements in radiation therapy. This chamber has a sensitive volume of 0,6 cm^3, with a length of 23,0 mm and a radius of 3,05 mm [46], [61], [103]. The central electrode has a 1,1 mm diameter and is made of aluminium. The wall has an outside coating of 0,335 mm polymethyl methacrylate (PMMA) and an inside coating of 0,09 mm graphite [46], [103]. It has a nominal response of 10 nC/Gy and operates at a voltage ranging from 100 V to 400 V [61], [103]. The chamber is shown in Figure 18.



Figure 18: PTW 30013 Farmer chamber used in absorbed dose to water measurements.

2.4.1. Stability verification procedure

Before the measurements, the stability of the dosimetry system was performed. The dosimetry system comprises an ionization chamber, an electrometer, and their respective connecting cables. This verification is crucial to ensure accurate dose readings and it should be checked before each dose measurement.

The verification is performed using an encapsulated radioactive isotope. For this purpose, a radioactive check device type 48010 manufactured by PTW [102] is used, shown in Figure 19. This device is charged with a ^{90}Sr source of 20 MBq, which as has

a half-life of 28,7 years. The system includes a thermometer that indicates the temperature inside the capsule.



Figure 19: PTW Radioactive Check Device type T48010.

The electrometer must be connected for, at least, 24 hours to be stable. Before checking the chamber stability while exposed to the source, it is necessary to check for charge leakages by taking dose readings first with only the electrometer and then with the electrometer and the cable. Once these checks are completed, the PTW 30013 Farmer ionization chamber is inserted inside the capsule of the source using an applicator. It is important to align the reference of the chamber with the reference of the source. The chamber should be allowed to stabilize for at least 15 minutes before any measurements are taken. For the actual chamber stability process, the ionization chamber is connected to the connection cable, that is already connected to the electrometer. The measurement process is controlled using the Mephysto software. Five measurements are recorded for the following configurations: electrometer only,

electrometer and cable, and electrometer, cable, and ionization chamber with the chamber positioned on the source. The recorded readings must be corrected for air pressure and for the decay factor of ^{90}Sr.

The maximum deviation accepted at IPO is 1%.

2.4.2. Solid water slab phantom

The RW3 slab phantom used for this study is manufactured by PTW (PTW, Freiburg, Germany) [102]. The phantom was designed to be water equivalent and it is a composition of Polystyrol and TiO_2 [88], [104]. The RW3 solid phantom consists of one plate with a thickness of 1 mm, two plates of 2 mm, one plate of 5 mm, and 29 plates that are each 10 mm thick, allowing for depth dose measurements down to 10 cm in 1 mm increments [104], [105]. Since the density of the phantom is higher than that of water, a correction factor provided in the instruction manual of the slab phantom should be applied to determine the absorbed dose [105]. The reference point of the chamber is taken to be at the centre of the cavity volume. Therefore, to have the chamber's centre at 10 cm depth, 9,3 cm of solid water was placed on top of the solid water phantom with the chamber insert. The setup can be seen in Figure 20.

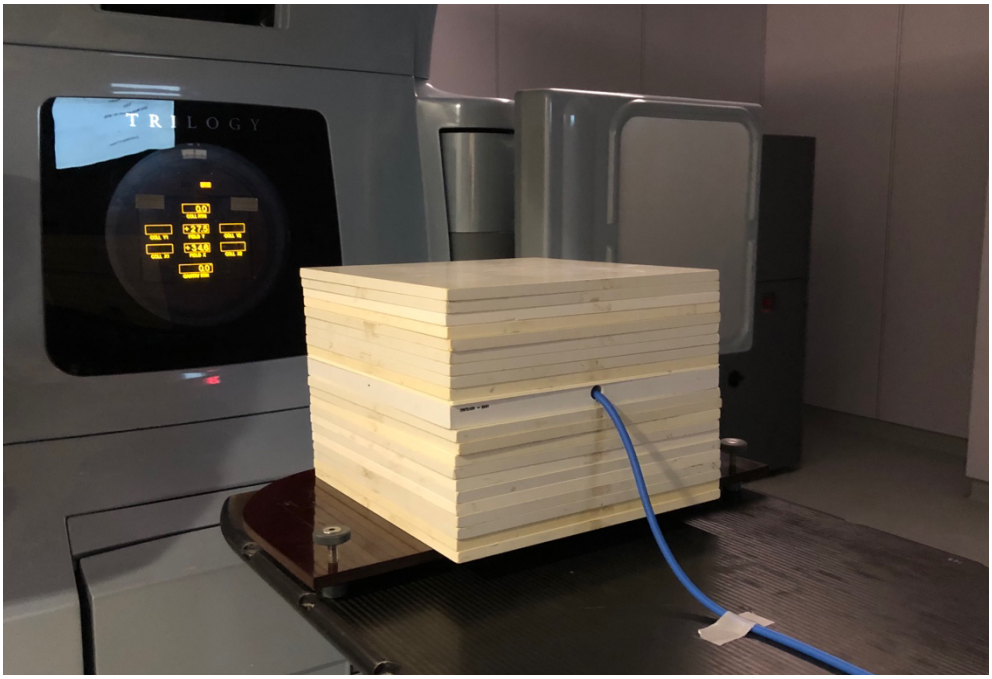


Figure 20: Setup for absorbed dose determination, assembled with RW3 slab phantom.

All the influence quantities, such as temperature and pressure, must be registered. Sometimes, the temperature inside the phantom insert may not be equal to the air temperature, so all the temperature readings were performed with a thermometer inside the phantom insert, the place where the ionization chamber was posteriorly placed.

Typically, this setup is used when time is limited and for periodic dose verification, as it assembles much faster than the water tank setup.

2.4.3. Water tank phantom

The water tank used is manufactured by PTW and it has acrylic walls with a thickness of 2 cm. The detector is attached to a movable arm, allowing the chamber to move in three dimensions. It has a scanning range of 60,0 cm × 50,0 cm × 40,8 cm [106].

For this setup, the reference point of the chamber is positioned at a depth of 10 cm using the TRUFIX system, on the central axis at the centre of the cavity volume. This setup can be seen in Figure 21.



Figure 21: Setup for absorbed dose determination, assembled with a water phantom.

The temperature registered was the water temperature, measured using an immersion thermometer.

In both setups, the chamber was connected to a PTW UNIDOS (PTW, Freiburg, Germany) [102] electrometer. Prior to measurements, the chamber undergoes irradiation for pre-heating. For each photon beam energy, the charge measurement was repeated at least three times.

The absorbed dose to water at the depth of dose maximum was calculated using both the worksheet provided by the IAEA, in 2004, and using the worksheet developed during this work.

2.5. Multicentre survey on dosimetry of small fields practices

Another survey was developed, this time focusing on the relative dosimetry practices for small fields with photon beams. The main goal was to assess the consistency of output factors for field sizes equal to or smaller than 3 cm × 3 cm and to understand the procedures used to measure them, in order to evaluate the correct implementation of the TRS-483 protocol recommendations. The survey covers various aspects of small field dosimetry, from equipment details to measurement methodologies, output correction factors determination, and verification and validation of the measurements. Each section is designed to gather comprehensive data to evaluate the consistency and accuracy of measurements across different centres. The collected data will help estimate the uncertainties associated with these measurements and to find inconsistencies in the methodology between centres. The survey was divided in 5 sections:

- Radiotherapy service details
- Equipment characterization
- Setup and methodology for small field output factors measurement
- Determination of field output factors
- Training and competency, verification and validation, and incident reporting

This survey can be fully accessed in Attachment 4.

Radiotherapy Service Details

Like the survey on absolute dose, this survey also contains a section on basic contact information. This section gathers basic contact information about the institution and the responsible physicist.

Equipment Characterization

The aim of this section was to gather details about the equipment. Understanding the equipment and detectors used is crucial for correlating the measurement techniques with the resulting data. Variations in equipment can lead to discrepancies in measurement outcomes. This section requests details about:

- linear accelerators, including manufacturer, model, and collimation system.
- detectors used, including their model, manufacturer, and the type of measure (OF, lateral profile or PDD).
- photon energies used for small fields.
- reference field size and small field sizes dimensions.

Setup and Methodology for Small Field Output Factors Measurement

This section details the methodology of the measurements, aiming to identify the potential sources of variability and ensure the process is consistent and repeatable. Information required includes:

- SSD and measurement depth.
- detector centring methodology.
- measurement methodology.
- minimum number of measurements and acceptance criteria.

Determination of Field Output Factors

Different methods and correction factors can significantly affect the accuracy of output factor measurements. This section aims to capture these differences to understand their impact on the results. The questions include:

- methodology for determining output factors.
- dependencies assessed for various detectors.

- methodology for determining the field output correction factors applied.
- field output factors reporting.
- associated uncertainties.

Training and Competency, Verification and Validation, and Incident Reporting

This section aims to evaluate the competency of the personnel, verify if regular verifications are done and capture how institution handle incidents.

2.6. Remote audit: small field OF

All 20 Radiotherapy facilities in Portugal were approached to submit their field output factors measured at the LINAC commissioning. The objective was to analyse the correct application of field output correction factors, the correct determination of small field OFs, compare these values and identify potential discrepancies between centres.

The information requested included:

- LINAC model
- Setup (SSD and depth of measurement)
- Beam energy and MUs prescribed for OF measurements
- Detector models used
- Nominal field size and FWHM of each non reference field measured
- Raw charge readings
- Calculated OF

To ensure accurate comparisons of field OFs, it is necessary that the LINAC, beam energy and the setup used are the same. The beam output is a function of the energy of the beam energy, so it is important to know the beam energy and only compare field output factors measured with the same energy.

Since different detectors have varying responses to radiation, it is important to account for potential differences in the measurements. It is also essential to request the nominal field size and FWHM, since FWHM is the recommended measure for reporting output factors. IAEA TRS-483 [9] recommends that any publication of small field data, such as field output factors, should include clear explanations of how the field size is defined. Detector response and perturbation are influenced by the FWHM at the

measurement depth, rather than by the collimator setting. For this reason, the field size should be specified by the FWHM of the lateral beam profile at the measurement depth. To facilitate establishing a relationship between FWHM and collimator setting, it is also advised that both the FWHM and the geometrical field size be recorded when reporting small field data.

The raw charge readings provide the data necessary for calculating output factors, and the calculated OF is the primary value being compared across different facilities. By comparing the two values, it is possible to verify if the OF were correctly determined and if the adequate correction factors were applied.

2.7. On-site measurements at pilot-centre: small field OF

For this audit stage, a checklist to verify the if the methodology was implemented following the TRS-483 [9] protocol recommendations. This checklist includes the steps that must be followed in order to determine small field OFs, and the recommended value or tolerance for each of them. The aim is to verify each part of the process in order and following an objective methodology. This document can be consulted in Attachment 5.

Field output factors were measured following the recommendations outlined in IAEA TRS-483 [9].

The measurements were performed in a water tank phantom, shown in Figure 22, with the detectors positioned at a depth of 5 cm and with SSD of 95 cm. At IPO, measurements were made on a Varian TrueBeam linear accelerator (Varian Medical Systems, Palo Alto, CA, USA) [101]. This part of the work was carried out using photon beams with nominal energies of 6 MV and 6 MV FFF. The reference field size was 10 cm × 10 cm, and the non-reference field sizes measured were 1 cm × 1 cm, 2 cm × 2 cm, and 3 cm × 3 cm. The field sizes were defined by the LINAC jaws, with the MLC retracted.



Figure 22: Setup for field output factors determination, assembled with a water phantom.

The measurements were performed with the PTW 60019 MicroDiamond detector (PTW Freiburg, Germany) [102], and with the PTW 6023 MicroSilicon detector (PTW Freiburg, Germany) [102]. Both detectors are shown in Figure 23. MicroDiamond is a synthetic diamond detector, that was designed to be water equivalent in megavoltage photon beams and is reliable in field sizes ranging from 1 to 40 cm^2 [107], [108]. This detector consists of a single crystal layer with a thickness of 1 μm and an active volume of 0,004 mm^3. It has a cylindrical shape with a radius of 1,1 mm and a height of 0,001 mm [88], [89], [109], [110] The reference point is located 1,0 mm away from the detector tip [88]. MicroSilicon detector is a p-type silicon diode detector. It has an active volume of 0,030 mm^3, a 0,75 mm radius and a 0,018 mm height [111]. Its reference point is located 0,9 mm from the detector tip. Both detectors operate at 0 V bias. The IAEA TRS-483 [9] recommends that they should be oriented parallel to the beam, due to the asymmetries in the detector structure.

The detector was connected to a PTW UNIDOS electrometer.

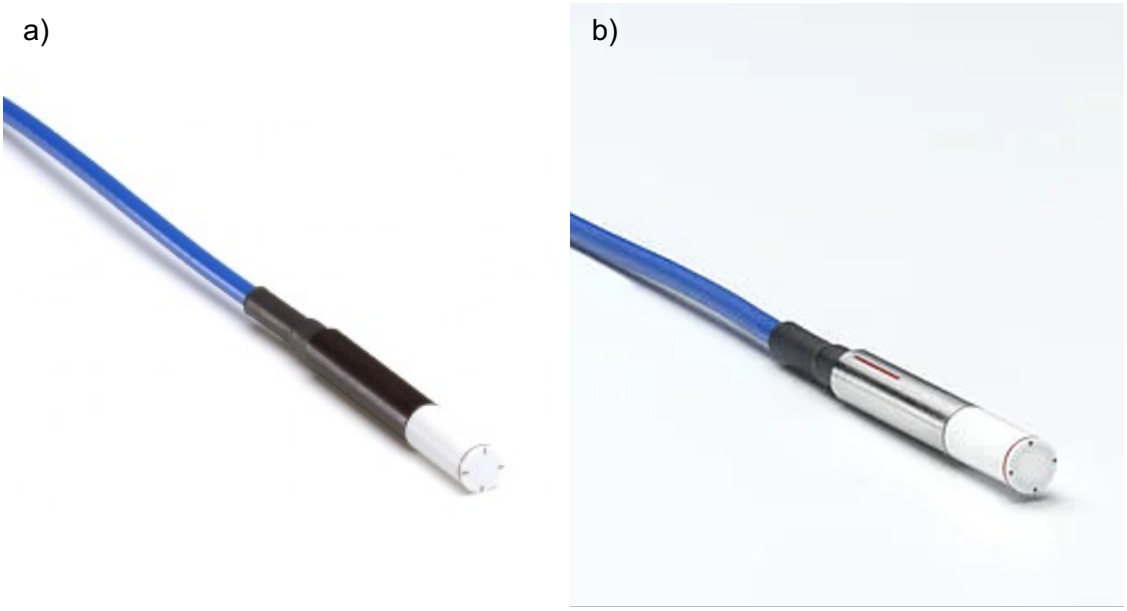


Figure 23: a) PTW 60019 MicroDiamond; b) PTW 6023 MicroSilicon

Since minor adjustments in the collimator position can lead to significant variations in the absorbed dose to water at the field's centre, an alignment procedure and FWHM determination were conducted each time the field was set or reset by moving the collimator, before OF measurements.

Before the OF measurements, for water tank alignment, beam centre adjustment was performed at two depths for the 10 ×10 cm^2 field: 50 mm and 150 mm, for beam inclination determination. A tolerance level of 0,1º was applied.

For each field, for OF and profile measurements, the lateral alignment of the detectors along the beam central axis was performed distinctly in the 3D water phantom, at 50 mm depth, following the steps listed below:

- CAX alignment, following the procedure available in the dosimetry software Mephysto MC2 (PTW Freiburg, Germany) [102], namely the CenterCheck tool, which was used for positioning the detector at the radiological centre of the beam via analysis of the in-plane and cross-plane profile measurements, at two different depths. A small step size of 1 mm was used for CAX check.
- CAX correction, repositioning (centering) of the detector after acquiring lateral beam profiles along crossline and in-line directions.

All relative measurements were performed using the same scanning direction to avoid mechanical hysteresis.

For OFs determination, the correction factor $k_{Q_{clin},Q_{msr}}^{f_{clin},f_{ms}}$ provided by the TRS-483 [9] was applied.

2.8. Uncertainties determination

2.8.1. Absolute dose determination

The uncertainty budget was determined based on the survey's answers, the protocol TRS-398 [8] and the article on the uncertainty in the determination of the absorbed dose to water by Castro et al [98]. The uncertainty budget for the determination of absorbed dose to water was organised in 4 parts:

1. Dosimetry system: uncertainties associated with the ionization chamber and the electrometer
2. Beam quality: uncertainty in k_Q determination
3. Correction factors for influence quantities: uncertainties associated with air pressure, ionic recombination, and polarity correction factors
4. Reference conditions: uncertainties related to field size, SSD, and depth

The first three parts pertain to the quantities that are measured and directly affect the dose value, while the fourth part is related to the establishment of reference conditions.

Dosimetry system

In this part, it was considered all the uncertainties associated with the dosimetry system, ionization chamber and electrometer.

The ionization chamber calibration factor, $N_{D,w}$, has an associated uncertainty given by the calibration laboratory. Since the electrometer was calibrated concurrently with the ionization chamber, the calibration factor $N_{D,w}$ is the only calibration factor applied. If the two equipments had been calibrated separately, the electrometer would have its own calibration factor, k_{elec}, with an associated uncertainty, given by the calibration laboratory.

The dosimetry system stability was evaluated using the stability measurements obtained with the ^{90}Sr check source, as suggested by Castro et al [98]. To determine the uncertainty associated with the stability measurements, we centred a rectangular

distribution on the reference dose value. The range of the measurements was calculated as the difference between the highest and lowest values.

The uncertainty in electrometer readings, represented as u_{elec}, considers both the reproducibility and resolution of the electrometer. The term reproducibility denotes the consistency of a measurement, which can be estimated by analysing the standard deviation of the charge readings. The total uncertainty of the electrometer reading is calculated as the quadratic sum of these two uncertainties:

$$u_{elec} = \sqrt{u(reading)^2 + u(resolution)^2} \tag{31}$$

Beam quality

Since k_Q was determined according to the equation given in TRS-398 [8], the uncertainty considered was the one provided in the same protocol. It is important to note that the uncertainty associated to the correction factor differs from the 2000 edition and the 2024 edition of the protocol.

Correction factors for influence quantities

This section contains the uncertainties associated with air pressure correction factor k_{TP}, polarity correction factor k_{pol}, and ionic recombination correction factor k_s.

The standard uncertainty of the air pressure correction factor, k_{TP}, was determined considering the uncertainties associated with the measurements of temperature and pressure. For each measurement, it was considered the uncertainty of the reading and the uncertainty of the calibration. The reading uncertainties are type B uncertainties with a rectangular probability distribution. Since the thermometer and the barometer are digital devices, the uncertainty u of the resolution is given by:

$$u = \frac{\Delta}{\sqrt{3}} \tag{32}$$

Where Δ is the resolution of the equipment.

The uncertainty associated with each measurement is the quadratic sum of the two uncertainties, reading and calibration. For instance, the uncertainty associated with the temperature measurement is determined by:

$$u(T) = \sqrt{u\left(T_{reading}\right)^2 + u(T_{calibration})^2} \tag{33}$$

Temperature and pressure are correlated quantities, so the uncertainty of the air pressure correction factor k_{TP} determination has to consider both measurements and the influence they have in the calculated value of k_{TP}. The uncertainty associated is, then, given by:

$$u(k_{TP}) = \sqrt{\left(\frac{\mathrm{d}k_{TP}}{\mathrm{d}T}\right)^2 u^2(T) + \left(\frac{\mathrm{d}k_{TP}}{\mathrm{d}P}\right)^2 u^2(P)} \quad (34)$$

If the relative humidity is between 20% and 80%, there is no need to apply a correction factor, resulting in no associated uncertainty for this parameter.

The uncertainty of the polarity correction factors depends on the uncertainty of the readings with both positive and negative polarities. Since it is a type A uncertainty, the uncertainty was determined based on their standard deviation. Since these values were measured with the same dosimetry system as the charge for absolute dose, the uncertainty associated with the dosimetry system is not considered in the standard uncertainty of the polarity correction factor. The standard uncertainty of the measurement is obtained dividing the standard deviation of the measurements by the square root of the number of measurements. The standard uncertainty of the polarity correction is the combined uncertainty of the measurements with positive, M_+, and negative polarity, M_-:

$$u\left(k_{pol}\right) = \sqrt{u(M_+)^2 + u(M_-)^2} \quad (35)$$

In addition to the uncertainty of the charge measurements to determine M_{normal} and $M_{reduced}$, estimating the uncertainty associated with the ionic recombination correction factor requires evaluating the uncertainty of the two-voltage method and the polynomial fit of the expression of k_s. The uncertainty is, then, given by:

$$u(k_s) = \sqrt{u(M_{normal})^2 + u(M_{reduced})^2 + u(\text{two-voltage method})^2 + u(\text{pol. fit})^2} \quad (36)$$

Reference conditions

The possibility of inaccuracy during the setup of reference conditions can be associated either with the setting of the field size, the positioning of the chamber at the source-to-surface distance, SSD, or in the measurement depth, z_{ref}. According to the TRS-398 [8], the three components combined result in a relative standard uncertainty of 0,3%, however this value depends on user and equipment.

Since relative standard uncertainties are being dealt with, the uncertainties of each component are combined in quadrature to obtain the combined standard uncertainty, which represents the relative uncertainty in determining the absorbed dose to water.

2.8.2. Field output factors determination

The uncertainty budget was organised in 3 parts:

1. Dosimetry system: uncertainties associated with the ionization chamber and the electrometer
2. Uncertainty in $k_{Q_{clin},Q_{msr}}^{f_{clin},f_{msr}}$ determination
3. Reference conditions: uncertainties related to field size of the reference field and the clinical field, SSD, and depth of measurement

Since field output factors are a relative measurement, the there was no need to approach the uncertainties associated with correction factors for influence quantities.

Dosimetry system

The detector calibration factor, $R_{D,w}$, has an associated uncertainty provided by the calibration laboratory. The uncertainty associated with long-term stability was the one provided by the manufacturer.

The uncertainty of the charge readings must account for the reading in the reference field and the reading in the clinical field. For the reference field size, the uncertainty was obtained in the same way as for dose determination, considering the reproducibility of the measurements and the resolution of the electrometer. The uncertainty associated with the small field size electrometer readings was calculated following the same steps and considering the smallest field size.

Field output factor correction factor

The field OF correction factor $k_{Q_{clin},Q_{msr}}^{f_{clin},f_{msr}}$ applied was provided TRS-483 [9], so it was considered the uncertainty that this protocol indicates. The value of the uncertainty associated with $k_{Q_{clin},Q_{msr}}^{f_{clin},f_{msr}}$ differs with the field size.

Reference conditions

The uncertainties associated with SSD and detector positioning are equal to those determined for absorbed dose. The uncertainty of the reference field size is also equal to the uncertainty of the field size determined for the uncertainty budget of the absorbed dose measurement.

The uncertainty of the clinical field size was determined based on the resolution of Mephysto, the software that analyses the beam profiles, which determines the FWHM. This uncertainty was estimated considering the smallest field size.

2.9. Audit report

A report of the outcome of the audit was created. This report briefly describes the methodology used, the results obtained, and the main conclusions of the dosimetric audit conducted at the Radiotherapy Service of IPO-Porto. The report includes:

- Centre characterization.
- Description of the on-site measurements: this section covers both absorbed dose determination and field output factors determination
- Absolute dose determination: the deviation of the absolute dose to the desired value is analysed, as well as the difference between the absolute dose values calculated in the two worksheets.
- Field output factors determination: calculation of the OF for each small field size and comparison of the values determined with two different detectors.
- Uncertainties: estimation of the uncertainties associated with absorbed dose to water determination and field output factors determination.
- Conclusions and recommendations: in this section, some recommendations for potential improvements of dosimetry practices were included.

The complete report can be consulted in Attachment 6.

3. Results and discussion

Of the 20 centres contacted, only 6 responded in full or in part to the surveys sent out. The small number of responses reduces the analysis and conclusions that can be drawn, although it does not compromise the proposed methodology.

In addition, there were constraints in scheduling visits to carry out the on-site measurements, due to the lack of response or availability of the centres contacted, which prevented them from being carried out before this work was submitted.

3.1. Multicentre survey on dosimetry practices in absolute dose

Besides IPO-Porto, five other facilities participated in this stage of the study. All six centres reported using ionization chambers for reference dosimetry, as highlighted by the most widely used dosimetry protocols, TRS-398 [8] and TG-51 [15]. Table 2 lists the ionization chambers used across the centres involved in this study along with the number of centres employing each chamber.

Table 2: Overview of the ionization chamber models used to measure absolute dose across different RT facilities.

Ionization chamber model	n
PTW 30010 Farmer	2
PTW 30013 Farmer	1
PTW 31002 Semiflex	3
IBA CC13	1

All the participating centres reported that they follow the guidelines of the IAEA TRS-398 [8] protocol. Out of the 6 facilities, four of them reported that they use the worksheet provided by IAEA, for absorbed dose to water determination. The remaining two facilities use their own worksheet, that already include updated values for the beam quality correction factor k_Q and the volume averaging correction factor k_{vol} for FFF beams. One of the facilities that still uses the IAEA worksheet, to the calculated dose value applies, posteriorly, the k_{vol} factor provided by the IAEA TRS-483 [9], for 10 MV FFF beams.

The six centres perform reference dosimetry measurements in water tank phantoms. All equipment (ionization chambers, thermometers, and barometers) used had valid calibration certificates.

All participants reported conducting a chamber pre-heating process. The methodology to ensure the stabilization of the chamber varies among facilities. In one centre, the chamber is left to stabilize for 5 minutes, while in two centres, it stabilizes for 15 minutes each, and in two others, the stabilization period is extended to 30 minutes. Additionally, in one facility, stabilization is determined not by time but by irradiating monitor units, where the chamber is exposed to 300 MUs before starting measurements. There is a different methodology from centre to centre as there is no universal rule to verify the stabilisation of the ionization chamber. However, it is recommended that the chamber stabilizes for at least 15 minutes, or as per the manufacturer's recommendation. It is also advisable to irradiate the chamber with a large number of MUs (e.g. 1000 Mus) and to check the stability of the current variation.

Regarding charge measurements, only one centre reported using a criterion for accepting or rejecting charge readings, based on a 1,0% standard deviation threshold.

The adopted tolerance levels follow the TRS-398, that indicates that the maximum tolerance limit for dose deviation is 2%. These limits differ from centre to centre and the values are shown in Table 3. One of the centres did not report its tolerance level for dose deviation.

The adopted tolerance levels follow the TRS-398 [8] guidelines, which indicate that the maximum tolerance limit for dose deviation is 2,0%. The adopted limits vary from centre to centre, and the values are shown in Table 3. One of the centres did not report its tolerance level for dose deviation. None of the surveyed centres reported estimating the uncertainties associated with the process, so they also do not take this value into account when defining dose deviation tolerance limits.

Table 3: Overview of the tolerance level for dose deviation adopted by the participating RT facilities.

Tolerance level for dose deviation	n
0,5%	1
1,0%	2
1,5%	1
2,0%	1

3.2. On-site measurements at pilot-centre: absolute dose

3.2.1. Stability verification procedure

The reading obtained was 0,0769 Gy, while the reference was 0,0773 Gy, resulting in a deviation of 0,47%. The maximum tolerance limit for the deviation of the dose reading relative to the reference reading of an ionization chamber is 1%. This chamber's stability is within the tolerance limits; therefore, the system is considered stable. This limit ensures the accuracy and consistency of dose measurements.

3.2.2. Absolute dose determination

The absolute dose was determined using both the IAEA worksheet and the worksheet developed during this work. All calculated dose values, for the eight LINACs, obtained using both dose determination worksheets, are presented in the Table 4.

Table 4: Relative variations in dose and beam quality correction factor k_Q values, between the two dose determination worksheets, for each beam energy of IPO LINACs.

LINAC	Energy	New worksheet (2024)		IAEA worksheet (2000)		Variation (%)	
		Dose (cGy/MU)	k_Q	Dose (cGy/MU)	k_Q	Dose	k_Q
1	6 MV	0,9975	0,9900	0,9996	0,9920	0,2%	0,2%
1	10 MV	1,0007	0,9760	1,0055	0,9807	0,5%	0,5%
2	6 MV SRS	1,0015	0,9910	1,0036	0,9928	0,2%	0,2%
2	6 MV	1,0057	0,9890	1,0080	0,9916	0,2%	0,2%
2	15 MV	1,0005	0,9690	1,0059	0,9744	0,5%	0,5%
3	6 MV	0,9921	0,9900	0,9943	0,9918	0,2%	0,2%
3	15 MV	0,9941	0,9700	0,9990	0,9746	0,5%	0,5%
4	6 MV	0,9982	0,9900	1,0002	0,9920	0,2%	0,2%
4	10 MV	0,9944	0,9730	0,9997	0,9779	0,5%	0,5%
5	6 MV	1,0046	0,9896	1,0069	0,9917	0,2%	0,2%
5	15 MV	0,9888	0,9696	0,9940	0,9747	0,5%	0,5%
6	4 MV	0,9994	0,9960	1,0007	0,9973	0,1%	0,1%
6	10 MV	0,9986	0,9766	1,0033	0,9811	0,5%	0,5%
7	6 MV	0,9961	0,9920	0,9960	0,9920	0,0%	0,0%

7	10 MV	0,9996	0,9760	1,0043	0,9807	0,5%	0,5%
8	6 MV	0,9978	0,9890	1,0001	0,9913	0,2%	0,2%
8	10 MV	0,9960	0,9750	1,0010	0,9797	0,5%	0,5%
8	15 MV	0,9930	0,9694	0,9982	0,9745	0,5%	0,5%
8	6 MV FFF	0,9989	0,9957	0,9989	0,9941	0,0%	0,2%
8	10 MV FFF	1,0016	0,9833	1,0004	0,9872	0,1%	0,4%

Additionally, a graph of the dose values, for the TrueBeam linear accelerator, is shown in Figure 24. It displays the dose values for each beam energy available obtained for the two worksheets for the TrueBeam LINAC, at IPO, and the tolerance limits, allowing for a graphical comparison of the differences.

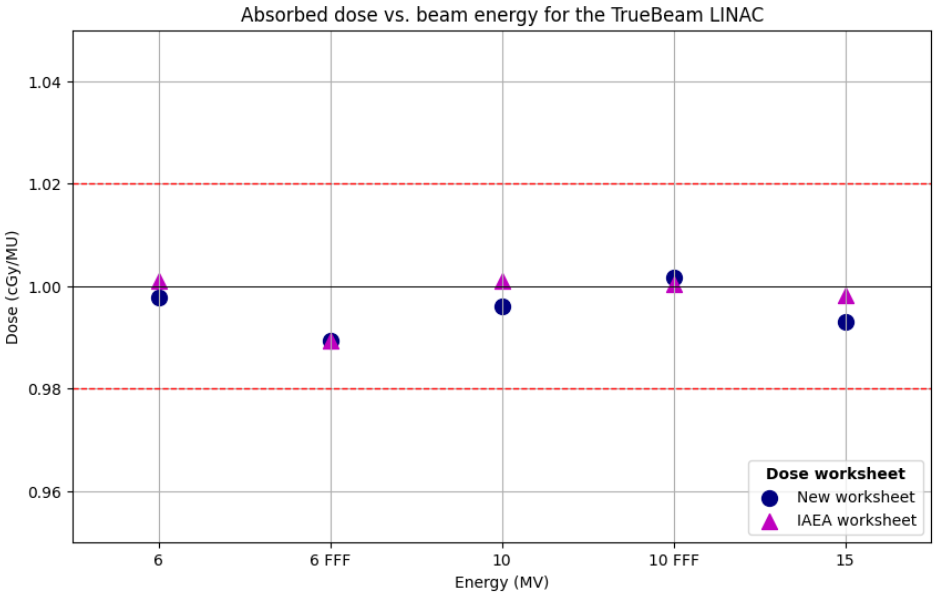


Figure 24: Absorbed dose determined for each beam energy for the TrueBeam LINAC, calculated using the IAEA worksheet and the new worksheet. The red line indicates the tolerance limit of 2%.

As expected, for photon beams with flattening filter, the difference between the dose determined with the two worksheets is proportional to the difference between the beam quality correction factors k_Q.

However, for FFF beams, the difference in the dose is not proportional. Specifically, for 6 MV FFF, despite a beam correction factor k_Q variation of 0,2%, the dose variation is negligible due to the application of the volume averaging factor k_{vol}. For instance, for a PTW 30013 Farmer ionization chamber with a thimble length of 2.3 cm and an SSD of 100 cm, k_{vol} is approximately 1,002 at this beam quality, resulting in

a dose variation of 0,2%. The same occurs with the 10 MV FFF beam, where the 0,4% variation in the k_Q value does not lead to a proportionate variation in the absolute dose value. In this example, the volume averaging factor k_{vol} introduces a 0,3% variation, resulting in a 0,1% difference in dose.

Regardless of the worksheet used, all calculated dose values fall within tolerance limits. It's important to note that the uncertainty associated with these calculated dose values should be taken into account when making dose adjustments. Further details on this topic will be discussed in Chapter 3.5.1.

3.3. Multicentre survey on dosimetry of small fields practices

Besides IPO-Porto, 6 national RT facilities took part in this study. The Table 5 presents an overview of the LINACs involved and energies used for small field dosimetry, as well as the setup used to determine field output factors.

Table 5: Overview of the number of LINACs and respective setups for field output factors determination.

Manufacturer	Model	SSD (cm)	Depth (cm)	Energy (MV)	n
Varian	TrueBeam	95	5	6	3
				10	1
				6 FFF	2
	Clinac	95	5	6	1
Elekta	Versa HD	90	10	6	2
				10	2
				15	1
				6 FFF	3
				10 FFF	2

As previously mentioned, there is no standard detector for small-field dosimetry, as indicated by physicists who have stated the use of three different types of detectors: diamond detector, diode detector, and ionization chamber. Four institutions reported that they use more than one detector for field output factors measurements, which is the recommended practice by the IAEA TRS-483 [9]. The Table 6 details the detectors used to measure field outputs.

Table 6: Overview of the detectors used for field output factors determination.

Type	Detector model	n
Diamond detector	PTW 60019 MicroDiamond	3
Diode detector	PTW 60016 MicroSilicon	1
	IBA RAZOR diode	2
Ionization chamber	PTW 31010 Semiflex	2
	PTW 31016 Pin-point	2

Out of the seven participant centres, in four of them the $k_{Q_{clin},Q_{msr}}^{f_{clin},f_{msr}}$ correction factor is applied in the determination output factors, using the values given by the IAEA TRS-483 [9]. At the remaining three centres, the field output factors are not corrected.

Following the TRS-483 [9] protocol, field output factors should be reported based on the equivalent square small field size S_{clin} rather than the nominal field size. Although the nominal value might be the same, the actual field size can vary slightly between centres, due to small differences in the aperture of the field, caused by the position of the jaws or the MLC. However, only two centres reported their field OFs based on S_{clin}.

The majority of the centres preferred direct measurements over the intermediate field method, that was only used by 2 facilities.

3.4. Field output factors determination

3.4.1. On-site measurements at pilot-centre

Locally, the field output factors were determined with two different detectors: a MicroDiamond and a MicroSilicon, both manufactured by PTW (PTW Freiburg, Germany) [102], for a Varian TrueBeam LINAC, for 3 nominal field sizes (1 cm × 1 cm, 2 cm × 2 cm, and 3 cm × 3 cm).

The field output factors were obtained using their field size defined by the FWHM. The equivalent square small field size, S_{clin}, was calculated using Equation (25). The equivalent square small size, S_{clin}, as a function of the nominal square field size is shown in Table 7.

Table 7: S_{clin} measured for the TrueBeam small field sizes, as a function of the nominal square field sizes.

Nominal field size (cm × cm)	MicroDiamond S_{clin} (cm)		MicroSilicon S_{clin} (cm)	
	6 MV	6 MV FFF	6 MV	6 MV FFF
1 × 1	0,923	0,891	0,918	0,888
2 × 2	1,914	1,890	1,911	1,887
3 × 3	2,925	2,903	2,922	2,902

The measured field size differs for each detector. The field sizes measured with the MicroSilicon are smaller than those measured with the MicroDiamond. These field size values were used to estimate the correction factor $k_{Q_{clin},Q_{msr}}^{f_{clin},f_{msr}}$ for each field OF.

According to TRS-483 [9], to facilitate establishing a relationship between FWHM and collimator setting, it is advised that both the FWHM and the geometrical field size is recorded when reporting small field data. Accordantly, field OFs values are reported as a function of the nominal field size. The calculated field output factors for the two photon beam energies are presented in the charts in Figure 25.

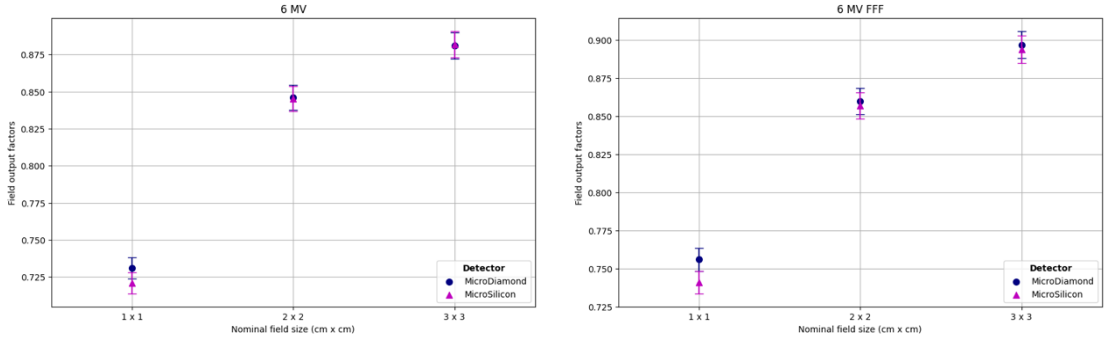


Figure 25: Field output factors, and respective uncertainty, for 3 field sizes (1 cm × 1 cm, 2 cm × 2 cm, and 3 cm × 3 cm), determined with MicroDiamond and MicroSilicon detectors, for 6 MV and 6 MV FFF photon beams.

Table 8 presents the values of the field output factors measured with the MicroDiamond and the MicroSilicon detectors, and the relative standard deviation (SD) for a photon beam with 6 MV and a photon beam with a 6 MV FFF energy.

Table 8: Field Output Factors determined with MicroDiamond and MicroSilicon detectors and relative standard deviation (SD) of the values, for photon beams with energies 6 MV and a 6 MV FFF.

Nominal field size (cm × cm)	**6 MV**			**6 MV FFF**		
	1 × 1	**2 × 2**	**3 × 3**	**1 × 1**	**2 × 2**	**3 × 3**
MicroDiamond	0,731 ± 0,007	0,846 ± 0,009	0,881 ± 0,009	0,756 ± 0,008	0,860 ± 0,009	0,897 ± 0,009
MicroSilicon	0,721 ± 0,007	0,845 ± 0,009	0,882 ± 0,009	0,741 ± 0,007	0,857 ± 0,009	0,894 ± 0,009
SD (%)	0,74	0,04	0,05	1,01	0,17	0,19

Since the measurements were performed on the same linear accelerator, under the same conditions, the slight difference in the measured values can be attributed to the intrinsic characteristics of the detectors. The values of the field output factors measured with the MicroDiamond and the MicroSilicon detectors for both 6 MV and 6 MV FFF photon beams are relatively close. The standard deviations indicate that the variability in measurements between the two detectors is relatively low, with slightly higher variability observed for the 1 cm field size, especially with the 6 MV FFF beam. Though, these results demonstrate consistency between the readings of the two detectors.

It is also important to note that the field output correction factor applied to the MicroSilicon measurements corresponds to a previous version of the detector, PTW 60017 Diode E, as there are no published correction factors specific to this detector. Weber at al. (2020) [111] and McGrath et al. (2022) [112] concluded that the MicroSilicon readings require less corrections, due to its more water-equivalent design. While performing measurements with the MicroSilicon, it is important to keep in mind the lack of correction factors. Given the lack of specific correction factors for the MicroSilicon, it is recommended to continue using the MicroDiamond detector for measurements until further information or correction factors for the MicroSilicon are available.

3.4.2. Remote audit

Six facilities submitted their field output factors for the LINACs and setups shown in Table 5. Field output factors values were compared by LINAC and beam energy.

Since only one centre with a Varian Clinac LINAC submitted their field output factors, these data were not considered in the comparative study.

For the Varian LINACs, measurements were conducted with an SSD of 95 cm at a depth of 5 cm, and output factors were analysed for 6 MV and 6 MV FFF energies. Since only one of the three facilities using a Varian TrueBeam LINAC submitted field output factors for a 10 MV beam, the analysis for this energy was not conducted.

For two of the centres, the field OFs were given based on the nominal field size. The only centre that reported its field OFs as a function of S_{clin} was IPO; these values were previously presented in Chapter 3.4.1, in Table 7.

The mean field output factors for this LINAC model are presented in Table 9, showing the field output factors average values $\Omega_{Q_{clin},Q_{msr}}^{f_{clin},f_{msr}}$, relative standard deviations (SD), and the number of beams considered.

Table 9: Mean and standard deviation of field OFs submitted, and number of beams considered for photon beams with energies 6 MV and a 6 MV FFF, for Varian TrueBeam LINACs.

Nominal field size (cm × cm)	**6 MV**			**6 MV FFF**		
	$\Omega_{Q_{clin},Q_{msr}}^{f_{clin},f_{msr}}$	**SD (%)**	n	$\Omega_{Q_{clin},Q_{msr}}^{f_{clin},f_{msr}}$	**SD (%)**	n
1 × 1	0,731	-	1	0,756	-	1
2 × 2	0,840	0,53	3	0,856	0,29	2
3 × 3	0,878	0,27	3	0,895	0,50	2

One of the centres did not apply a correction factor to the calculation of their field OFs, so it was applied the correction factor provided by the TRS-483 [9] protocol to their measurement. As this centre reported its OFs as a function of nominal field size, the correction was applied considering that field size value.

Table 10: Mean and standard deviation of field OFs with the TRS-483 correction factor applied, and number of beams considered for photon beams with energies 6 MV and a 6 MV FFF, for Varian TrueBeam LINACs

Nominal field size (cm × cm)	**6 MV**			**6 MV FFF**		
	$\Omega_{Q_{clin},Q_{msr}}^{f_{clin},f_{msr}}$	**SD (%)**	n	$\Omega_{Q_{clin},Q_{msr}}^{f_{clin},f_{msr}}$	**SD (%)**	n
1 × 1	0,731	-	1	0,756	-	1
2 × 2	0,841	0,27	3	0,858	0,26	2
3 × 3	0,879	0,07	3	0,895	0,23	2

It can be observed that, after applying the correction factor $k_{Q_{clin},Q_{msr}}^{f_{clin},f_{msr}}$, the standard deviation among the values decreases, highlighting the necessity of applying this factor.

The standard deviation increases as the field size decreases, reflecting the different detector responses in small fields. However, due to limited sampling, comments regarding 1 cm fields cannot be made. Nonetheless, the standard deviation for 2 × 2 cm^2 and 3 × 3 cm^2 fields at both energies is below 1%, indicating good agreement in beam characteristics among the TrueBeam machines at participating centres.

For the Elekta Versa HD LINACs, the same analysis method was used. The measurements were conducted with an SSD of 90 cm at a depth of 10 cm, and output factors were analysed for 6 MV, 6 MV FFF, 10 MV and 10 MV FFF energies. Since only one facility utilizes 15 MV beams for small field dosimetry, an analysis of this energy was not conducted. The calculated field output factors were compared, for each energy and field size.

The average of the field output factors $\Omega_{Q_{clin},Q_{msr}}^{f_{clin},f_{msr}}$ values submitted by the centres, relative standard deviations, and the number of beams considered for 6 MV and 6 MV FFF energies are presented in Table 11. The values for 10 MV and 10 MV FFF energies are presented in Table 12.

Table 11: Mean and standard deviation of field OFs submitted, and number of beams considered for photon beams with energies 6 MV and a 6 MV FFF, for Elekta Versa HD LINACs.

Nominal field size (cm × cm)	**6 MV**			**6 MV FFF**		
	$\boldsymbol{\Omega_{Q_{clin},Q_{msr}}^{f_{clin},f_{msr}}}$	**SD (%)**	$\boldsymbol{n}$	$\boldsymbol{\Omega_{Q_{clin},Q_{msr}}^{f_{clin},f_{msr}}}$	**SD (%)**	$\boldsymbol{n}$
1 × 1	0,671	0,42	2	0,695	1,29	3
2 × 2	0,793	1,41	2	0,823	0,99	3
3 × 3	0,838	1,41	2	0,869	1,09	3

Table 12: Mean and standard deviation of field OFs submitted, and number of beams considered for photon beams with energies 10 MV and a 10 MV FFF, for Elekta Versa HD LINACs.

Nominal field size (cm × cm)	10 MV			10 MV FFF		
	$\Omega_{Q_{clin},Q_{msr}}^{f_{clin},f_{msr}}$	SD (%)	n	$\Omega_{Q_{clin},Q_{msr}}^{f_{clin},f_{msr}}$	SD (%)	n
1 × 1	0,639	0,28	2	0,670	0,48	2
2 × 2	0,798	0,99	2	0,831	0,97	2
3 × 3	0,856	0,99	2	0,886	1,21	2

Two of the centres did not apply a correction factor to the calculation of their field OFs, it was applied the correction factor provided by the TRS-483 [9] protocol to their measurement. Once again, the S_{clin} was not reported. The mean field output factors $\Omega_{Q_{clin},Q_{msr}}^{f_{clin},f_{msr}}$, with the TRS-483 correction factor applied, for 6 MV and 6 MV FFF are presented in Table 13, and the data for 10 MV and 10 MV FFF are presented in Table 14.

Table 13: Mean and standard deviation of field OFs with the TRS-483 correction factor applied, and number of beams considered for photon beams with energies 6 MV and a 6 MV FFF, for Elekta Versa HD LINACs.

Nominal field size (cm × cm)	6 MV			6 MV FFF		
	$\Omega_{Q_{clin},Q_{msr}}^{f_{clin},f_{msr}}$	SD (%)	n	$\Omega_{Q_{clin},Q_{msr}}^{f_{clin},f_{msr}}$	SD (%)	n
1 × 1	0,672	0,24	2	0,697	0,49	3
2 × 2	0,799	0,58	2	0,831	0,49	3
3 × 3	0,845	0,48	2	0,873	0,54	3

Table 14: Mean and standard deviation of field OFs with the TRS-483 correction factor applied, and number of beams considered for photon beams with energies 10 MV and a 10 MV FFF, for Elekta Versa HD LINACs.

Nominal field size (cm × cm)	10 MV			10 MV FFF		
	$\Omega_{Q_{clin},Q_{msr}}^{f_{clin},f_{msr}}$	SD (%)	n	$\Omega_{Q_{clin},Q_{msr}}^{f_{clin},f_{msr}}$	SD (%)	n
1 × 1	0,640	0,46	2	0,671	0,29	2
2 × 2	0,804	0,15	2	0,837	0,09	2
3 × 3	0,863	0,03	2	0,893	0,22	2

Except for 6 MV FFF, for the Elekta Versa HD LINACs, the standard deviation of the field OFs also decreases when the correction factor $k_{Q_{clin},Q_{msr}}^{f_{clin},f_{msr}}$ is applied. For 6 MV FFF energy, this trend is not observed because the correction factor values are very close to 1.

This occurrence highlights the importance of correcting the output factor values for the detector and field size, as these factors influence the values.

The standard deviations estimated for different field sizes indicate variability in measurement results. Generally, smaller fields tend to exhibit higher standard deviations, suggesting increased uncertainty in measurements.

The relative standard deviation for all field sizes analysed for 6 MV, 10 MV and 10 MV FFF is below 1. These results indicate a high level of agreement among centres using the Elekta Versa HD LINACs.

This suggests consistent and reliable dosimetric measurements across different field sizes and beam energies, enhancing confidence in the consistency of radiation delivery.

Additionally, since the field OFs were provided based on the nominal field size, it was not possible to analyse differences in the actual field size and assess whether these differences in collimator positioning caused variations in the OF values.

The consistency of results could be improved with more samples to estimate mean values and standard deviations. The limited sampling underscores the need for additional measurements to enhance statistical precision. Nevertheless, the small standard deviation obtained for field OFs suggests consistent and reliable dosimetric measurements across different RT facilities.

3.5. Uncertainties determination

In this section, the estimated uncertainty budgets for absolute dose measurements and field output factors will be presented. Both were estimated based on the equipment used and measurement methodology at the pilot centre, IPO-Porto.

3.5.1. Uncertainties associated with absolute dose determination

Dosimetry system:

The ionization chamber used was a PTW 30013 Farmer, with a calibration uncertainty of 2,2% as quoted in the calibration certificate, with a coverage factor k of 2. This means that the relative standard uncertainty of the chamber calibration is 1,1%. Since the electrometer and the ionization chamber were calibrated together, the electrometer does not have a separate calibration uncertainty.

The uncertainty in electrometer readings, represented as u_{read}, considers both the reproducibility and resolution of the electrometer. Across all considered photon beams, the maximum standard uncertainty observed in the charge readings was 0,008 nC, with a corresponding mean value of 24,31 nC. Consequently, the associated relative uncertainty amounts to 0,03%. The resolution of the electrometer is 0,01 nC, and considering a charge mean value of 24,31, this results in an uncertainty of 0,04%. The total uncertainty of the electrometer reading is, then, calculated as the quadratic sum of these two uncertainties:

$$u_{read} = \sqrt{0{,}03^2 + 0{,}04^2} = 0{,}05\% \quad (37)$$

As mentioned before, the dosimetry system of the dosimetry system evaluated using the stability measurements obtained with the ^{90}Sr check source. To determine the uncertainty associated with the stability measurements, we centered a rectangular distribution on the reference dose value. The range of the measurements was calculated as the difference between the highest and lowest values, resulting in a range of 0,0004 Gy. The half-range was then determined to be $2{,}0 \times 10^{-4}$ Gy. For a rectangular distribution, the standard uncertainty is given by dividing the half range by the square root of 3, yielding an uncertainty of approximately $1{,}15 \times 10^{-4}$ Gy. When expressed as a percentage of the mean value (0,0773 Gy), this corresponds to a percentual uncertainty of about 0,15%.

Beam quality:

According to the TRS-398 [8] the uncertainty associated with the beam quality correction factor k_Q determination, using equation (13) given by this protocol is 0,6%. If the correction factor applied was the one provided by the 2000 edition of this protocol, the uncertainty would be 1,0%

Correction factors for influence quantities:

The resolution of the thermometer is 0,1 ºC, resulting in an uncertainty of resolution of 0,06 ºC. As the thermometer used had no valid calibration certificate, the calibration uncertainty considered was the calibration uncertainty quoted in the certificate of a similar thermometer, which is 0,16ºC. The standard uncertainty associated with the temperature measurement is calculated as:

$$u(T) = \sqrt{0{,}06^2 + 0{,}16^2} = 0{,}17 \tag{38}$$

Similarly, for pressure measurement, the resolution of the barometer is 0,01 kPa, resulting in an uncertainty of resolution of 0,006 kPa. The calibration uncertainty of the barometer is 0,06 kPa. The standard uncertainty associated with pressure measurement is given by:

$$u(P) = \sqrt{0{,}006^2 + 0{,}06^2} = 0{,}06 \tag{39}$$

The uncertainty was calculated, using equation (10), relative to a thermometer reading, T, of 22,0ºC and a barometer reading, P, of 100,0 kPa. Under these conditions, air pressure correction, k_{TP}, is equal to 1,020.

$$u(k_{TP}) = \sqrt{\left(\frac{\mathrm{d}k_{TP}}{\mathrm{d}T}\right)^2 u^2(T) + \left(\frac{\mathrm{d}k_{TP}}{\mathrm{d}P}\right)^2 u^2(P)} =$$

$$= \sqrt{\left(\frac{1}{293{,}25} \cdot \frac{101{,}325}{P}\right)^2 u^2(T) + \left(\frac{(273{,}25+T) \times 101{,}325}{293{,}25} \cdot \frac{1}{P^2}\right)^2 u^2(P)} =$$

$$= \sqrt{\left(\frac{1}{293{,}25} \cdot \frac{101{,}325}{100{,}00}\right)^2 0{,}17^2 + \left(\frac{(273{,}25+22{,}0) \times 101{,}325}{293{,}25} \cdot \frac{1}{100{,}00^2}\right)^2 0{,}06^2} =$$

$$= 0{,}0008 \tag{40}$$

This represents a 0,08% relative standard uncertainty.

The standard uncertainty of the M_+ and M_- measurements was obtained dividing the standard deviation of the measurements by the square root of the number of measurements. The maximum uncertainty calculated was 0,06% for M_+ and 0,04% for M_-, so the combined uncertainty is:

$$u(k_{pol}) = \sqrt{0{,}06^2 + 0{,}04^2} = 0{,}07\% \quad (41)$$

The uncertainties associated with M_{normal} and $M_{reduced}$ were calculated the same way as the uncertainties of M_+ and M_-. The maximum uncertainty calculated was 0,03% for M_{normal} and 0,01% for $M_{reduced}$.

The uncertainty associated with the two-voltage method was considered to be the difference between the expected value from the Boag theory and the value measured, which were under 0,03%, according to Castro et al [98], [113].

Regarding the polynomial fit error, the maximum deviation found between the values of k_s determined by the numerical solution of Boag's transcendental equations [114], and determined from the quadratic fit was 0,1%, which corresponds to an uncertainty of 0,06%, as reported by Weinhous et al [113].

$$u(k_s) = \sqrt{0{,}03^2 + 0{,}01^2 + 0{,}03^2 + 0{,}06^2} = 0{,}07\% \quad (42)$$

Reference conditions

Considering the measurement of the radiation field size with a film detector, the maximum deviation between the radiation field size and the light field size is 0,5 mm, so the uncertainty is estimated to be 0,29 mm, resulting in a relative uncertainty of 0,29%.

The SSD was mainly checked using the pointer, which smallest scale division is 2,0 mm. Considering a rectangular distribution, the standard deviation will be 1,2 mm. The relative standard deviation is 0,12%.

The uncertainty estimated pertained to the depth positioning of the chamber in the water tank phantom, and not in the slab phantom, due to its widespread utilization and recommended status. In the water tank phantom, the ionization chamber was positioned at the reference depth with a TRUFIX system, which is a detector positioning system designed for positioning accuracy. The alignment accuracy has an uncertainty of 0,1 mm, which means an uncertainty of 0,06 mm. Another source of uncertainty is the error of the movement array of the beam analyser. Since the resolution of the system is

0,01 mm, the standard uncertainty is 0,006 mm. Combining both uncertainty components in quadrature, the standard uncertainty of the depth is 0,06 mm, and since the desired depth is 100 mm, the relative standard uncertainty is 0,06%.

Since relative standard uncertainties are being dealt with, the uncertainties of each component were combined in quadrature to obtain the combined standard uncertainty, which represents the relative uncertainty in determining the absorbed dose to water. The ionization chamber calibration uncertainty is the most significant source of uncertainty.

Table 15: Uncertainty budget of the determination of absorbed dose to water.

Source of Uncertainty	**Standard uncertainty (%)**
Dosimetry system	
Ionization chamber calibration factor, $\boldsymbol{N_{D,w}}$	1,10
Dosimetry system stability	0,15
Electrometer calibration factor, $\boldsymbol{k_{elec}}$	-
Electrometer reading	0,05
Beam quality	
Determination of $\boldsymbol{k_{Q,Q_0}}$	0,60
Correction factors for influence quantities	
Air pressure correction, $\boldsymbol{k_{TP}}$	0,08
Polarity correction, $\boldsymbol{k_{pol}}$	0,07
Ionic recombination correction, $\boldsymbol{k_s}$	0,07
Reference conditions	
Field size	0,29
Source-to-surface distance, SSD	0,12
Measurement depth, $\boldsymbol{z_{ref}}$	0,06
Combined standard uncertainty (%)	1,30

The highest contribution for the total uncertainty was the uncertainty of the ionization chamber calibration factor, $N_{D,w}$. For example, in a centre where the chamber's calibration uncertainty is 1,0%, the combined standard uncertainty of the process decreases to 1,2%.

The combined standard uncertainty value does not vary significantly between centres, as the uncertainty of the chamber's calibration factor consistently hovers around 1,0%, the $k_Q$value applied is the same, and the uncertainties associated with the equipment (electrometer, thermometer, barometer) are similar.

The previous version of TRS-398 [8] presents an uncertainty of 1,0% associated with k_Q calculation. Therefore, when using the IAEA worksheet to determine absorbed dose, the uncertainty associated with the determination of k_Q increases from 0,6% to 1,0%, resulting in a combined relative standard uncertainty of 1,5%. For this reason, it is recommended to use the updated values of k_Q, since they have a lower associated uncertainty. The uncertainty associated with the electrometer reading is a function of the charge readings standard deviation. This value can be reduced, if the charge readings have a lower standard deviation.

Uncertainties should always be reported. Therefore, it's important to update Figure 24 with the associated uncertainties: 1,3% for the absolute dose calculated using the new worksheet and 1,5% for the absolute dose calculated using the IAEA worksheet. The updated graph, incorporating the absolute dose values and associated uncertainties, can be found in Figure 26.

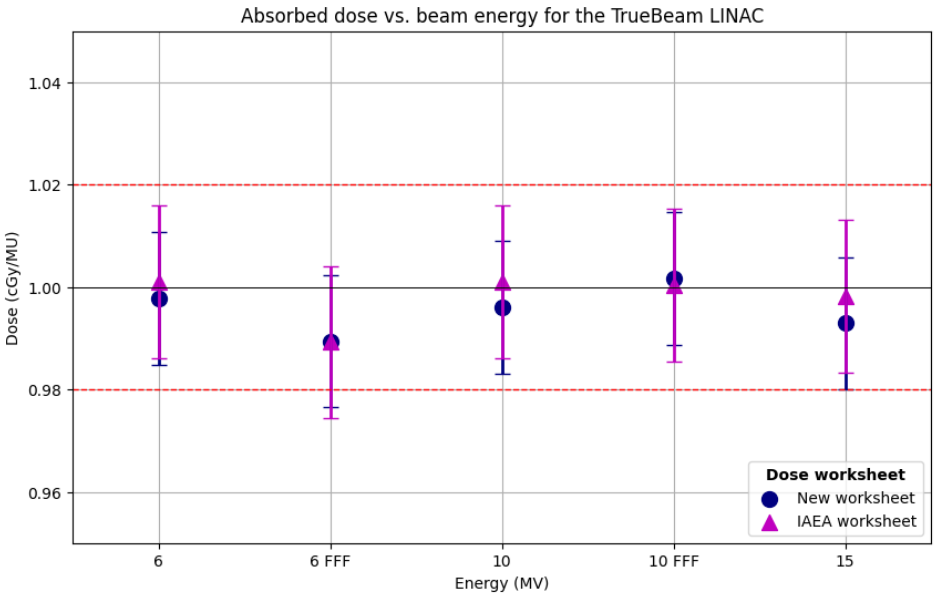


Figure 26: Absorbed dose determined for each beam energy for the TrueBeam LINAC, calculated using the IAEA worksheet and the new worksheet, and respective uncertainties. The red line indicates the tolerance limit of 2%.

Even though all absorbed dose values are within the tolerance limits, it's important to note that the lower limit of the uncertainty interval of the dose value calculated for the 6 MV FFF photon beam falls below the tolerance limit. So, considering the worst-case scenario where the dose value is 1,3% below the measured value, it would be outside the acceptance interval. For this reason, it's important to acknowledge the uncertainty interval when defining dose deviation tolerance limits.

3.5.2. Uncertainties associated field output factors determination

The uncertainty budget was determined considering the calculation of the field OF of the smallest field size, since it's the case where the uncertainty will be higher.

Dosimetry system

According to its calibration certificate, the calibration uncertainty of the diamond detector is 1,1%, with a coverage factor k of 2, which means that the relative standard uncertainty of the chamber calibration is 0,55%. The uncertainty associated with long-term stability of the diamond detector is 0,25%, according to its specifications provide by the manufacturer.

The resolution of the electrometer is 0,001 nC. For the reference field size, the standard deviation of the charge readings was 0,001 nC, for a mean value of 2,411 nC. So, the relative uncertainty is approximately 0,04%. For this charge reading, the uncertainty associated with the electrometer resolution is 0,04%. The uncertainty of the electrometer reading in the reference field size is:

$$u_{M_{msr}} = \sqrt{0{,}04^2 + 0{,}04^2} = 0{,}06\% \quad (43)$$

Considering the smallest field size, the mean charge reading was 1,046 and the standard deviation of the charge readings was also 0,001 nC, so the relative standard uncertainty is 0,10%. The uncertainty associated with the electrometer resolution is 0,10%. Therefore, the uncertainty of the electrometer reading in the small field size is:

$$u_{M_{clin}} = \sqrt{0{,}10^2 + 0{,}10^2} = 0{,}14\% \quad (44)$$

Field OF correction factor

The value of the field OF uncertainty increases as the field size decreases. Table 16 shows the field OF correction uncertainty for each field size, measured with a PTW

60019 microDiamond. This way, the uncertainty of the measurement will also be different for each field size. The uncertainty budget was determined considering the maximum uncertainty possible, which is the uncertainty for a square small field size of 0,5 cm.

Table 16: Field OF uncertainty and its respective relative standard uncertainty, according to TRS-483 [9].

Square small field size, S_{clin} (cm)	**Standard uncertainty (%)**
0,5	0,8
1,0	0,5
2,0	0,4
3,0	0,4
5,0	0,3
10,0	0,3

Measurement conditions:

The uncertainty of the reference field size is equal to the uncertainty of the field size determined for the uncertainty budget of the absorbed dose measurement, which is a relative uncertainty of 0,29%.

The uncertainty of the clinical field size was determined based on the resolution of the system that is used to analyse the beam profiles, and to determine FWHM. Its resolution is 0,01 mm, resulting in an uncertainty of 0,006 mm, and, for the smallest field size, a relative standard uncertainty of 0,12%.

The SSD of 95,0 cm was mainly checked using the pointer, which smallest scale division is 2,0 mm. Considering a rectangular distribution, the standard deviation will be 1,2 mm. The relative standard deviation is 0,13%.

The detector was positioned at the reference depth with a TRUFIX system, which is a detector positioning system designed for positioning accuracy. The alignment accuracy has an uncertainty of 0,1 mm, which means an uncertainty of 0,06 mm. Another source of uncertainty is the error of the movement array of the beam analyser. Since the resolution of the system is 0,01 mm, the standard uncertainty is 0,006 mm. Combining both uncertainty components in quadrature, the standard uncertainty of the depth is 0,06 mm, and since the desired depth is 50 mm, the relative standard uncertainty is 0,12%.

Since relative standard uncertainties are being dealt with, the uncertainties of each component are combined in quadrature to obtain the combined standard uncertainty, which represents the relative uncertainty in determining the small field output factors.

Table 17: Uncertainty budget of field output factors determination.

Source of Uncertainty	**Standard uncertainty (%)**
Dosimetry system	
Detector calibration factor, $\boldsymbol{R_{D,w}}$	0,55
Detector long-term stability	0,25
Electrometer reading of $\boldsymbol{M_{msr}}$	0,06
Electrometer reading of $\boldsymbol{M_{clin}}$	0,14
Field OF correction factor	
Determination of $\boldsymbol{k_{Q_{clin},Q_{msr}}^{f_{clin},f_{msr}}}$	0,80
Measurement conditions	
Reference field size	0,29
Clinical field size	0,12
Source-to-surface distance, SSD	0,13
Measurement depth, $\boldsymbol{z_{ref}}$	0,12
Combined standard uncertainty (%)	1,00

Considering the smallest field, the uncertainty associated with the determination of the field OF correction factor becomes the most significant source of uncertainty, followed by the detector calibration factor.

4. Conclusions

An audit methodology was developed for absolute dose determination and small field output factors based on TRS-398 [8] and TRS-483 [9] recommendations and other main guidelines. This methodology was previously tested in the Radiotherapy Department of IPO-Porto. The audit methodology was based on two pre-visit surveys, the remote report of raw small field OFs measurements and an on-site visit of the auditing team for measurements performance.

An email for 20 Radiotherapy centres was sent with the two surveys and an excel file for raw measurements report of output factors for field sizes ranging from 1×1 cm^2 to 3×3 cm^2. An on-site visit would be scheduled later, to carry out measurements with an independent dosimetry system. At the same time, a calculation worksheet for determining absolute dose was developed, reflecting the changes proposed by the revision of TRS 398, as well as several checklists to support the audit.

Only a total of six Radiotherapy centres responded to the surveys, and not all of them answered all the questions. The visit to carry out on-site measurements was not scheduled until now, due to logistical constraints or unavailability of the contacted centres.

Overall, the audit methodology developed in the work showed to be robust to characterize dosimetry practices regarding absolute dose and small field output factors determination, and to identify discrepancies between centres. At the same time, the surveys allowed the uncertainties calculation associated with each of the dosimetric processes. However, the small number of responses received prevented a more consistent multicentre analysis. And the impossibility of carrying out on-site measurements in the various centres audited, prevented full validation of the methodology designed.

Analysing the responses received allowed to conclude that, in general, the protocols TRS-398 and TRS-483 were well implemented.

Tolerance levels for dose deviation ranged from 0,5% to 2,0% among the surveyed centres, in accordance with TRS-398 guidelines. However, none of the centres had yet carried out a calculation of the uncertainty associated with absorbed dose measurements. It is crucial to consider the uncertainty interval when establishing dose deviation tolerance limits. The dose values obtained varied by a maximum of 0,50% when calculated using the new worksheet compared to the IAEA worksheet, highlighting

the importance of using the updated worksheet. Furthermore, the uncertainty associated with calculations using the new worksheet is also lower, enabling more reliable dose values.

Regarding small field output factors, no centre had yet estimated the associated uncertainties. Additionally, some centres did not apply the correction factors, as recommended by TRS-483, despite the analysis demonstrating their importance in correcting detector readings. The comparison of field output factors showed consistent results, highlighting concordance across centres. However, these results could be more robust if there were more participating centres.

This work is of great importance to increase the confidence and the strengthen of all involved institutions and professionals. Also, allows the cooperation among the Portuguese medical physics community to uniformize dosimetric practices and promote peer discussion about these subjects.

4.1. Future work

Overall, while this study provides valuable insights into current dosimetry practices, the limited response rate and methodological constraints underscore the challenges in conducting multicentre surveys in clinical settings. Future studies should aim to address these challenges to enhance the robustness and generalizability of findings in the field of radiation dosimetry.

The future work will include visits to perform on-site measurement in different centres. The on-site measurements will allow to verify the correct application of the dosimetric protocols and to identify if the dosimetry practices differ across different centres.

In the future, it would be advantageous to compare the small field output factors from a greater number of machines and across multiple centres. This comparative analysis could provide valuable insights into the consistency and reliability of small field output factor measurements across different radiation therapy facilities

Incorporating uncertainty analysis into dosimetry practice evaluations is also essential. Future work should emphasize the estimation and reporting of uncertainties associated with absorbed dose measurements and field output factors determination to provide a comprehensive assessment of dosimetric accuracy.

References

[1] J. Ferlay *et al.*, “Global Cancer Observatory: Cancer Today.” [Online]. Available: https://gco.iarc.who.int/today

[2] A. Chougule, “Status of cancer treatment by radiotherapy and requirement of radiation oncology medical physicists in Asia Oceania federation of organizations for medical physics region,” *J Cancer Res Ther*, vol. 19, no. 3, pp. 567–572, Jul. 2023, doi: 10.4103/jcrt.jcrt_51_21.

[3] “Radiotherapy Risk Profile: Technical Manual,” Geneva, 2008.

[4] J. Izewska, W. Lechner, and P. Wesolowska, “Global availability of dosimetry audits in radiotherapy: The IAEA dosimetry audit networks database,” *Phys Imaging Radiat Oncol*, vol. 5, pp. 1–4, Jan. 2018, doi: 10.1016/j.phro.2017.12.002.

[5] R. A. S. Thomas *et al.*, “Radiotherapy reference dose audit in the United Kingdom by the National Physical Laboratory: 20 years of consistency and improvements,” *Phys Imaging Radiat Oncol*, vol. 3, pp. 21–27, Jul. 2017, doi: 10.1016/j.phro.2017.07.005.

[6] C. H. Clark, N. Jornet, and L. P. Muren, “The role of dosimetry audit in achieving high quality radiotherapy,” *Phys Imaging Radiat Oncol*, vol. 5, pp. 85–87, Jan. 2018, doi: 10.1016/j.phro.2018.03.009.

[7] “Comprehensive QA for Radiation Oncology: Report of AAPM Radiation Therapy Committee Task Group 40,” College Park, 1994.

[8] *Absorbed Dose Determination in External Beam Radiotherapy*, (Rev.1)., vol. no. 398. Vienna: International Atomic Energy Agency, 2024. doi: 10.61092/iaea.ve7q-y94k.

[9] *Dosimetry of Small Static Fields Used in External Beam Radiotherapy*, no. 483. in Technical Reports Series. Vienna: INTERNATIONAL ATOMIC ENERGY AGENCY, 2017. [Online]. Available: https://www.iaea.org/publications/11075/dosimetry-of-small-static-fields-used-in-external-beam-radiotherapy

[10] T. K. Yeung, K. Bortolotto, S. Cosby, M. Hoar, and E. Lederer, “Quality assurance in radiotherapy: evaluation of errors and incidents recorded over a 10 year period,” *Radiotherapy and Oncology*, vol. 74, no. 3, pp. 283–291, Mar. 2005, doi: 10.1016/j.radonc.2004.12.003.

[11] D. van der Merwe *et al.*, “Accuracy requirements and uncertainties in radiotherapy: a report of the International Atomic Energy Agency,” *Acta Oncol (Madr)*, vol. 56, no. 1, pp. 1–6, Jan. 2017, doi: 10.1080/0284186X.2016.1246801.

[12] M. A. Bolt, C. H. Clark, T. Chen, and A. Nisbet, “A multi-centre analysis of radiotherapy beam output measurement,” *Phys Imaging Radiat Oncol*, vol. 4, pp. 39–43, Oct. 2017, doi: 10.1016/j.phro.2017.12.001.

[13] International Atomic Energy Agency. and Quality Assurance Team for Radiation Oncology., *Comprehensive audits of radiotherapy practices : a tool for quality improvement*. International Atomic Energy Agency, 2007.

[14] M. Pasler, V. Hernandez, N. Jornet, and C. H. Clark, “Novel methodologies for dosimetry audits: Adapting to advanced radiotherapy techniques,” *Phys Imaging Radiat Oncol*, vol. 5, pp. 76–84, Jan. 2018, doi: 10.1016/j.phro.2018.03.002.

[15] P. R. Almond *et al.*, “AAPM’s TG-51 protocol for clinical reference dosimetry of high-energy photon and electron beams,” *Med Phys*, vol. 26, no. 9, pp. 1847–1870, Sep. 1999, doi: 10.1118/1.598691.

[16] D. Eaton, S. Bolton, R. Thomas, and C. Clark, “Inter-departmental dosimetry audits-development of methods and lessons learned,” *J Med Phys*, vol. 40, no. 4, pp. 183–189, Oct. 2015, doi: 10.4103/0971-6203.170791.

[17] C. H. Clark *et al.*, “Radiotherapy dosimetry audit: Three decades of improving standards and accuracy in UK clinical practice and trials,” 2015, *British Institute of Radiology*. doi: 10.1259/bjr.20150251.

[18] L. Humbert-Vidan, T. Sander, D. J. Eaton, and C. H. Clark, “National audit of a system for rectal contact brachytherapy,” *Phys Imaging Radiat Oncol*, vol. 1, pp. 1–5, Jan. 2017, doi: 10.1016/j.phro.2016.12.001.

[19] W. Lechner *et al.*, “A multinational audit of small field output factors calculated by treatment planning systems used in radiotherapy,” *Phys Imaging Radiat Oncol*, vol. 5, pp. 58–63, Jan. 2018, doi: 10.1016/j.phro.2018.02.005.

[20] S. Dufreneix, J. Bellec, S. Josset, and L. Vieillevigne, “Field output factors for small fields: A large multicentre study,” *Physica Medica*, vol. 81, pp. 191–196, Jan. 2021, doi: 10.1016/j.ejmp.2021.01.001.

[21] K. Manolova Sergieva, “Dosimetry Audit in Modern Radiotherapy,” in *Radiation Oncology*, IntechOpen, 2022. doi: 10.5772/intechopen.100941.

[22] J. Izewska, T. Bokulic, P. Kazantsev, P. Wesolowska, and D. van der Merwe, “50 Years of the IAEA/WHO postal dose audit programme for radiotherapy: what can we learn from 13756 results?,” *Acta Oncol (Madr)*, vol. 59, no. 5, pp. 495–502, May 2020, doi: 10.1080/0284186X.2020.1723162.

[23] T. Kron, A. Haworth, and I. Williams, “Dosimetry for audit and clinical trials: Challenges and requirements,” in *Journal of Physics: Conference Series*, Institute of Physics Publishing, 2013. doi: 10.1088/1742-6596/444/1/012014.

[24] “Dosimetry Audit,” 2023, *ESTRO, Teddington, United Kingdom* .

[25] “RADIATION PROTECTION NO 159 EUROPEAN COMMISSION GUIDELINES ON CLINICAL AUDIT FOR MEDICAL RADIOLOGICAL PRACTICES (DIAGNOSTIC RADIOLOGY, NUCLEAR MEDICINE AND RADIOTHERAPY),” 2009. [Online]. Available: http://www.clinicalaudit.net/img/Proceedings2003.pdf

[26] O. Casares-Magaz, L. G. Marcu, Y. Prezado, E. Koutsouveli, and M. Brambilla, “EFOMP survey results on national radiotherapy dosimetry audits,” *Physica Medica*, vol. 84, pp. 10–14, Apr. 2021, doi: 10.1016/j.ejmp.2021.03.020.

[27] M. C. Lopes *et al.*, “Treatment planning systems dosimetry auditing project in Portugal,” *Physica Medica*, vol. 30, no. 1, pp. 96–103, Feb. 2014, doi: 10.1016/j.ejmp.2013.03.008.

[28] T. Santos and F. Social Europeu, “IAEA supported national IMRT audit in Portugal National report UNIÃO EUROPEIA,” 2018.

[29] N. Miri, J. Lehmann, K. Legge, B. J. Zwan, P. Vial, and P. B. Greer, “Remote dosimetric auditing for intensity modulated radiotherapy: A pilot study,” *Phys Imaging Radiat Oncol*, vol. 4, pp. 26–31, Oct. 2017, doi: 10.1016/j.phro.2017.11.004.

[30] Kh. Masood, A. Ullah, A. Hussain, Kh. Mahmood, G. R. Hart, and W. Muhammad, “Comparison of level-I, -II and -III dosimetry quality audits for MV-photon beams emitted from medical linear accelerators,” *International Journal of Radiation Research*, vol. 18, no. 3, Jul. 2020.

[31] E. Seravalli *et al.*, “Auditing local methods for quality assurance in radiotherapy using the same set of predefined treatment plans,” *Phys Imaging Radiat Oncol*, vol. 5, pp. 19–25, Jan. 2018, doi: 10.1016/j.phro.2018.01.002.

[32] Y. Tsang, A. Carver, N. Groom, C. Harris, C. Faivre-Finn, and D. Eaton, “A multi-centre dosimetry audit on advanced radiotherapy in lung as part of the isotoxic IMRT study,” *Phys Imaging Radiat Oncol*, vol. 4, pp. 17–21, Oct. 2017, doi: 10.1016/j.phro.2017.11.001.

[33] V. Hernandez, J. Saez, M. Pasler, D. Jurado-Bruggeman, and N. Jornet, “Comparison of complexity metrics for multi-institutional evaluations of treatment plans in radiotherapy,” *Phys Imaging Radiat Oncol*, vol. 5, pp. 37–43, Jan. 2018, doi: 10.1016/j.phro.2018.02.002.

[34] J. Lehmann *et al.*, “Dosimetric end-to-end tests in a national audit of 3D conformal radiotherapy,” *Phys Imaging Radiat Oncol*, vol. 6, pp. 5–11, Apr. 2018, doi: 10.1016/j.phro.2018.03.006.

[35] S. Russo *et al.*, “Multicenter evaluation of a synthetic single-crystal diamond detector for CyberKnife small field size output factors,” *Physica Medica*, vol. 32, no. 4, pp. 575–581, Apr. 2016, doi: 10.1016/j.ejmp.2016.03.005.

[36] Y. Akino, H. Mizuno, Y. Tanaka, M. Isono, N. Masai, and T. Yamamoto, “Inter-institutional variability of small-field-dosimetry beams among HD120 ™ multileaf collimators: a multi-institutional analysis,” *Phys Med Biol*, vol. 63, no. 20, p. 205018, Oct. 2018, doi: 10.1088/1361-6560/aae450.

[37] S. Russo *et al.*, “Multi-site evaluation of the Razor stereotactic diode for CyberKnife small field relative dosimetry,” *Physica Medica*, vol. 65, pp. 40–45, Sep. 2019, doi: 10.1016/j.ejmp.2019.07.027.

[38] C. Talamonti *et al.*, “Community approach for reducing small field measurement errors: Experience over 24 centres,” *Radiotherapy and Oncology*, vol. 132, pp. 218–222, Mar. 2019, doi: 10.1016/j.radonc.2018.10.012.

[39] Y. Akino, H. Mizuno, M. Isono, Y. Tanaka, N. Masai, and T. Yamamoto, “Small-field dosimetry of TrueBeam flattened and flattening filter-free beams: A multi-institutional analysis,” *J Appl Clin Med Phys*, vol. 21, no. 1, pp. 78–87, Jan. 2019, doi: 10.1002/acm2.12791.

[40] F. H. Attix, *Introduction to Radiological Physics and Radiation Dosimetry*, 1st ed. Germany: John Wiley & Sons, Inc., 1986.

[41] “ICRU Report 33: Radiation quantities and units ,” Washington D. C., 1980.

[42] E. B. Podgorsak, *Radiation Physics for Medical Physicists*, 3rd ed. Cham: Springer International Publishing, 2016. doi: 10.1007/978-3-319-25382-4.

[43] C. Eduardo de Almeida and C. Salata, “Absolute, Reference, and Relative Dosimetry in Radiotherapy,” in *Dosimetry*, IntechOpen, 2022. doi: 10.5772/intechopen.101806.

[44] E. B. Podgorsak, *Radiation Oncology Physics: A Handbook for Teachers and Students*. Vienna: International Atomic Energy Agency, 2005.

[45] M. R. McEwen and J. Taank, “Examining the influence of humidity on reference ionization chamber performance,” *Med Phys*, vol. 44, no. 2, pp. 694–702, Feb. 2017, doi: 10.1002/mp.12057.

[46] Y. Kato, H. Fuse, K. Shinoda, K. Miyamoto, and T. Fujisaki, “Thermal Equilibration in the Cavity Volume of a Farmer Ion Chamber for Routine Dosimetry,” *Int J Med Phys Clin Eng Radiat Oncol*, vol. 04, no. 04, pp. 268–272, 2015, doi: 10.4236/ijmpcero.2015.44032.

[47] M. McEwen, “Ionisation chamber dosimetry – updates and challenges,” in *International Symposium on Standards, Applications and Quality Assurance in Medical Radiation Dosimetry* , Ottawa: National Research Council Canada, 2019.

[48] R. Alfonso *et al.*, “A new formalism for reference dosimetry of small and nonstandard fields,” *Med Phys*, vol. 35, no. 11, pp. 5179–5186, Nov. 2008, doi: 10.1118/1.3005481.

[49] W. Parwaie, S. Refahi, M. Ardekani, and B. Farhood, “Different dosimeters/detectors used in small-field dosimetry: Pros and cons,” *J Med Signals Sens*, vol. 8, no. 3, p. 195, 2018, doi: 10.4103/jmss.jmss_3_18.

[50] J. P. Vaqué, “Contributions to new challenges in radiotherapy. From Small Field Dosimetry to Stereotactic Body Radiation Therapy,” Doctoral Thesis, Universitat Politècnica de Catalunya, Barcelona, 2015.

[51] P. Papaconstadopoulos, “On the detector response and the reconstruction of the source intensity distribution in small photon fields,” Doctoral Thesis, McGill University, 2016.

[52] G. F. Knoll, *Radiation Detection and Measurement*, 4th ed. John Wiley & Sons, Inc., 2010.

[53] H. Maselesele, “Development of a dosimetry audit methodology for advanced radiotherapy,” Doctoral Thesis, University of the Witwatersrand, Johannesburg, 2023.

[54] M. S. Huq, P. Andreo, and H. Song, “Comparison of the IAEA TRS-398 and AAPM TG-51 absorbed dose to water protocols in the dosimetry of high-energy photon and electron beams,” *Phys Med Biol*, vol. 46, no. 11, pp. 2985–3006, Nov. 2001, doi: 10.1088/0031-9155/46/11/315.

[55] A. El Hajami *et al.*, “Evaluation of the performance of an ionization chamber cylindrical (PTW) by the ELEKTA linear accelerator: Case of pulsed radiation,” *J Phys Conf Ser*, vol. 1292, no. 1, p. 012006, Aug. 2019, doi: 10.1088/1742-6596/1292/1/012006.

[56] “Common Dosimeters,” OncologyMedicalPhysics.com.

[57] P. Kazantsev *et al.*, “The IAEA remote audit of small field dosimetry for testing the implementation of the TRS-483 code of practice,” *Med Phys*, May 2024, doi: 10.1002/mp.17109.

[58] B. Casar, E. Gershkevitsh, I. Mendez, S. Jurković, and M. S. Huq, “A novel method for the determination of field output factors and output correction factors for small static fields for six diodes and a microdiamond detector in megavoltage photon beams,” *Med Phys*, vol. 46, no. 2, pp. 944–963, Feb. 2019, doi: 10.1002/mp.13318.

[59] J. U. Wuerfel, “Dose measurements in small fields,” 2013.

[60] L. Wilke *et al.*, “ICRU report 91 on prescribing, recording, and reporting of stereotactic treatments with small photon beams,” *Strahlentherapie und Onkologie*, vol. 195, no. 3, pp. 193–198, Mar. 2019, doi: 10.1007/s00066-018-1416-x.

[61] PTW, “Detectors for Ionizing Radiation: Including Codes of Practice,” Oct. 2023

[62] S. Clemente *et al.*, “A multi-center output factor intercomparison to uncover systematic inaccuracies in small field dosimetry,” *Phys Imaging Radiat Oncol*, vol. 5, pp. 93–96, Jan. 2018, doi: 10.1016/j.phro.2018.03.007.

[63] I. J. Das *et al.*, “Report of AAPM Task Group 155: Megavoltage photon beam dosimetry in small fields and non-equilibrium conditions,” Oct. 01, 2021, *John Wiley and Sons Ltd*. doi: 10.1002/mp.15030.

[64] B. Casar, “Small field dosimetry on linear accelerators,” 2022, *EURADOS WG9 WEBINAR*.

[65] H. Palmans, P. Andreo, M. S. Huq, J. Seuntjens, K. E. Christaki, and A. Meghzifene, “Dosimetry of small static fields used in external photon beam radiotherapy: Summary of TRS-483, the IAEA–AAPM international Code of Practice for reference and relative dose determination,” *Med Phys*, vol. 45, no. 11, pp. e1123–e1145, Nov. 2018, doi: 10.1002/mp.13208.

[66] H. Bagheri *et al.*, “An overview on small-field dosimetry in photon beam radiotherapy: Developments and challenges,” *J Cancer Res Ther*, vol. 13, no. 2, p. 175, 2017, doi: 10.4103/0973-1482.199444.

[67] M. M. Aspradakis *et al.*, “IPEM report 103: Small field MV photon dosimetry,” 2010. [Online]. Available: https://api.semanticscholar.org/CorpusID:115627935

[68] A. Megahed, G. Hassan, K. Ereiba, and E. Alashkar, “Problems Affecting Accurate Dose Measurement in Small-Field for Linear Accelerator,” *Asian Pacific Journal of Cancer Prevention*, vol. 24, no. 8, pp. 2757–2764, Aug. 2023, doi: 10.31557/APJCP.2023.24.8.2757.

[69] I. J. Das, J. Morales, and P. Francescon, “Small field dosimetry: What have we learnt?,” 2016, p. 060001. doi: 10.1063/1.4954111.

[70] D. Ceska, “Technology innovations reference detector for small field - The T-ref chamber,” 2016.

[71] I. Silvestre, A. Subiel, S. Dimitriadis, J. Duane, J. Snaith, and M. Homer, “A practical approach to report output factors for the NPL Beam Data Acquisition Service. Emphasis in Small Fields.,” Middlesex, Dec. 2017.

[72] S. E. Lam, D. A. Bradley, and M. U. Khandaker, “Small-field radiotherapy photon beam output evaluation: Detectors reviewed,” *Radiation Physics and Chemistry*, vol. 178, p. 108950, Jan. 2021, doi: 10.1016/j.radphyschem.2020.108950.

[73] B. Casar *et al.*, “On dosimetric characteristics of detectors for relative dosimetry in small fields: a multicenter experimental study,” *Phys Med Biol*, vol. 69, no. 3, p. 035009, Feb. 2024, doi: 10.1088/1361-6560/ad154c.

[74] W. Culberson, “Understanding Solid-State Dosimeters and Their Increasing Role in Medical Physics Quality Assurance Measurements,” in *QA & Dosimetry Symposium*, Lisbon, Feb. 2024.

[75] R. Ravichandran, J. P. Binukumar, I. Al Amri, and C. A. Davis, “Diamond detector in absorbed dose measurements in high-energy linear accelerator photon and electron beams,” *J Appl Clin Med Phys*, vol. 17, no. 2, pp. 291–303, Mar. 2016, doi: 10.1120/jacmp.v17i2.5690.

[76] F. Marsolat *et al.*, “Diamond dosimeter for small beam stereotactic radiotherapy,” *Diam Relat Mater*, vol. 33, pp. 63–70, Mar. 2013, doi: 10.1016/j.diamond.2013.01.003.

[77] S. Deshpande, R. Kumar, Y. Ghadi, R. M. Nehru, and V. Kannan, “Dosimetry Investigation of MOSFET for Clinical IMRT Dose Verification,” *Technol Cancer Res Treat*, vol. 12, no. 3, pp. 193–198, Jun. 2013, doi: 10.7785/tcrt.2012.500318.

[78] H. Benmakhlouf and P. Andreo, “Spectral distribution of particle fluence in small field detectors and its implication on small field dosimetry,” *Med Phys*, vol. 44, no. 2, pp. 713–724, Feb. 2017, doi: 10.1002/mp.12042.

[79] S. B. Scarboro, D. S. Followill, R. M. Howell, and S. F. Kry, “Variations in photon energy spectra of a 6 MV beam and their impact on TLD response,” *Med Phys*, vol. 38, no. 5, pp. 2619–2628, May 2011, doi: 10.1118/1.3575419.

[80] M. Kannan, S. Saminathan, V. Chandraraj, G. R. D, and K. M. Ganesh, “Determination of small-field output factors for beam-matched linear accelerators using various detectors and comparison of detector-specific output correction factors using IAEA Technical Report Series 483 protocol,” *Reports of Practical Oncology and Radiotherapy*, vol. 28, no. 2, pp. 241–254, Jun. 2023, doi: 10.5603/RPOR.a2023.0024.

[81] D. S. McGregor and J. K. Shultis, “Sensor Types,” in *Encyclopedia of Sensors and Biosensors*, vol. 1, K. Ikebukuro, Ed., Elsevier, 2023.

[82] J. Th. M. Jansen, F. W. Schultz, and J. Zoetelief, “RADIATION SOURCES: TYPES AND SUITABILITY FOR DOSE DELIVERY TO TISSUES FOR STERILISATION,” in *Sterilisation of Tissues Using Ionising Radiations*, Elsevier, 2005, pp. 79–103. doi: 10.1533/9781845690779.2.79.

[83] P. A. Jursinic, “Characterization of optically stimulated luminescent dosimeters, OSLDs, for clinical dosimetric measurements,” *Med Phys*, vol. 34, no. 12, pp. 4594–4604, Dec. 2007, doi: 10.1118/1.2804555.

[84] R. Liuzzi *et al.*, “Dose–Response of TLD-100 in the Dose Range Useful for Hypofractionated Radiotherapy,” *Dose-Response*, vol. 18, no. 1, p. 155932581989408, Jan. 2020, doi: 10.1177/1559325819894081.

[85] P. Alvarez, S. F. Kry, F. Stingo, and D. Followill, “TLD and OSLD dosimetry systems for remote audits of radiotherapy external beam calibration,” *Radiat Meas*, vol. 106, pp. 412–415, Nov. 2017, doi: 10.1016/j.radmeas.2017.01.005.

[86] A. Karmakar, J. Wang, J. Prinzie, V. De Smedt, and P. Leroux, “A Review of Semiconductor Based Ionising Radiation Sensors Used in Harsh Radiation Environments and Their Applications,” *Radiation*, vol. 1, no. 3, pp. 194–217, Aug. 2021, doi: 10.3390/radiation1030018.

[87] S. Dieterich and G. W. Sherouse, “Experimental comparison of seven commercial dosimetry diodes for measurement of stereotactic radiosurgery cone factors,” *Med Phys*, vol. 38, no. 7, pp. 4166–4173, Jul. 2011, doi: 10.1118/1.3592647.

[88] J. M. Lárraga-Gutiérrez, P. Ballesteros-Zebadúa, M. Rodríguez-Ponce, O. A. García-Garduño, and O. O. G. de la Cruz, “Properties of a commercial PTW-60019 synthetic diamond detector for the dosimetry of small radiotherapy beams,” *Phys Med Biol*, vol. 60, no. 2, pp. 905–924, Jan. 2015, doi: 10.1088/0031-9155/60/2/905.

[89] Y. Akino, A. Gautam, L. Coutinho, J. Würfel, and I. J. Das, “Characterization of a new commercial single crystal diamond detector for photon- and proton-beam dosimetry,” *J Radiat Res*, vol. 56, no. 6, pp. 912–918, Nov. 2015, doi: 10.1093/jrr/rrv044.

[90] A. B. Rosenfeld, “Electronic dosimetry in radiation therapy,” *Radiat Meas*, vol. 41, pp. S134–S153, Dec. 2006, doi: 10.1016/j.radmeas.2007.01.005.

[91] R. Consorti *et al.*, “In vivo dosimetry with MOSFETs: Dosimetric characterization and first clinical results in intraoperative radiotherapy,” *International Journal of Radiation Oncology*Biology*Physics*, vol. 63, no. 3, pp. 952–960, Nov. 2005, doi: 10.1016/j.ijrobp.2005.02.049.

[92] Y. Akdeniz and Z. Yegingil, “Evaluation of an efficient calibration protocol for use in radiochromic film dosimetry for photon beams,” *Radiation Physics and Chemistry*, vol. 156, pp. 31–37, Mar. 2019, doi: 10.1016/j.radphyschem.2018.10.002.

[93] S. Devic, N. Tomic, and D. Lewis, “Reference radiochromic film dosimetry: Review of technical aspects,” *Physica Medica*, vol. 32, no. 4, pp. 541–556, Apr. 2016, doi: 10.1016/j.ejmp.2016.02.008.

[94] M. Schöpe, J. Sahlmann, K. Lorenz, A. Findeisen, T. Barthel, and G. Klautke, “Sweeping-beam technique with electrons for large treatment areas as total skin irradiation,” *Strahlentherapie und Onkologie*, vol. 198, no. 1, pp. 47–55, Jan. 2022, doi: 10.1007/s00066-021-01859-1.

[95] C. Andrés, A. del Castillo, R. Tortosa, D. Alonso, and R. Barquero, “A comprehensive study of the Gafchromic EBT2 radiochromic film. A comparison with EBT,” *Med Phys*, vol. 37, no. 12, pp. 6271–6278, Dec. 2010, doi: 10.1118/1.3512792.

[96] T. Miyatake *et al.*, “Evaluation of the spatial resolution of Gafchromic™ HD-V2 radiochromic film characterized by the modulation transfer function,” *AIP Adv*, vol. 13, no. 8, Aug. 2023, doi: 10.1063/5.0160754.

[97] International Atomic Energy Agency., *Accuracy requirements and uncertainties in radiotherapy*. 2016.

[98] P. Castro *et al.*, “Study of the uncertainty in the determination of the absorbed dose to water during external beam radiotherapy calibration,” *J Appl Clin Med Phys*, vol. 9, no. 1, pp. 70–86, 2008, doi: 10.1120/jacmp.v9i1.2676.

[99] B. McClean, “Uncertainty Analysis in Radiation Dosimetry,” 2024, *ESMPE, Prague*.

[100] Joint Committee for Guides in Metrology, “Evaluation of measurement data-Guide to the expression of uncertainty in measurement,” 2008. [Online]. Available: www.bipm.org

[101] “https://www.varian.com”.

[102] “https://www.ptwdosimetry.com/en/.”

[103] S. Ketelhut, “Measurement of chamber correction factors kch for medium-energy therapeutic X-rays,” Jun. 2019, *Physikalisch-Technische Bundesanstalt, Berlin*.

[104] H. R. Baghani, S. Andreoli, and M. Robatjazi, “On the measurement of scaling factors in the RW3 plastic phantom during high energy electron beam dosimetry,” *Phys Eng Sci Med*, vol. 46, no. 1, pp. 185–195, Mar. 2023, doi: 10.1007/s13246-022-01209-0.

[105] "RW3 Slab Phantom T29672 and T40006.1.001: Instruction Manual," Freiburg, 2009.

[106] W. Cruz, G. Narayanasamy, N. Papanikolaou, and S. Stathakis, "Dosimetric comparison of water phantoms, ion chambers, and data acquisition modes for LINAC characterization," *Radiat Meas*, vol. 82, pp. 108–114, Nov. 2015, doi: 10.1016/j.radmeas.2015.09.005.

[107] A. Ralston, M. Tyler, P. Liu, D. McKenzie, and N. Suchowerska, "Over-response of synthetic microDiamond detectors in small radiation fields," *Phys Med Biol*, vol. 59, no. 19, pp. 5873–5881, Oct. 2014, doi: 10.1088/0031-9155/59/19/5873.

[108] V. De Coste *et al.*, "Is the PTW 60019 microDiamond a suitable candidate for small field reference dosimetry?," *Phys Med Biol*, vol. 62, no. 17, pp. 7036–7055, Aug. 2017, doi: 10.1088/1361-6560/aa7e59.

[109] G. Reggiori *et al.*, "Use of PTW-microDiamond for relative dosimetry of unflattened photon beams," *Physica Medica*, vol. 38, pp. 45–53, Jun. 2017, doi: 10.1016/j.ejmp.2017.05.046.

[110] I. Ciancaglioni *et al.*, "Dosimetric characterization of a synthetic single crystal diamond detector in clinical radiation therapy small photon beams," *Med Phys*, vol. 39, no. 7Part1, pp. 4493–4501, Jul. 2012, doi: 10.1118/1.4729739.

[111] C. Weber *et al.*, "Small field output correction factors of the microSilicon detector and a deeper understanding of their origin by quantifying perturbation factors," *Med Phys*, vol. 47, no. 7, pp. 3165–3173, Jul. 2020, doi: 10.1002/mp.14149.

[112] A. N. McGrath, S. Golmakani, and T. J. Williams, "Determination of correction factors in small MLC-defined fields for the Razor and microSilicon diode detectors and evaluation of the suitability of the IAEA TRS-483 protocol for multiple detectors," *J Appl Clin Med Phys*, vol. 23, no. 7, Jul. 2022, doi: 10.1002/acm2.13657.

[113] M. S. Weinhous and J. A. Meli, "Determining P ion, the correction factor for recombination losses in an ionization chamber," *Med Phys*, vol. 11, no. 6, pp. 846–849, Nov. 1984, doi: 10.1118/1.595574.

[114] J. W. Boag, E. Hochhäuser, and O. A. Balk, "The effect of free-electron collection on the recombination correction to ionization measurements of pulsed radiation,"

Phys Med Biol, vol. 41, no. 5, pp. 885–897, May 1996, doi: 10.1088/0031-9155/41/5/005.

Attachments

Attachment 1



Survey on dosimetry practices in Radiotherapy

Introduction

This survey is part of the research being conducted for a master's thesis in Medical Physics. Its purpose is to perform a multicentre evaluation of absolute dose measurements with photon and the related measurements procedures to identify discrepancies among centers.

The answers will be used to estimate uncertainties associated with absolute dose measurements and develop a report on best practices.

Thank you for your time and cooperation.

Diana Silva | up202103123@edu.fc.up.pt

Radiotherapy service details	
Institution name	
City	
Medical physicist name	
Email address	

IPOPORTO
INSTITUTO PORTUGUÊS DE ONCOLOGIA DO PORTO FG, EPE

Equipment characterization			
Linear accelerators (LINACs)			
Manufacturer	Model	Available photon energies	
		○ 4 MV ○ 15 MV ○ 6 MV ○ 6 MV FFF ○ 10 MV ○ 10 MV FFF ○ Other:	
Ionization chambers			
Ionization chambers used to measure absolute dose	Calibration laboratory	Calibration date	Calibration uncertainty quoted in the calibration certificate
Stabilization time of the chamber	○ 0 minutes ○ 15 minutes ○ 5 minutes ○ 30 minutes ○ Other:		
Do you preheat the chamber?	○ Yes ○ No		
The chamber's stability is verified prior to measurements?			
Electrometer			
Model			
Manufacturer			
Measurement resolution			
Calibration laboratory			
Calibration date			
Calibration uncertainty quoted in the calibration certificate			
Calibrated concurrently with the ionization chamber?	○ Yes ○ No		
If not, do you apply the correction factor k_{elec}?	○ Yes ○ No		

IPOPORTO
INSTITUTO PORTUGUÊS DE ONCOLOGIA DO PORTO FG, EPE

Thermometer	
Model	
Manufacturer	
Measurement resolution	
Calibration laboratory	
Calibration date	
Calibration uncertainty quoted in the calibration certificate	
Which is the temperature used for the calculation of the correction factor k_{TP}?	○ Room temperature ○ Water temperature
Barometer	
Model	
Manufacturer	
Measurement resolution	
Calibration laboratory	
Calibration date	
Calibration uncertainty quoted in the calibration certificate	

IPOPORTO
INSTITUTO PORTUGUÊS DE ONCOLOGIA DO PORTO FG, EPE

Set-up		
Set-up	○ SSD	○ SAD
Distance measurement	○ Pointer ○ Lasers	○ Optical distance indicator (ODI)
Smallest scale division		
Phantoms		
Phantom used for reference dosimetry	○ Water phantom ○ Other:	○ Solid water
For solid water phantoms, how was the correction factor $h_{w/m}$ obtained?	○ Provided by the manufacturer ○ Other:	○ Calculated at the centre

Formalism for dose determination		
Which calibration protocol is used?	○ IAEA TRS-398 ○ Other:	○ AAPM TG-51
Which dose calculation worksheet do you use?	○ IAEA worksheet ○ Other:	○ Your own/your center's worksheet
Where is the PDD information taken from?	○ PDD determined during LINAC commissioning ○ PDD determined on the measurement day	
In 2024, an update of TRS-398 was published, which includes the revision of the beam quality correction factor values, k_Q, and proposes the use of the volume averaging correction factor, k_{vol}, for FFF beams.		
Do you use the beam quality correction factor, k_Q, updated values?	○ Yes	○ No
Do you apply the volume averaging correction factor, k_{vol}, for FFF beams?	○ Yes ○ Not applicable	○ No

IPOPORTO
INSTITUTO PORTUGUÊS DE ONCOLOGIA DO PORTO FG, EPE

Measurements		
How many charge readings are taken at minimum?	○ 1 ○ 2 ○ 3 ○ 4	○ 5 ○ Other:
Tolerance level for accepting or rejecting values	○ None	○ Yes (please specify):
Polarizing voltages ratio V_1/V_2 typically used	○ 3,0 ○ 3,5 ○ 4,0	○ 5,0 ○ Other:
Tolerance level for dose deviation	○ 0,5% ○ 1,0% ○ 1,5%	○ 2,0% ○ Other:
Are uncertainty limits applied to dose calculation?	○ Yes	○ No
If so, what's the maximum uncertainty admitted?	○ 0,5% ○ 1,0% ○ 1,5%	○ 2,0% ○ Other:

IPOPORTO
INSTITUTO PORTUGUÊS DE ONCOLOGIA DO PORTO FG, EPE

If you have any additional comments or suggestions related to absolute dose measurements, please, let us know.

Attachment 2

IPOPORTO

Worksheet for absorbed dose to solid water determination from high-energy photon beams

This file includes the formulas and data provided in the IAEA's TRS-398, which necessary for calculating the dose of high-energy photons in water or solid water.

This sheet was created following the guidelines outlined in the original TRS-398 (2000) and subsequently updated with the recommendations from the 2024 revision. In the TRS-398 published in 2000, k_Q is provided for a predefined set of values. For values not explicitly stated in the table, the corresponding value was determined using interpolation.

The TRS-398 revision, published in 2024, introduces a formula to calculate k_Q for each ionization chamber, based on the quality index, $TPR_{20,10}$. The values of **a** and **b** for each ionization chamber can be found in Appendix II of this report. This calculation sheet utilizes this formula.

Following the revision reccomendations, it was also included the calculation of volume averaging correction factor, k_{vol}, for FFF beams.

This worksheet was built to be used specifically in dose calculation in solid water, whereas the correction factor h_{wlm} is applied automatically. The correction factor h_{wlm} applied is the one provided by PTW for the RW3 Slab Phantom.

Additionally, there's also a section to fill in with the three dosimeter incorrect readings. The sheet calculates and returns the average and standard deviation of these measurements.

Only the grey cells should be filled. The results will appear in the blue cells.

Comments and feedback are greatly appreciated!

Diana Lopes Silva
e-mail: up202103123@fc.up.pt

Determination of the absorbed dose to solid water for high energy photon beams

User:		Date:	

1: Radiation treatment unit, ionization chamber and electrometer

LINAC:		Reference phantom:	
Nomimal acc potential (MV):		Reference field size (cm x cm):	
Nomimal dose rate (MU/min):		Reference depth, z_{ref} (g/cm²):	
		Set up:	
Ionization chamber model:		Reference distance (cm):	
Serial number:			

Correction factor for solid water: $h_{w/m} =$

Thimble length (cm):	
$N_{D,w}$ (Gy/nC):	
Beam quality ($TPR_{20,10}$):	

$$k_Q\left(\mathrm{TPR}_{20,10}\right) = \frac{1+\exp\left(\frac{a-0.57}{b}\right)}{1+\exp\left(\frac{a-\mathrm{TPR}_{20,10}}{b}\right)} =$$

a:
b:

2: Correction for influence quantities

Pressure, P (kPa):		Temperature, T (ºC):	
Reference conditions (calibration certificate):			
Pressure, P_0 (kPa):		Temperature, T_0 (ºC)	

$$k_{TP} = \frac{(273.2+T)}{(273.2+T_0)}\frac{P_0}{P} =$$

Humidity (%):	
Reference conditions (calibration certificate):	
Humidity (%):	

$$k_h =$$

$$k_{vol} = 1 + (0.0062Q - 0.0036)\left(\frac{100}{SDD}\right)^2 L^2 =$$

3: Dosimeter readings

$$k_{elec} =$$

Reading at +V₁, M₊ (nC):	
Reading at -V₁, M₋ (nC):	

$$k_{pol} = \frac{|M_+|+|M_-|}{2M} =$$

V₁ normal (V):		V₁/V₂:	
V₂ reduced (V):			
M₁ (nC):		M₁/M₂:	
M₂ (nC):			
Beam type:	pulsed	a₀:	
		a₁:	
$k_s = a_0 + a_1\left(\frac{M_1}{M_2}\right) + a_2\left(\frac{M_1}{M_2}\right)^2 =$		a₂:	

4: Uncorrected dosimeter reading

Uncorrected reading, M₁ (nC):	
Uncorrected reading, M₂ (nC):	
Uncorrected reading, M₃ (nC):	

$M =$ nC Standard Deviation:

Accelerator monitor units (MU):	

$M =$ nC/MU

5: Corrected dosimeter reading

$$M_Q = M\, k_{TP} k_h k_{elec} k_{pol} k_s k_{vol} h_{w/m} =$$ nC/MU

6: Absorbed dose rate to water

$$D_{w,Q}(z_{ref}) = M_Q N_{D,W,Q_0} k_{Q,Q_0} =$$ Gy/MU

Depth of dose maximum, z_{max} (g/cm²):	
PDD at z_{max} (%)	

$$D_{w,Q}(z_{max}) = 100\frac{D_{w,Q}(z_{ref})}{PDD\,(z_{ref})} =$$ Gy/MU

Deviation:

Ideal charge, M: nC

Attachment 3

IPOPORTO
INSTITUTO PORTUGUÊS DE ONCOLOGIA DO PORTO F.G, EPE

CHECKLIST DOSIMETRIC AUDIT

Department:	
Date:	

Nº	Item	Check	Value/Tolerance
ABSOLUTE DOSE VERIFICATION			
PRE-MEASUREMENT VERIFICATIONS			
	Ionization chamber model used for absolute dose measurement (FF photon beams)		Farmer type; cylindrical
	Ionization chamber model used for absolute dose measurement (FFF photon beams)		Farmer type or Semiflex; cylindrical
	Ionization chamber certified calibration laboratory		Primary standards dosimetry laboratory (PSDL) or, a secondary standards dosimetry laboratory (SSDL)
	Validity of the ionization chamber calibration certificate		Valid
	Ionization chamber stability verification		< 1%
	Electrometer model used for absolute dose measurement		Adequate
	Electrometer certified calibration laboratory		Primary standards dosimetry laboratory (PSDL) or, a secondary standard dosimetry laboratory (SSDL)
	Validity of the electrometer calibration certificate		Valid
	Electrometer calibrated concurrently with the ionization chamber		Yes
	k_{elec} correction factor		If applicable
	Polarization factors		< 1 year

IPOPORTO
INSTITUTO PORTUGUÊS DE ONCOLOGIA DO PORTO F.G, EPE

CHECKLIST DOSIMETRIC AUDIT

Nº	Item	Check	Value/Tolerance
	Thermometer model used for absolute dose measurement		Adequate
	Thermometer certified calibration laboratory		Adequate
	Validity of the Thermometer calibration certificate		Valid
	Barometer model used for absolute dose measurement		Adequate
	Barometer certified calibration laboratory		Adequate
	Validity of the Barometer calibration certificate		Valid
	REFERENCE SETUP		
	Phantom		Water phantom
	Water phantom alignment (beam inclination)		< 0.5º
	SSD		100 cm
	Field size		10 × 10 cm^2
	CAX measuring step		< 2 mm
	Ionization chamber alignment: CAX		< 0.5 mm
	Measurement depth, z_{ref}		10 cm
	Reference point of the chamber		On the central axis at the centre of the cavity volume
	Ionization chamber alignment: CAX		< 0.5 mm

IPOPORTO
INSTITUTO PORTUGUÊS DE ONCOLOGIA DO PORTO F.G, EPE

CHECKLIST DOSIMETRIC AUDIT

Nº	Item	Check	Value/Tolerance
	Dosimetric system stabilization time		Min 15 min or recommended by manufacturer
	Thermometer and barometer stabilization time		Min 15 min
	MEASUREMENTS		
	Ionization chamber warm up		Min 1000 Mus and check stability of current variation
	Tolerance level for accepting or rejecting measured values		SD < 0.05 nC
	DOSE CALCULATION		
	Dose calculation worksheet		With quality correction factor updated values (2024 TRS-398 update)
	%D @ 10 cm determination		Commission or recent PDD ($\Delta TPR_{20,10}$ < 1% from the reference)
	Quality correction factor determination (k_Q)		Quality correction factor updated values (2024 TRS-398 update)
	Average volume correction factor (k_{vol})		If a farmer type chamber is used
	k_{TP} determination		T_0 and P_0 values from the ionization chamber calibration certificate
	Polarizing voltages ratio V_1 / V_2 used for k_s determination		4
	k_{pol} and k_s correction factors		Applied
	Correction for influence quantities		Applied
	Uncertainty budget calculation in the determination of absorbed dose to water under reference conditions		Performed
	Tolerance level for dose deviation		> calculated uncertainty

IPOPORTO
INSTITUTO PORTUGUÊS DE ONCOLOGIA DO PORTO F.G, EPE

CHECKLIST DOSIMETRIC AUDIT

OBS:

Date:	Responsable:

Attachment 4



Survey on relative dosimetry of small fields practices

Introduction

This survey is part of the research being conducted for a master's thesis in Medical Physics. Its purpose is to perform a multicentre evaluation of small field output factors with photon beams for field sizes equal to or smaller than 3 cm × 3 cm and the related measurements procedures to identify discrepancies among centres.

The answers will be used to estimate uncertainties associated with output factors measurements and develop a report on best practices in small fields dosimetry.

Additionally, an Excel sheet has been sent for you to fill in with the measured values to determine the output factors.

Thank you for your time and cooperation.

Diana Silva | up202103123@edu.fc.up.pt

Radiotherapy service details	
Institution name	
City	
Medical physicist name	
Email address	

IPOPORTO
INSTITUTO PORTUGUÊS DE ONCOLOGIA DO PORTO FG, EPE

Equipment characterization	
Linear accelerator (LINAC)	
Model	
Manufacturer	
Collimation system	
Photon energies (used for small fields)	○ 4 MV ○ 6 MV FFF ○ 6 MV ○ 10 MV FFF ○ 10 MV ○ Other:
Field size defined by	○ MLC aperture ○ Jaws ○ Circular fixed aperture collimator ○ Other:
Reference field dimension	
Non-reference small fields dimensions (defined by collimator settings)	

Detectors used in small field dosimetry			
Model	Manufacturer	Orientation	Type of measure

IPOPORTO
INSTITUTO PORTUGUÊS DE ONCOLOGIA DO PORTO FG, EPE

Setup and methodology for small field output factors measurement		
SSD (cm)		
Depth (cm)		
Detector centering methodology		
For CAX correction, which profile step (mm) do you use?		
Do you perform profiles for CAX correction for each field, before measuring?		
○ Yes	○ No	
Do you perform and average measurements taken in the following two situations: moving the collimator from a smaller or from a larger field size and then back to the correct field size?		
○ Yes	○ No	
Do you perform individual non-reference field size measurements interleaving the reference field measurements?		
○ Yes	○ No	
Do you perform output factor measurements with at least two different detectors?		
○ Yes	○ No	
How many measures are taken at minimum?	○ 1 ○ 2 ○ 3 ○ 4	○ 5 ○ Other:
Tolerance level for accepting or rejecting values	○ None	○ Yes (please specify):

IPOPORTO
INSTITUTO PORTUGUÊS DE ONCOLOGIA DO PORTO FG, EPE

Determination of field output factors		
Methodology		
Ratio of detectors readings methodology	○ Direct measured ratio of detector readings ○ Intermediate field method also known as the "daisy-chaining" method	
If a Daisy-chaining method is applied:		
Intermediate field f_{int} used		
Ionization chamber used in f_{int}		
Readings		
Ionization chamber:		
Corrected for influence quantities?	o Yes	o No
Recombination and polarity correction factors dependence with field size were assessed?	o Yes	o No
Solid-state detector:		
Temperature and dose rate dependencies were assessed?	o Yes	o No
Scintillator detector:		
Which methodology was used to estimate Cerenkov effect correction factor?		

Correction factors	
Correction factors applied to field output factors	○ None ○ Correction factors from TRS-483 ○ Correction factors from another publication:
Determination of the equivalent square small field size, S_{clin}, for output correction factors selection	○ FWHM at the measurement depth, derived from the beam profiles acquired with different detectors ○ FWHM at the measurement depth, measured with film dosimetry ○ Collimator aperture settings ○ Other:
Output factors reporting	
How do you report field output factors?	○ As a function of the equivalent square field size defined by the full width at half maximum (FWHM) of the beam profiles ○ As a function of the nominal field size
Do you report field output factors with the associated uncertainty?	○ Yes ○ No
If so, what's the methodology to determine this uncertainty?	

Training and competency	
What training do staff members receive regarding small field dosimetry measurements?	
Verification and validation	
How often are the output factor measurements verified?	
Do you perform any comparison with reference data or other facilities? If yes, please describe it.	
Incident reporting	
Have there been any incidents or deviations related to small field dosimetry measurements?	
How are such incidents investigated and addressed?	

IPOPORTO
INSTITUTO PORTUGUÊS DE ONCOLOGIA DO PORTO FG, EPE

Please provide any additional comments, observations, or suggestions related to small field dosimetry measurements at your facility.

Attachment 5

IPOPORTO
INSTITUTO PORTUGUÊS DE ONCOLOGIA DO PORTO F.G, EPE

CHECKLIST DOSIMETRIC AUDIT

Department:	
Date:	

Nº	Item	Check	Value/Tolerance
SMALL FIELD OFs VERIFICATION			
PRE-MEASUREMENT VERIFICATIONS			
	Small field dimensions		
	Detectors used for OF measurements		Diode type unshielded; Diamond detector; micro-ionization chamber The detector size is such that the volume averaging correction is not larger than 5%.
	Detector verification		Valid (< 2 years)
	Electrometer model used		Adequate
	Electrometer voltage		0 V, if a solid-state detector is used
	Thermometer		If a micro-ionization chamber is used
	Barometer		If a micro-ionization chamber is used
	MEASUREMENT SETUP		
	Phantom		Water phantom
	Water phantom alignment (beam inclination)		< 0.1º
	SSD		Variable, depending on the commissioning data specifications

IPOPORTO
INSTITUTO PORTUGUÊS DE ONCOLOGIA DO PORTO F.G, EPE

CHECKLIST DOSIMETRIC AUDIT

Nº	Item	Check	Value/Tolerance
	Reference field size		10 × 10 cm^2
	CAX measuring step		0.1 mm
	Beam profiles measuring step		1 mm
	Measurement depth		Variable, depending on the commission data specifications
	Detector orientation		Parallel (solid-state detectors)
	Reference point of the detector		According to the manufacturer specifications
	Dosimetric system stabilization time		Min 15 min or recommended by manufacturer
	Thermometer and barometer stabilization time		Min 15 min, if a micro-ionization chamber is used
	MEASUREMENTS		
	Detector warm up		Min 1000 MUs and check stability of current variation
	Beam profiles acquired at the measurement depth, for FWHM determination		Performed
	OF measurements: CAX correction for each field, before measuring		Performed
	OF measurements: detector readings taken in the following two situations: moving the collimator from a smaller or from a larger field size and then back to the correct field size		Performed
	OF measurements: tolerance level for accepting or rejecting measured values		SD < 0.005 nC
	OF CALCULATION		
	Determination of the output correction factors based on FWHM at the measurement depth, derived from the beam profiles acquired		Performed (TRS-483)

IPOPORTO
INSTITUTO PORTUGUÊS DE ONCOLOGIA DO PORTO F.G, EPE

CHECKLIST DOSIMETRIC AUDIT

OBS:

Date:	Responsable:

Attachment 6





Audit report

Diana Lopes Silva
Master in Medical Physics
Department of Physics and Astronomy
Faculty of Sciences of University of Porto

June 2024

Table of contents

1. Introduction ... 3
1.1. Audit objectives ... 3
1.2. Audit outline ... 4
2. Materials and methods ... 5
2.1. Centre characterization ... 5
2.2. Pre-visit survey ... 5
2.3. On-site measurements ... 6
2.3.1. Absorbed dose determination of photon beams ... 6
2.3.2. Field output factors determination ... 8
2.4. Post-visit analysis ... 10
2.4.1. Uncertainties ... 10
2.4.2. Tolerance limits ... 11
3. Results ... 12
3.1. Absorbed dose ... 12
3.1.1. Methodology analysis for absorbed dose determination ... 12
3.1.2. Absorbed dose deviation ... 12
3.1.3. Absorbed dose uncertainty ... 14
3.2. Field output factors ... 15
3.2.1. Methodology analysis for field output factors determination ... 15
3.2.2. Field output factors determination ... 15
3.2.3. Field output factors uncertainty ... 18
4. Conclusions and recommendations ... 19
References ... 21

1. Introduction

Radiotherapy is a complex multi-step process that involves ionizing radiation, requiring a high level of accuracy at every step [1]. Inadequate clinical dosimetry places the patient at risk, as the dose has an impact on local tumour control and radiation toxicity, consequently affecting quality of life [1], [2]. Due to this, it is very important to ensure safe radiotherapy with consistent doses, and dosimetry audits are an effective way of checking whether the quality of dosimetry in radiotherapy centres is adequate for the treatment objectives [2], [3], [4]. In addition to testing each system, there is also the need to ensure even more consistency between different systems and medical facilities [3]. Several authors and studies report that dosimetry audits reduce uncertainty and increase the consistency of dosimetry between different institutions [5], [6], [7], [8].

This report briefly describes the methodology used, the results obtained, and the main conclusions of the dosimetric audit conducted at the Radiotherapy Service of Portuguese Oncology Institute of Porto (IPO-Porto) between April and May 2024.

1.1. Audit objectives

This audit had two main objectives:

1. **Verification of the methodology used for absolute dose measurements of photon beams.**
   - Verification of the correct application of the IAEA TRS-398 [9] protocol.
   - Introduction of the methodology proposed by the revision of this protocol, published in 2024, that includes several updates, such as: updated k_Q values and the respective equation to obtain them; introduction of the volume averaging correction factor k_{vol}, that is only applied to FFF beams and corrects the underestimated dose reading that happens when the sensitive area of the chamber is not uniformly irradiated.
2. **Verification of the methodology used for small field dosimetry, particularly the field output factors.**
   - Verification of the correct application the IAEA TRS-483 [10] protocol.

1.2. Audit outline

The audit encompassed the following steps:

1. **Pre-visit survey:** In April, a survey on dosimetry practices in Radiotherapy was conducted among the medical physicists responsible for each linear accelerator. The survey included questions about equipment, dosimetry measurements, and dose determination.
2. **On-site measurements:** From April to May, dose verification of IPO-Porto's linear accelerators was monitored.
3. **Post-visit analysis:** This step involved evaluating the methodologies used for absolute dose and field output factors measurements, analysing the measured values, and estimating associated uncertainties.

2. Materials and methods

2.1. Centre characterization

IPO-Porto is an institution specialised in oncological treatment, research and education. IPO-Porto is equipped with 8 linear accelerators (LINACs) manufactured by Varian (Varian Medical Systems, Palo Alto, USA) [11]. The LINAC models include Clinac (4), TrueBeam (1), Trilogy (2) and Novalis (1). During this audit, 19 photon beams with energies between 4 MV and 15 MV were analysed, distributed as show in Figure 1.

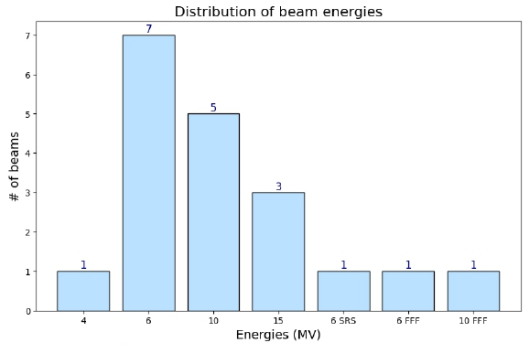


Figure 1: Distribution of beam energies.

2.2. Pre-visit survey

A survey on dosimetry practices in radiotherapy was sent to IPO-Porto's medical physicists. The aim of the survey was to evaluate the measurement procedures used to determine absolute dose and to identify any discrepancies among LINACs. The answers were also utilised to estimate the uncertainties associated with absolute dose measurements. The survey's questions were organized in the following sections:

- Equipment characterization (manufacturer, model and photon beam energies available)
- Detectors characterization (manufacturer, model and uncertainties quoted in the respective calibration certificates)
- Measurement set-up
- Formalism for dose determination and correction factors used to determine absolute dose to water
- Absolute dose measurements

2.3. On-site measurements

2.3.1. Absorbed dose determination of photon beams

Absorbed dose was determined following the IAEA Code of Practice TRS-398 [9]. The refence conditions were a depth of 10 cm at a source-to-surface distance (SSD) of 100 cm, and a field size of 10 cm × 10 cm.

The chamber used was a PTW 30013 Farmer (PTW, Freiburg, Germany) [12], which is the standard ionization chamber for absolute dose measurements in radiation therapy. This chamber has a sensitive volume of 0,6 cm^3, with a length of 23,0 mm and a radius of 3,05. It operates at a voltage ranging from 100 V to 400 V [69], [85]. Prior to dose measurements, the chamber's stability was checked. The chamber is shown in Figure 2.



Figure 2: PTW 30014 Farmer chamber used in absorbed dose measurements.

For dose measurements, two setups were assembled: one with solid water slab phantoms and the other with a water tank phantom.

The reference point of the chamber is taken to be at the centre of the cavity volume. Therefore, to have the chamber's centre at 10 cm depth in the solid water setup, 9,3 cm of solid water was placed on top of the solid water phantom with the chamber insert, since the chamber plate insert is displaced by 7 mm from the centre. The RW3 slab phantom used for this study was manufactured by PTW (PTW, Freiburg, Germany). The RW3 solid phantom consists of one plate with a thickness of 1 mm, two plates of 2 mm, one plate of 5 mm, and 29 plates that are each 10 mm thick, allowing for depth dose measurements down to 10 cm in 1 mm increments. Since the density of the phantom is higher than that of water, a correction factor provided in the instruction manual of the

slab phantom should be applied to determine the absorbed dose. Typically, this setup is used when time is limited, as it assembles much faster than the water tank setup.

For the water tank setup, the reference point of the chamber is positioned at a depth of 10 cm using the TRUFIX system (PTW, Freiburg, Germany. The water tank has a scanning range of 60,0 cm × 50,0 cm × 40,8 cm. Both setups can be seen in Figure 3.

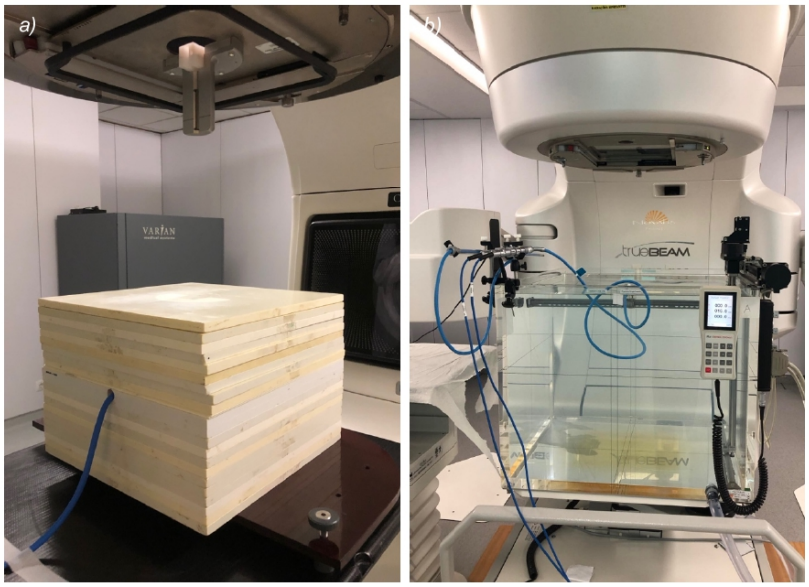


Figure 3: a) Setup assembled with RW3 slab phantom; b) Setup assembled with a water phantom

The chamber was connected to a PTW UNIDOS (PTW, Freiburg, Germany) electrometer. Before measuring, the chamber undergoes irradiation for pre-heating, i.e. until a stable reading is obtained. For each photon beam energy, the charge measurement was repeated at least three times.

All the influence quantities, such as temperature and pressure, were registered. Since the temperature inside the phantom insert may differ from the air temperature, the temperature readings were performed with a thermometer inside the solid water phantom insert, where the ionization chamber was later placed. For the water tank measurement, the water temperature was considered.

The absorbed dose to water at the depth of dose maximum was calculated using both the worksheet provided by the IAEA and the worksheet developed during this work base in TRS-398 [9] revision. In both cases, the air pressure correction, k_{TP}, the polarity correction factor k_{pol}, and the ionic recombination correction factor k_s were applied. The new worksheet includes the updated k_Q values, which differ from those provided in the 2000 version of the protocol and used in IAEA worksheet. This variation propagates to the calculated dose value. For FFF energies, the new worksheet also applies the volume averaging correction factor k_{vol} in the dose determination.

2.3.2. Field output factors determination

Field output factors were measured following the recommendations outlined in IAEA Codes of Practice TRS-483 [10]. The measurements were performed in a water phantom, shown in Figure 4, with the detectors positioned at a depth of 5 cm and with SSD of 95 cm. Measurements were made on a Varian TrueBeam linear accelerator (Varian Medical Systems, Palo Alto, CA, USA) [11].

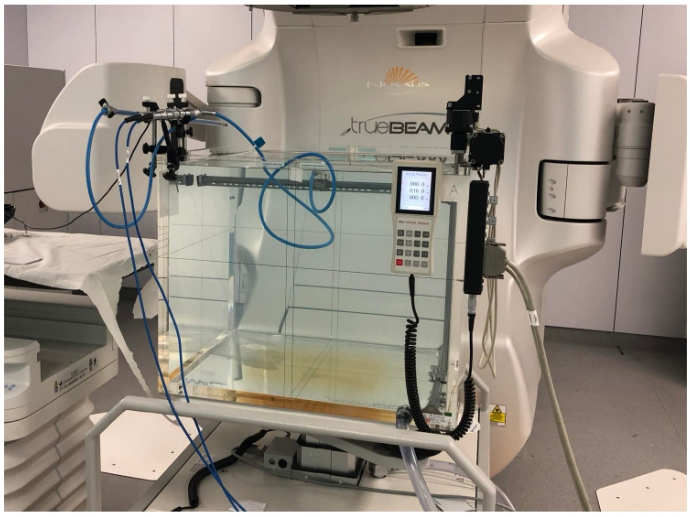


Figure 4: Setup for field output factors determination, assembled with a water phantom.

This part of the work was carried out using photon beams with nominal energies of 6 MV and 6 MV FFF. The reference field size was 10 cm × 10 cm, and the non-reference field sizes measured were 1 cm × 1 cm, 2 cm × 2 cm, and 3 cm × 3 cm. The field sizes were defined by the LINAC jaws.

The measurements were performed with the PTW 60019 MicroDiamond detector (PTW Freiburg, Germany) [12], and with the PTW MicroSilicon 6023 detector (PTW Freiburg, Germany) [12]. Both detectors are shown in Figure 5.

PTW 60019 MicroDiamond synthetic is diamond detector, water equivalent in megavoltage photon beams and it is reliable in field sizes ranging from 1 to 40 cm2. The MicroDiamond detector consists of a single crystal layer with a thickness of 1 μm and an active volume of 0,004 mm³. The reference point is located 1,0 mm away from the detector tip. PTW MicroSilicon 6023 detector is a p-type silicon diode detector. It has an active volume of 0,030 mm3, a 0,75 mm radius and a 0,018mm height. Its reference point is located 0,9 mm from the detector tip. Both detectors operate at 0 V bias. The IAEA TRS-483 [10] recommends that they should be oriented parallel to the beam, due to the asymmetries in the detector structure.

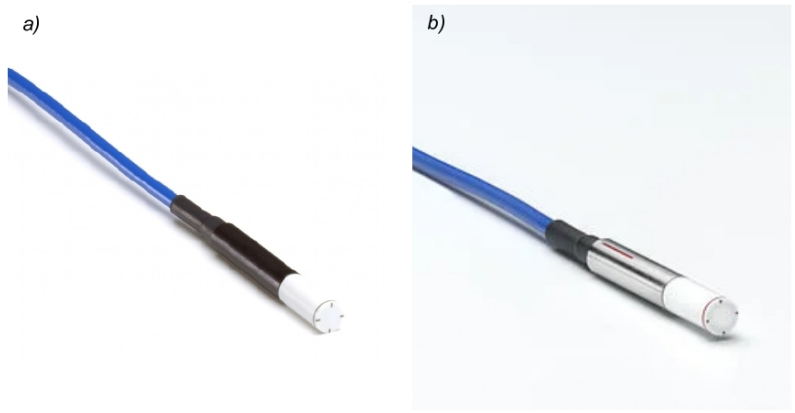


Figure 5: a) PTW 60019 MicroDiamond; b) PTW MicroSilicon 6023

The detector was connected to a PTW UNIDOS electrometer. For each field size, at the measurement depth, it was performed profile measurements, and the detector was positioned according to its CAX. The field size is defined by its FWHM.

For OFs determination, it was applied the correction factor $k_{Q_{clin},Q_{msr}}^{f_{clin},f_{msr}}$ given by the TRS-483 [10]. The correction factor value was estimated for each field size defined by the FWHM.

2.4. Post-visit analysis

The final stage of the audit involved the analysis of the data collected from the survey and the on-site measurements. The surveys were analysed to understand the dosimetry practices, the consistency of the methodology used by the different medical physicists and the dose values obtained were compared with the desired value to ensure they were within the tolerance limits. Additionally, an uncertainty budget was developed for the absorbed dose determination, and another was created for the output factors determination.

2.4.1. Uncertainties

The estimated or measured value of the dose, $D_{w,meas}$, should always be reported with an associated uncertainty:

$$D_{w,true} = D_{w,meas} \pm u$$

The "true" value, $D_{w,true}$, lies in the interval $\left[D_{w,meas} - u,\ D_{w,meas} + u\right]$, as exemplified in Figure 6.

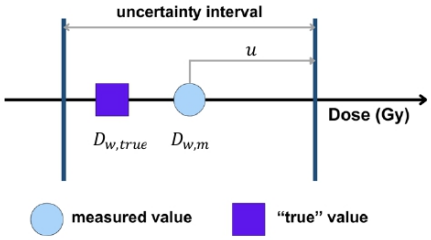


Figure 6: Exemplification of the uncertainty interval.

The uncertainty budget is the compilation of all input uncertainties [13]. According to the IAEA, each user should have the responsibility to establish an uncertainty budget for their determination of absorbed dose to water. [9]. Based on the survey information, two uncertainty budgets were calculated: one for absorbed dose measurements and another for field output factors. These are presented in Chapter 3.

2.4.2. Tolerance limits

The percentage relative deviation of the dose value is estimated following this equation:

$$\Delta_r(\%) = \left(\frac{D_w}{D_{w,meas}} - 1\right) \times 100$$

$D_{w,meas}$ is the measured absorbed dose value, and D_w is the desired dose value, which is 1 cGy/MU.

3. Results

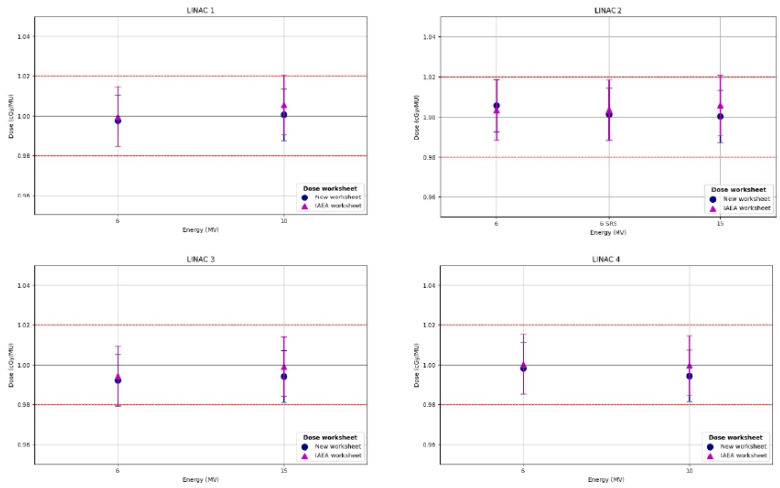
3.1. Absorbed dose

3.1.1. Methodology analysis for absorbed dose determination

Generally, the methodology applied follows the guidelines recommended by the IAEA TRS-398 code of practice [9]. The Farmer-type chamber used, which is the standard dosimeter for reference dosimetry, is being utilized correctly. However, it was noted that for some dose measurements, the chamber was not allowed sufficient time to stabilize. For this chamber model, it is recommended that the chamber should stabilize for at least 15 minutes. Despite these good practices, recommendations for potential improvements will be provided in Chapter 4.

3.1.2. Absorbed dose deviation

The charts presented in Figure 7 show the values of the calculated absorbed dose to water using the new and the IAEA worksheets. In the charts, it can also be seen the tolerance limits and estimated uncertainties, that will be presented in detail in Chapter 3.1.3.



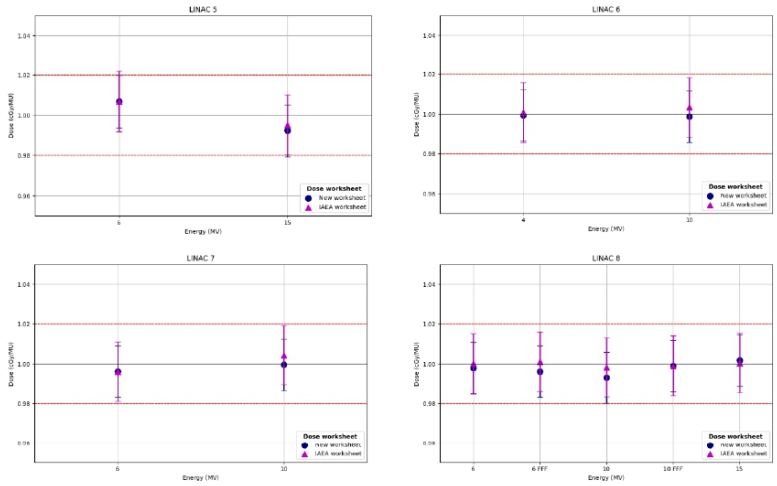


Figure 7: Dose (Gy/MU) per energy (MV), for each LINAC. Blue: dose value determined by the new worksheet. Green: dose value determined by the IAEA worksheet. The red line indicates the tolerance limit of 2%.

For photon beams with flattening filter, the difference between the dose determined with the two worksheets is proportional to the difference between the beam quality correction factors k_Q determined with the respective worksheet. For FFF beams, the difference in the dose won't be proportional due to the volume averaging correction factor k_{vol}.

Despite the worksheet used, all calculated dose values are within the tolerance limits. It's important to note that the uncertainty associated with the calculated dose values should be considered in dose adjustments. Even if the estimated dose value is within the tolerance limits, some values within the uncertainty interval may exceed these limits.

3.1.3. Absorbed dose uncertainty

The uncertainty budget estimated for absorbed dose determination at IPO can be seen in Table 1. The combined relative standard uncertainty is the quadratic sum of all the relative standard uncertainties associated with the process of dose measuring.

Table 1: Uncertainty budget of the determination of absorbed dose to water.

Source of Uncertainty	Standard uncertainty (%)
Dosimetry system	
Ionization chamber calibration factor, $N_{D,w}$	1,10
Long-term stability	0,15
Electrometer calibration factor, k_{elec}	-
Electrometer reading	0,05
Beam quality	
Determination of k_{Q,Q_0}	0,60
Correction factors for influence quantities	
Air pressure correction, k_{TP}	0,08
Polarity correction, k_{pol}	0,07
Ionic recombination correction, k_s	0,07
Reference conditions	
Field size	0,29
Source-to-surface distance, SSD	0,12
Measurement depth, z_{ref}	0,06
Combined standard uncertainty (%)	1,30

The highest contribution for the total uncertainty was the uncertainty of the ionization chamber calibration factor, $N_{D,w}$.

The previous version of TRS-398 presents an uncertainty of 1,0% associated with k_Q calculation. Therefore, when using the IAEA worksheet to determine absorbed dose, the uncertainty associated with the determination of k_Q increases from 0,6% to 1,0%, resulting in a combined relative standard uncertainty of 1,5%. For this reason, it is recommended to use the updated values of k_Q, since they have a lower associated uncertainty. The uncertainty associated with the electrometer reading is a function of the charge readings standard deviation. This value can be reduced, if the charge readings have a lower standard deviation.

3.2. Field output factors

3.2.1. Methodology analysis for field output factors determination

Field output factors were determined following the methodology proposed by the IAEA TRS-483 [10].

Both detectors used are suitable for small fields dosimetry, due to their small sensitive volume. TRS-483 [10] does not provide a correction factor for small fields measured with PTW MicroSilicon 6023, so the correction factor applied to this detector readings was the correction factor given for the previous version of this detector, the PTW 60017 unshielded diode. It is recommended to contact the manufacturer to verify if this correction factor is still valid or to search for an appropriate correction factor in the literature. Hence, using another detector is recommended for comparing values under these circumstances.

3.2.2. Field output factors determination

Before measuring field output factors, dose profiles for each field size were measured with the two detectors used for field output factors. The field size measured with each detector differs, as it can be seen in Figure 8.

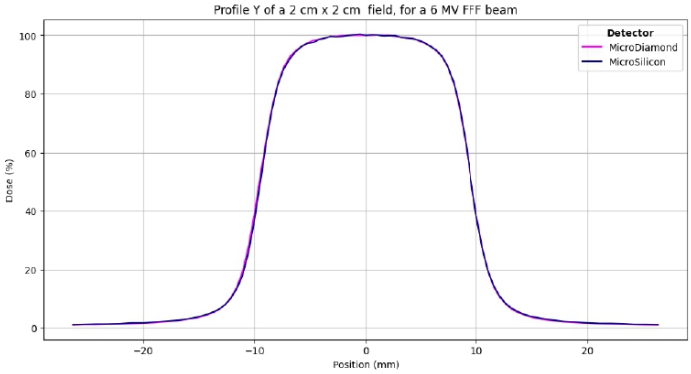


Figure 8: Profile X of a 2 cm × 2 cm field, for a 6 MV beam, at a depth of 5 cm, measured with MicroDiamond and MicroSilicon.

The field size and penumbra measured with the MicroSilicon detector is slightly smaller due to the larger sensitive region of the microdiamond detector (diameter of 2.2 mm), compared to the 1.5 mm for the MicroSilicon detector. The measured penumbral widths are dependent on detector volume and measurement step size.

As mentioned before, the field output factors were obtained using their field size defined by the FWHM, since this value doesn't equal the nominal field size for small fields. The equivalent square small size, S_{clin}, is given by:

$$S_{clin} = \sqrt{AB}$$

A and B correspond to the in-plane and cross-plane dosimetric field widths, respectively, defined as the FWHM of the dose profiles at the measurement depth. S_{clin} as a function of the nominal square field size, measured with each detector for 6 MV and 6 MV FFF, is shown in **Erro! A origem da referência não foi encontrada.**.

Table 2: S_{clin} measured for the TrueBeam small field sizes, as a function of the nominal square field sizes.

Nominal field size (cm × cm)	MicroDiamond S_{clin} (cm)		MicroSilicon S_{clin} (cm)	
	6 MV	6 MV FFF	6 MV	6 MV FFF
1 × 1	0,923	0,891	0,918	0,888
2 × 2	1,914	1,890	1,911	1,887
3 × 3	2,925	2,903	2,922	2,902

The calculated field output factors for the two photon beam energies are presented in Figure 9.

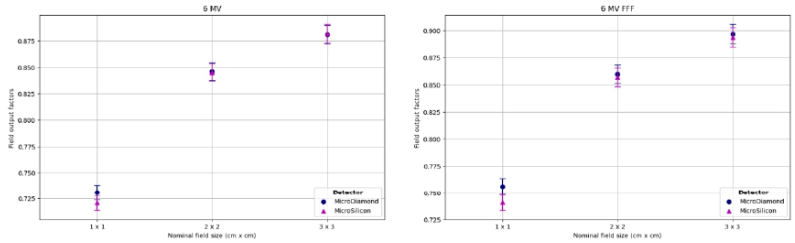


Figure 9: Field output factors, and respective uncertainty, for 3 nominal field sizes (3 cm, 2 cm, and 1 cm), determined with MicroDiamond and MicroSilicon detectors, for 6 MV and 6 MV FFF photon beams.

Table 3 and Table 4 present the values of the field output factors measured with the MicroDiamond and the MicroSilicon detectors, for 3 field sizes (1 cm × 1 cm, 2 cm × 2 cm, and 3 cm × 3 cm) for a photon beam with 6 MV and a photon beam with a 6 MV FFF energy, respectively.

Table 3: Field Output Factors determined with MicroDiamond and MicroSilicon detectors and relative standard deviation (SD) of the values determined with, for a 6 MV photon beam.

Nominal field size (cm × cm)	1 × 1	2 × 2	3 × 3
MicroDiamond	0,731	0,846	0,881
MicroSilicon	0,721	0,845	0,882
SD (%)	0,74	0,04	0,05

Table 4: Field Output Factors determined with MicroDiamond and MicroSilicon detectors and relative standard deviation (SD) of the values determined with, for a 6 MV FFF photon beam.

Nominal field size (cm × cm)	1 × 1	2 × 2	3 × 3
MicroDiamond	0,756	0,860	0,897
MicroSilicon	0,741	0,857	0,894
SD (%)	1,01	0,17	0,19

Since the measurements were performed on the same linear accelerator, under the same conditions, the slight difference in the measured values can be attributed to the intrinsic characteristics of the detectors.

It is also important to note that the field output correction factor applied to the MicroSilicon measurements corresponds to a previous version of the detector, PTW 60017 Diode E, as there are no published correction factors specific to this detector. Weber at al. (2020) [14] and McGrath et al. [15] concluded that the MicroSilicon readings require less corrections, due to its more water-equivalent design. While performing measurements with the MicroSilicon, it is important to keep in mind the lack of correction factors. The manufacturer has been contacted and has requested information from the specialist in this area in Freiburg. It is recommended to continue measuring the field output factors with the MicroDiamond, as it has published correction factors.

However, the MicroSilicon is still a valid detector to use for dose profiles measurements.

Though, these results demonstrate consistency between detectors for small output factors determination of this linear accelerator.

3.2.3. Field output factors uncertainty

The uncertainty budget estimated for the field output factors determination at IPO-Porto can be found in Table 5.

Table 5: Uncertainty budget of field output factors determination.

Source of Uncertainty	Standard uncertainty (%)
Dosimetry system	
Detector calibration factor, $\boldsymbol{R_{D,w}}$	0,55
Detector long-term stability	0,25
Electrometer reading of $\boldsymbol{M_{msr}}$	0,06
Electrometer reading of $\boldsymbol{M_{clin}}$	0,14
Field OF correction factor	
Determination of $\boldsymbol{k_{Q_{clin},Q_{msr}}^{f_{clin},f_{msr}}}$	0,80
Reference conditions	
Reference field size	0,29
Clinical field size	0,12
Source-to-surface distance, SSD	0,13
Measurement depth, $\boldsymbol{z_{ref}}$	0,12
Combined standard uncertainty (%)	1,00

The factor that most contributes to the uncertainty associated with field output factors determination is the uncertainty of the field correction factor, given by the TRS-483, followed by the detector's uncertainty.

4. Conclusions and recommendations

Overall, the dosimetry audit results show that the absorbed dose is within the reference standards defined by the IAEA [9], since for each audited beam the dose deviation was below 2%, and the dosimetry practices were performed according to the IAEA TRS-398 [9].

Despite all LINACs being correctly calibrated, some recommendations for potential improvements are noted:

1. The thermometer's calibration certificate was not valid – it is recommended to calibrate this equipment, according to the international standards.
2. The chamber's stability should be verified before taking absolute dose measurements.
3. The ionization chamber should stabilize for at least 15 minutes or as recommended by the manufacturer, before measurements.
4. It is recommended to experimentally determine the solid water correction factor for each beam energy and compare them with the values given by the phantom manufacturer's manual.
5. Absorbed dose determination must consider the updates in TRS-398 [9]:
    a. The dose must be calculated applying the updated values of k_{Q,Q_0}.
    b. For FFF beams, when using a Farmer chamber, the volume averaging correction k_{vol} should be applied.
    c. Alternatively, for FFF beams, dose measurement can also be performed with a smaller ionization chamber, such as a Semiflex.
6. Since there is no transversal methodology among medical physicists for accepting or rejecting a raw charge value, it is suggested that all physicists use the criterion of a standard deviation less than 0,005 nC.
7. It is suggested to adopt a transversal methodology regarding the threshold deviation for adjusting the dose, based on the uncertainty of the process.

Relative to the determination of small field output factors, all procedures were carried out in accordance with the recommendations of TRS 483 [10]. However, it is important to highlight the following points:

8. It is recommended to continue performing measurements with the MicroDiamond detector, since, according to the TRS 483 [10], it is a suitable detector for carrying

out small OF measurements and as it has appropriate correction factors published.

9. For MicroSilicon measurements, it is important to keep in mind that there are no suitable correction factors published, and it is ideal to wait for the manufacturer specialist's response.

References

[1] Radiotherapy Risk Profile: Technical Manual, Geneva, 2008.

[2] J. Izewska, W. Lechner, and P. Wesolowska, 'Global availability of dosimetry audits in radiotherapy: The IAEA dosimetry audit networks database', *Phys Imaging Radiat Oncol*, vol. 5, pp. 1–4, Jan. 2018, doi: 10.1016/j.phro.2017.12.002.

[3] R. A. S. Thomas *et al.*, 'Radiotherapy reference dose audit in the United Kingdom by the National Physical Laboratory: 20 years of consistency and improvements', *Phys Imaging Radiat Oncol*, vol. 3, pp. 21–27, Jul. 2017, doi: 10.1016/j.phro.2017.07.005.

[4] C. H. Clark, N. Jornet, and L. P. Muren, 'The role of dosimetry audit in achieving high quality radiotherapy', *Phys Imaging Radiat Oncol*, vol. 5, pp. 85–87, Jan. 2018, doi: 10.1016/j.phro.2018.03.009.

[5] S. Dufreneix, J. Bellec, S. Josset, and L. Vieillevigne, 'Field output factors for small fields: A large multicentre study', *Physica Medica*, vol. 81, pp. 191–196, Jan. 2021, doi: 10.1016/j.ejmp.2021.01.001.

[6] Y. Akino, H. Mizuno, Y. Tanaka, M. Isono, N. Masai, and T. Yamamoto, 'Inter-institutional variability of small-field-dosimetry beams among HD120 ™ multileaf collimators: a multi-institutional analysis', *Phys Med Biol*, vol. 63, no. 20, p. 205018, Oct. 2018, doi: 10.1088/1361-6560/aae450.

[7] C. Talamonti *et al.*, 'Community approach for reducing small field measurement errors: Experience over 24 centres', *Radiotherapy and Oncology*, vol. 132, pp. 218–222, Mar. 2019, doi: 10.1016/j.radonc.2018.10.012.

[8] S. Clemente *et al.*, 'A multi-center output factor intercomparison to uncover systematic inaccuracies in small field dosimetry', *Phys Imaging Radiat Oncol*, vol. 5, pp. 93–96, Jan. 2018, doi: 10.1016/j.phro.2018.03.007.

[9] *Absorbed Dose Determination in External Beam Radiotherapy*, (Rev.1)., vol. no. 398. Vienna: International Atomic Energy Agency, 2024. doi: 10.61092/iaea.ve7q-y94k.

[10] *Dosimetry of Small Static Fields Used in External Beam Radiotherapy*, no. 483. in Technical Reports Series. Vienna: INTERNATIONAL ATOMIC ENERGY AGENCY, 2017. [Online]. Available: https://www.iaea.org/publications/11075/dosimetry-of-small-static-fields-used-in-external-beam-radiotherapy

[11] 'https://www.varian.com'.

[12] 'https://www.ptwdosimetry.com/en/'.

[13] Joint Committee for Guides in Metrology, 'Evaluation of measurement data-Guide to the expression of uncertainty in measurement', 2008. [Online]. Available: www.bipm.org

[14] C. Weber *et al.*, 'Small field output correction factors of the MicroSilicon detector and a deeper understanding of their origin by quantifying perturbation factors', *Med Phys*, vol. 47, no. 7, pp. 3165–3173, Jul. 2020, doi: 10.1002/mp.14149.

[15] A. N. McGrath, S. Golmakani, and T. J. Williams, 'Determination of correction factors in small MLC-defined fields for the Razor and MicroSilicon diode detectors and evaluation of the suitability of the IAEA TRS-483 protocol for multiple detectors', *J Appl Clin Med Phys*, vol. 23, no. 7, Jul. 2022, doi: 10.1002/acm2.13657.